University of Stavanger

FACULTY OF SCIENCE AND TECHNOLOGY

MASTER'S THESIS

Study programme/specialisation: **Petroleum Technology, Drilling**	Autumn semester, 2020 Open
Author: **Rafael Alves Madeira**	…………………………………. (signature of author)
Programme coordinator: **Anita Malde** Supervisor(s): **Dan Sui**	
Title of master's thesis: **Twisted Elliptic Cylinder of Uncertainty: An Alternative Method to Calculate the Anti-Collision Safety Factor**	
Credits (ECTS): 30	
Keywords: Directional Drilling Anti-Collision Position Uncertainty Model Ellipsoid of Uncertainty ISCWSA Error Model Separation Factor Safety Factor Covariance Matrix Twisted Elliptic Cylinder of Uncertainty Peda-Curve Method	Number of pages: ……83……… + supplemental material/other: ………… Stavanger, Dec 3rd 2020 date/year

Twisted Elliptic Cylinder of Uncertainty

An Alternative Method to Calculate the Anti-Collision Safety Factor

Rafael Alves Madeira

Abstract

A precise anti-collision analysis is becoming even more important in the past few years, with the increasing amount of wells being drilled in highly congested fields. The costs associated with the production fields have increased substantially in recent years, and with that, the necessity to enhance the hydrocarbon recovery has also increased. One of the most adopted methods to enhance the recovery is to drill more wells in the same area.

Currently, the Ellipsoid Pedal-Curve method to calculate the Separation Factor is the most used and safe method. It is also the most conservative, and in many situations, it triggers an unnecessary early stop drilling due to limitations. This work aims to study a different method by using a different position uncertainty representation, a Twisted Elliptic Cylinder of Uncertainty, that can provide a more precise safety factor without triggering an early stop drilling situation and also keeping a safe operation.

The thesis utilizes the error model for Measuring While Drilling tools, provided by the The Industry Steering Committee on Wellbore Survey Accuracy (ISCWSA). The model has 27 generic error sources used to calculate both Ellipsoid of Uncertainty and the Cylinder of Uncertainty. The individual direction uncertainties were calculated using the Pedal-Curve method and the Cylinder Surface method introduced in this work. The individual uncertainties can be defined as the size of the position uncertainty in the direction of the closest point to reference in the offset well path. The comparison has shown that the Cylinder Surface method presents a more optimistic (smaller) separation factor results than the Pedal Radius, precisely indicating if the two wells have collided.

Three Separation Factor equations (ISCWSA, Equinor's, and a Simplified Version) were also compared throughout this work. The ISCWSA equation has shown more stability and robustness than the others, and it should be utilized as the main separation factor equation.

The results using the Twisted Elliptic Cylinder of Uncertainty as an alternative method to calculate the separation factor has shown a great potential to be used in the field, although it is still computationally demanding. The method still needs refinements, but it should be considered a viable method to determine the drilling operation's safety.

Keywords: directional drilling, anti-collision, position uncertainty model, ellipsoid of uncertainty, iscwsa error model, separation factor, safety factor, covariance matrix, twisted elliptic cylinder of uncertainty, pedal-curve method

Acknowledgments

First, I would like to thank my supervisor, Professor Dan Sui, for her guidance, support, and patience through each stage of this work.

In addition, I would like to also to thank my parents, Élia Maria and Carlos Miguel. They were always supportive throughout my entire life and were still there for me. My mother always believed in me and made me understand that I was able to overcome all problems and difficulties in life. To my dad, that is not with us anymore. I am pretty sure that, where ever my dad is, he is guiding and protecting me. Miss you so much, Dad!

Finally, I would more than ever thank my wife, Carolina. Without her help, patience, and support, I would never be able to complete the program. We all know the sacrifices that we have made in our lives to enable me to reach the end of this journey. Thank you for riding this path with me. Love you more than ever!

Contents

List of Figures

List of Tables

List of Symbols and Abbreviations

$Azi.$ Azimuth.

Azi_M Magnetic Azimuth.

Azi_T True Azimuth.

B_x Magnetometer measurements in x-axis.

B_y Magnetometer measurements in y-axis.

B_z Magnetometer measurements in z-axis.

B_{field} Magnetic Field Strength.

$C_{\mathbf{NEV}}$ Error covariance matrix in NEV-axes.

C_{hla} Error covariance matrix in HLA-axes.

D Center to Center Distance.

Dip Magnetic Field Inclination.

G_x Accelerometer measurements in x-axis.

G_y Accelerometer measurements in y-axis.

G_z Accelerometer measurements in z-axis.

G_{field} Gravitational Constant.

$Inc.$ Inclination.

R_i Length of semi-axes of an ellipsoid along principal axes.

R_r Offset Wellbore Radius.

R_r Reference Wellbore Radius.

S_m Safety Margin.

$T_{hla}^{\mathbf{NEV}}$ Direction cosine matrix to transform NEV matrix to HLA..

ΔE Easting.

ΔN Northing.

ΔV Vertical Depth.

β Angle at kick-off point.

$\boldsymbol{\Delta r}$ Borehole displacement between successive survey stations.

$\boldsymbol{e_{i,k}}$ The ith error source at the kth trajectory station.

$\frac{\delta \boldsymbol{p}}{\varepsilon_i}$ Weighting function of the i_{th} error source on the survey measurement.

$\frac{d\boldsymbol{r}}{d\boldsymbol{p}}$ The effect on the borehole position due to changes in survey measurement vector.

λ Eigenvalue of a given covariance matrix.

ϕ Dogleg.

ρ_i Propagation coefficients.

σ Magnitude of the weighting function.

σ_E^2 Variance in E-measurements.

σ_N^2 Variance in N-measurements.

σ_V^2 Variance in V-measurements.

σ_1 Directional Uncertainty from the reference well to offset well.

σ_2 Directional Uncertainty from the offset well to the reference well.

σ_{pa} Project-ahead Uncertainty.

$\varepsilon^{scalefactor}$ Scale factor error term.

k Dimensionless Scaling Factor.

l/min Liters Per Minute.

r Vector representing the NEV coordinate system.

BGGM BGS Geomagnetic Model.

BGS British Global Survey.

BHA Bottom Hole Assembly.

C-C Center to Center Distance.

DL Dogleg.

DLS Dogleg Severity.

DSATS Drilling Systems Automation Technical Section.

EOU Ellipsoid of Uncertainty.

G Global Error Source.

HLA Borehole Coordinate System.

I2C Inter-Integrated Circuit.

IFR In-Field Referencing.

ISCWSA The Industry Steering Committee on Wellbore Survey Accuracy.

KOP Kick-off Point.

LWD Logging While Drilling.

MASD Minimum Allowable Separation Distance.

MCM Minimum-Curvature Method.

MD Measured depth.

MWD Measurement While Drilling.

NEV Global Coordinate System.

R Random/Uncorrelated Error Source.

ROP Rate Of Penetration.

RPM Rotations Per Minute.

RSS Rotary Steerable System.

RSS Root-of-Sum-of-Squares.

S Systematic Error Source.

SPE Society of Petroleum Engineers.

TECoU Twisted Elliptic Cylinder of Uncertainty.

TVD True Vertical Depth.

UTM Universal Transverse Mercator.

WOB Weight On Bit.

WPTS SPE Wellbore Positioning Technical Section.

Chapter 1

Introduction

1.1 Background

The enhancement of the oil and gas recovery on already mature fields is leading companies worldwide to increase the number of wellbores in the same area. This situation makes the probability of hitting another well to grow, potentially leading to financial and life losses. The importance of increasing the accuracy of determining the wellbore position is also enlarging.

In the past few years, the Directional Drilling technologies have improved substantially, allowing the wellbore considered challenging until recently to be successfully concluded. The sensors used to calculate the wellbore position were also upgraded, and consequentially, the accuracy of the measurements was improved.

The directional drilling technique's main objective is to combine methods and practices to design and drill a wellbore by controlling its trajectory to reach an operational or geological target (Mitchell & Miska, 2016). The particular subject of controlling the wellbore trajectory in a crowded field can be a strenuous task. An unplanned well crossing can have severe economic and health consequences, and therefore, a meticulously performed anti-collision analysis is necessary to ensure the operation's safety.

A typical anti-collision analysis process starts by collecting the necessary data (location, position uncertainties) from the offset wells in the vicinity where the well is planned to be constructed. It is also necessary to determine the error model that will be used while drilling on a particular well, and because of that is important to calculate the planned wellbore's position uncertainty. The end product of the analysis is to determine how safe the current well plan is to be drilled. If the planned well path is not safe enough according to the requirements, the trajectory is altered until it is safe to be executed. The process is repeated for every offset well in the same area.

The Separation (or Safety) Factor along the trajectory indicates how close two well paths are to each other. At the current state, there is not an industry-standard form to calculate the factor. However, the most accurate equation is done by a ratio between the Center to Center distance and the uncertainties size for each point. The Center to Center Distance (C-C) is the distance between a point in the reference well and the closest point in the offset well (Jamieson et al., 2007).

The position uncertainty of a well path at a specific depth is caused due to many different error sources, and it can be geometrically expressed as an Ellipsoid of Uncertainty. The Ellipsoid radius in the direction of the closest point at the offset well is commonly calculated by the Pedal-Curve Method. The Pedal method is considered the safest method but also, it can also be very conservative, with the safety factor generated by the method indicating a nonexistent collision.

Alternatively, the uncertainty can be represented by a surface that envelops the well path, and it has the shape of an elliptic cylinder. In this thesis, the results from the Pedal-Curve method using the Ellipsoid of Uncertainty will be compared with the results from the Elliptic Cylinder Surface Distance method. The comparison will indicate if the Cylinder of Uncertainty and the method to calculate the safety factor are a viable way to represent the uncertainty and a wellbore can be drilled safely.

1.2   Objectives

The Pedal-Curve method is considered the safest method to calculate the size of the position uncertainty in the direction from a point in the well path to another point in the offset well. It is also very conservative, and the results are dependent on the direction the reference well is approaching the offset well.

In certain situations, the safety factor calculated by the Pedal-Curve radius can erroneously indicate that the two wells (reference and offset) have collided. With the increased number of wells in the same area, it is increasing the necessity to reduce the proximity between wells without compromising the personnel and operation's safety.

The ellipses of uncertainty at a particular depth can be derived from a 2D cut of the ellipsoid, with the center at a point in the well path and orthogonal to the trajectory direction. A series of ellipses of uncertainty separated by a small distance in the well path, and connected in a chain, form a surface of uncertainty around the well path. This surface is called the Twisted Elliptic Cylinder of Uncertainty, and in this thesis, it is presented as an alternative method to calculate the position uncertainty.

If an imaginary line could be drawn between a point at the reference well and its closest point found at the offset well, this line would be called Center to Center Distance (C-C). The size of the position uncertainty in the direction of the closest point at the offset well can be calculated by finding the radius of the intersecting point of the C-C line and cylinder surface for both reference and offset wells.

The radius derived by the cylinder of uncertainty will be used to calculate the wells' safety factor. The results will be compared with the results from the ellipsoid of uncertainty using the pedal-curve radius method. The main objective is to determine if the Cylinder of Uncertainty can be precisely indicated when the two well paths have in factor collided, being less pessimistic than the Pedal-Curve methods.

Since there is no industry standard method to calculate the safety factor, three versions of the equation will be used throughout this work. The equation provided by The Industry Steering Committee on Wellbore Survey Accuracy (ISCWSA), is the most recommended equation due to its robustness and stability. A more realistic and field-tested safety factor equation, provided by Equinor, a Norwegian state-owned energy company, was also used in this work. Lastly, the simplified version of the equation that was recently mentioned

by Mansouri et al. (2020) will also be used. As a secondary objective, the equations'
performance will also be evaluated. The most adequated equation that should be used
together with the cylinder of uncertainty will be determined.

1.3 Outline

This document comprises the following chapters:

1. **Introduction**: presents the background and basic information about the current
   state of the anti-collision process and the objective of the thesis.

2. **Directional Drilling**: the basic concepts of Well Planning and Directional Drilling
   techniques are presented. The wellbore position concepts are also introduced.

3. **Error Model**: in this chapter, the error model provided by ISCWSA is described
   in detail and the means to calculate the position uncertainty of a wellbore. The
   Ellipsoid of Uncertainty and Twisted Elliptic Cylinder will be introduced and the
   methods to calculate them.

4. **Anti-Collision**: in the anti-collision chapter, the basis of the anti-collision analysis
   is introduced. Step by step, the methodology to find the separation factors will be
   laid down through the text. In the end, the three separation factors used throughout
   this work are also presented.

5. **Case of Study**: the chapter describes the data and implementation routine used
   through the thesis. A comparison between the different methods of calculating the
   separation factors is also made in this chapter.

6. **Conclusion and Future Work**: the results are summarized and presented in this
   chapter. The author recommends future works to the future students of the theme.

Chapter 2

Directional Drilling

2.1 Well Planning

A Well Plan is a detailed study of a proposed wellbore and includes a vast number of data describing each well construction aspect of the well path that will be drilled. It is an important subject, and perhaps the most demanding aspect of Well Construction and Drilling Engineering subjects (Adams & Charrier, 1985).

Even with a variety of planning methods and practices across the oil industry, the well planning result should always be a plan that considers the safety, the minimum cost of the operations, and the usability that satisfies the reservoir engineer's requirements for the oil and gas production. Unfortunately, it is very difficult to accomplish all of these wells' objectives due to geology and drilling equipment constraints.

The main objectives of Well Planning are:

1. **Safety**: The personnel safety is the highest priority in well planning. In some cases, the plan must be modified in the drilling phase when unforeseen drilling problems endanger human lives (Adams & Charrier, 1985). The wellbore's safety is a second priority where the wellbore is designed to minimize the risk of blowouts, well collision, and other operational problems.

2. **Usability**: The final wellbore path must be usable to justify the efforts. The well needs sufficient hole diameters, the material used in hole and conditions without producing irreparable damage. The well path should be optimized to maximize the exposure to the reservoir, increasing the hydrocarbon production.

3. **Minimize Cost**: The well plan has also the objective to maintain the operational costs to a minimum without jeopardizing the safety of the personnel and the well.

In a very simplified way, well planning starts with the geologists and reservoir engineers defining the geological targets and the best angle to enter to those targets, especially in the reservoir areas. It might be necessary for the well path to penetrate to multiple targets until it reaches the final and main target. The well path design needs to meet all the necessary target requirements at the lowest possible cost. In order to meet those targets, safety, and cost requirements, in most of the situations, a Directional Well must be created.

2.2 Directional Drilling

Directional Drilling can generally be defined as the science of controlling a wellbore direction along a predetermined trajectory to intersect a designated subsurface target. It combines all activities, methods, and practices required to design and drill a wellbore to reach a target or multiple targets that are not directly positioned below the wellhead (Mitchell & Miska, 2016).

Today, most oil and gas production comes from directional wells drilled onshore or offshore, even environmentally sensitive locations (Mitchell & Miska, 2016). Production enhancement is reached by drilling high inclination angles wells and correctly entering the reservoir using the directional drilling techniques.

The recent improvements in the drilling technology have gradually increased the wellhead's horizontal departure, enabling the Extended Reach well types. Also, the development of the Logging While Drilling (LWD) tools made possible the guiding of the wellbore path based on real-time measurements of the formation rather than following a predetermined trajectory, called Geosteering, potentially maximizing the contact area of the well with the formation and improving the recovery of the hydrocarbons (Mitchell & Miska, 2016).

In response to the economic and environmental pressure, the use and number of directional wellbores have increased. A high number of wells drilled closely in the same field also increased the drilling operations' complexity, increasing the probability of a well collision. Because of the high probability, more sophisticated and precise drilling tools and technologies are required.
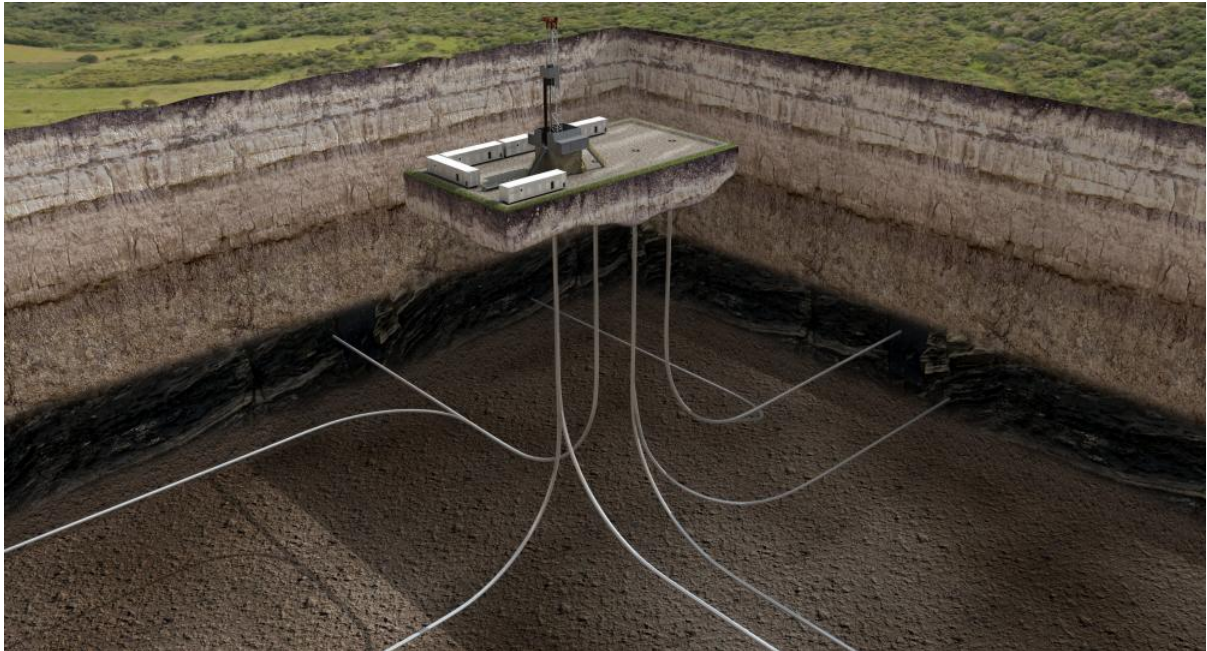
Figure 2.1: Multilateral Wells: Example of a Directional Drilling Application (Butler, 2018).

2.2.1 Directional Well Profiles

Defining the wellbore trajectory is a very important procedure in the well planning subject. Some of the trajectories are challenging, others require specialized equipment, while a few are impossible to be performed. The evolution of the Rotary Steerable System (RSS) in the past few years has allowed those complex operations to be completed with safety and precision.

In general, the Directional Well profiles can be divided into trajectories confined to one plane (2D trajectories) and more complex trajectories that are not restricted to one plane (3D trajectories). There are three basic 2D trajectories: Type I, II, and III. Additional 2D types are the Horizontal and Vertical Wells. The 3D well trajectories examples consist of Cluster Drilling and Designer Wells (Mitchell & Miska, 2016).

2D Well Trajectories

- **Type I - Slant-Type**: The well is confined in the vertical 2D plane, and it consists of a vertical section that ends at the Kick-off Point (KOP). The well starts to build up angle from the KOP until a certain depth where the desired inclination is reached. A tangent section is initiated, and it goes until the target is hit.

- **Type II - S-Type**: A S-type well starts with a vertical section until the KOP, followed by a build-up section. A tangent section comes after the desired inclination was reached in the build-up section and ends at a certain depth with a drop section. Sometimes, the inclination is reduced in the drop section to almost vertical until it hits the target.

- **Type III - J-Type**: The J-Type profile is normally used in Appraisal well to assess the extent of a newly discovered reservoir (Krishnan & Kulkarni, 2016). The well is kept vertical until the KOP. A build-up section starts, and the angle is kept increasing until the target is hit.
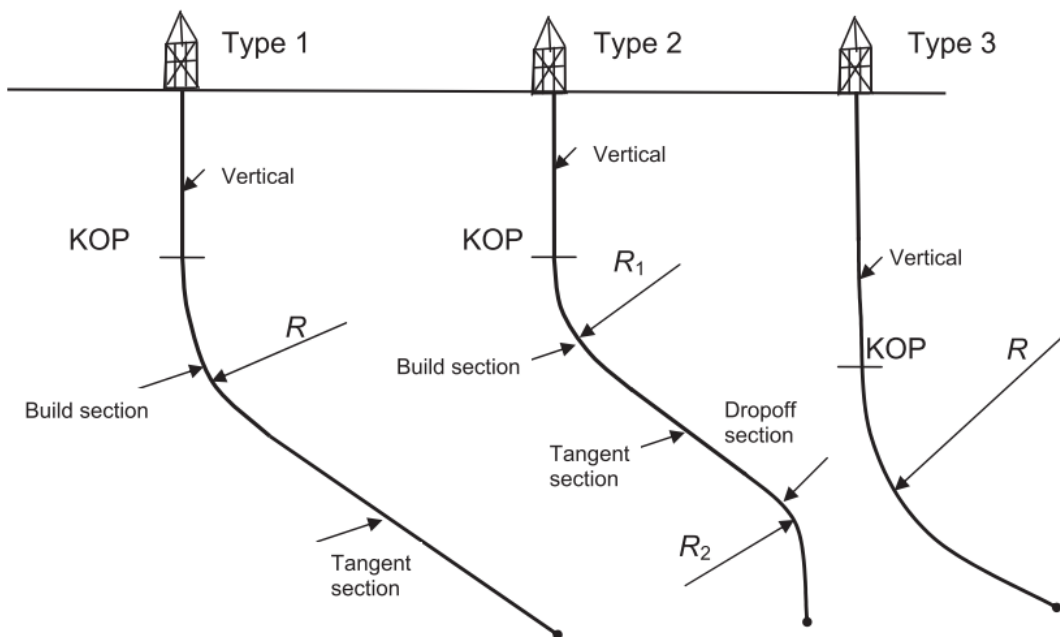
Figure 2.2: Example of Type I, II and II 2D Well Profile (Mitchell & Miska, 2016).

6

- **Additional Types: Vertical and Horizontal Wells**: The Vertical well is the simplest and economic well to be drilled and historically is the most common onshore well. Now a day is normally used to investigate geological marks or hazards. The Horizontal wells are wells with high inclination angles between 80°to 100°, with an ideal one being 90°of inclination. The Horizontal wells are drilled in the reservoir to potentially increase the wellbore contact and enhance the oil recovery. The well initiates with a vertical section, followed by a build-up segment, and ends with a horizontal section after the desired angles were achieved in the build-up section. Before it reaches horizontal, the well can have different profiles than just a build-up section, for example, a tangent section.
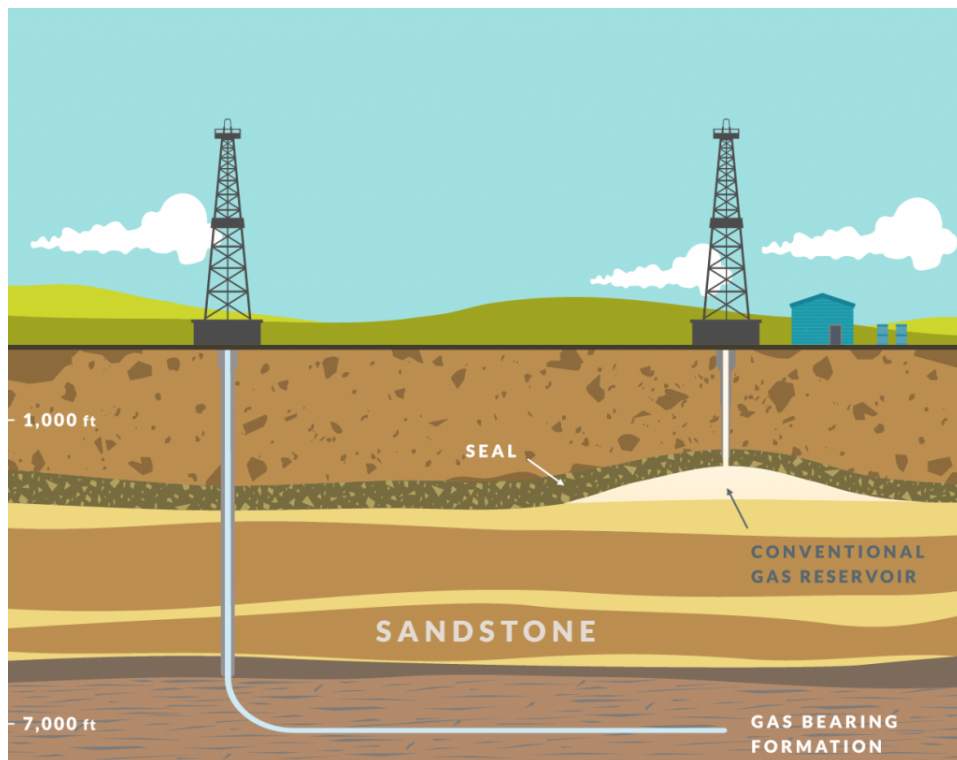
Figure 2.3: Examples of Vertical and Horizontal Wells (Cumming, 2017)

3D Well Trajectories

All the wellbores that are not confined to the vertical plane are considered to be a Three-Dimensional well. This type of well is necessary due to a variety of geological and engineering reasons. A few examples of designing a 3D well are avoiding subsurface hazards, intersecting multiple geological targets, avoiding collision with nearby wells, and many others. The most common types of 3D wells are the Cluster drilling and Designer wells.

The Cluster drilling (figure 2.4) is a combination of multiple tri-dimensional wells drilled from one offshore or onshore structure. This type of drilling is environmentally friendly, minimizing the drilling impacts and economical, reducing the amount of material and equipment necessary to perform the operations.

The Designer Wells (figure 2.5) are wells that involve a great change in the hole direction, with more than 30°Azimuth difference, combined with some changes in the hole inclination

7

(Mitchell & Miska, 2016). This type of well is designed to optimize the efficiency of the production or injection and hit multiple targets until reaching the main one.
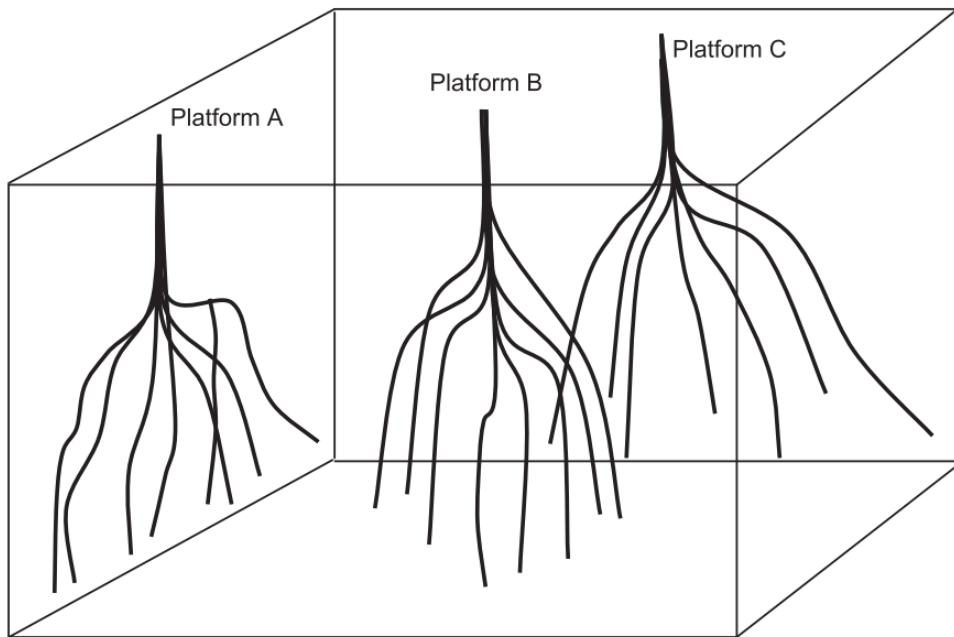
Figure 2.4: Example of a group of wells or Cluster (Mitchell & Miska, 2016).
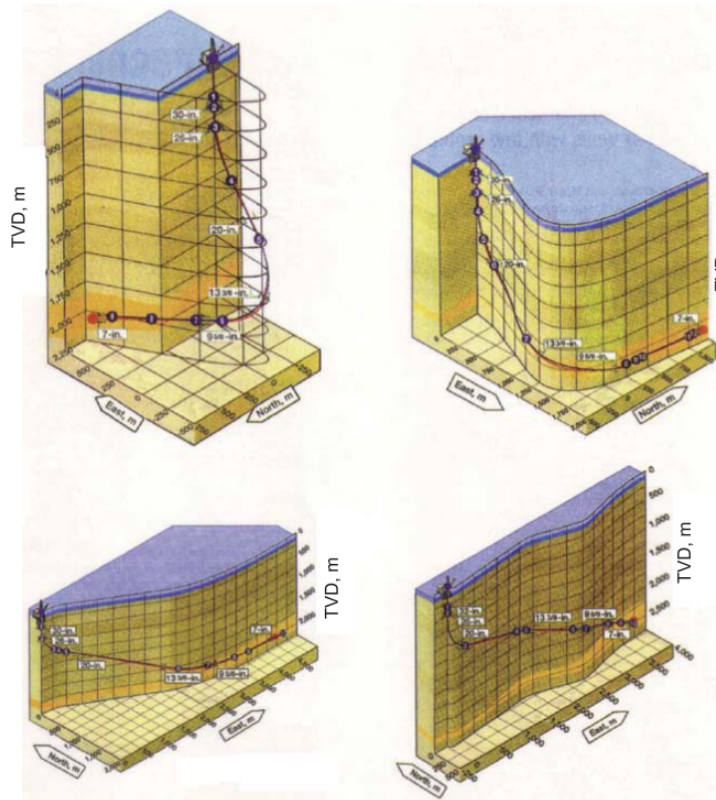
Figure 2.5: Examples of Designer Wells (Mitchell & Miska, 2016).

2.3 Wellbore Positioning Concepts

2.3.1 Magnetic Field

Earth's rotating core produces an enormous magnetic field with the magnetic flux lines coming externally from the South to the North Magnetic Poles. The Earth's geographic poles are located on its spin axis, while the magnetic poles are located around 1000 miles from the geographic poles. The Magnetic Declination is the angular separation between the geographic and magnetic poles.

The lines of the magnetic field flow externally from the South pole to the North pole, and the direction of the lines is called Magnetic North. Also, the flux lines have different "inclinations" depending on where the magnetic field is being measured. Since the lines are coming out of the Earth in the south pole and entering the north pole, they do not always align with Earth's surface horizontal component. The angle between the horizontal component and the flux line at a specific location is called Magnetic Inclination or Magnetic Dip angle. At the equator, the line is aligned with the horizontal component, but on the other hand, at the North or South is almost vertical, with the values being positive and negative, respectively. To fully define the Magnetic Field at any location is necessary to measure the Field Strength, in nano or micro Tesla, the Declination, and the Dip angle vector components.

The magnetic poles are not fixed in a specific position, but it slowly changes with time. Those changes are influenced by magnetic disturbances both inside and outside the Earth's, like solar storms, for example (Baker Hughes, 1998). To keep track of the field movement, the data collected from observatories worldwide are sent to the British Geological Survey institution, where a mathematical model of the Earth's magnetic field in its undisturbed state is developed. This geomagnetic model is called BGGM, and it is the most used model in the industry (Jamieson et al., 2007) to correct the magnetic tool measurements.

The magnetic rock's localized effects in the formation are the big source of errors in the magnetic surveying tool measurements. In order to reduce those errors, the In-Field Referencing (IFR) technique was developed. It measures the field strength, direction (declination), and vertical angle (Dip) in the drilling area's vicinity. Although it is not as standard service as the BGGM, the IFR is increasing in popularity fast since the demand for more accurate measurements is also increasing.

2.3.2 Global Coordinates

The representation of the geographic locations and the Earth's curvature on paper has an important subject to the human being since the beginning of time. As found out later in history, the Earth is not flat, and in fact, only areas of one square mile or less are considered flat (Baker Hughes, 1998). Many coordinate systems were created in order to overcome the issue.

Universal Transverse Mercator

The Universal Transverse Mercator (UTM) is a projection of the surface of an ellipsoidal representation of the Earth wrapped in a cylinder which touches the spheroid along the chosen meridian (Baker Hughes, 1998). The projection forms a map with a rectangular

grid system, with the grid lines heading northward, called Grid North. The Grid North is only identical to the True North at the chosen meridian that touches the cylinder. The angle between the Grid North and True North is called Convergence.
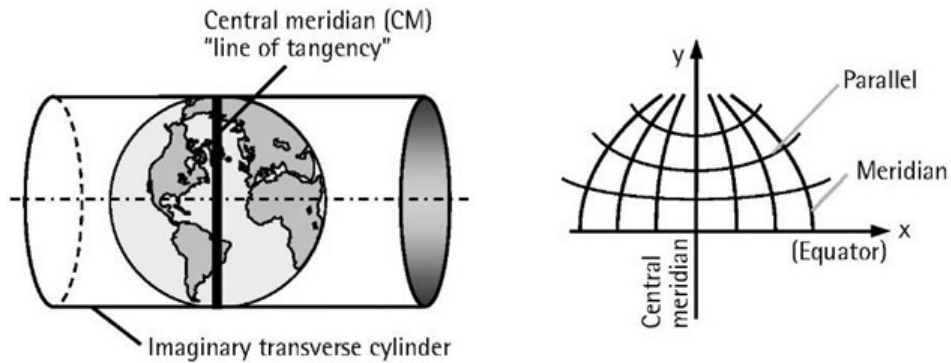
Figure 2.6: The UTM Projection (What-when-how, n.d.).

In this grid system, the world is divided into 60 zones with 6° between each zone. The counting starts from the west and goes toward the east, with zone 31 passing at the longitude 0° (Greenwich). Each zone is divided into sectors starting from the equator and covering 8° latitude going up to 84° North and 80° South. The complete UTM reference for any point is composed of the zone number, the Northing and Easting coordinates of the location.

The Northing is the distance measured in meters from the equator. The equator receives 0 values and measuring a location in the northern hemisphere, and it goes up to 10 000 000 m in the northern part. When measuring a location in the southern hemisphere, the equator receives the value of 10 000 000 m, and it decreases as it goes southward.

The Easting represents the distance in meters from the central meridian of the zone in which it lies (Baker Hughes, 1998). Each zone's central meridian receives a value of 500 000 m, increasing from west to east to avoid negative numbers.
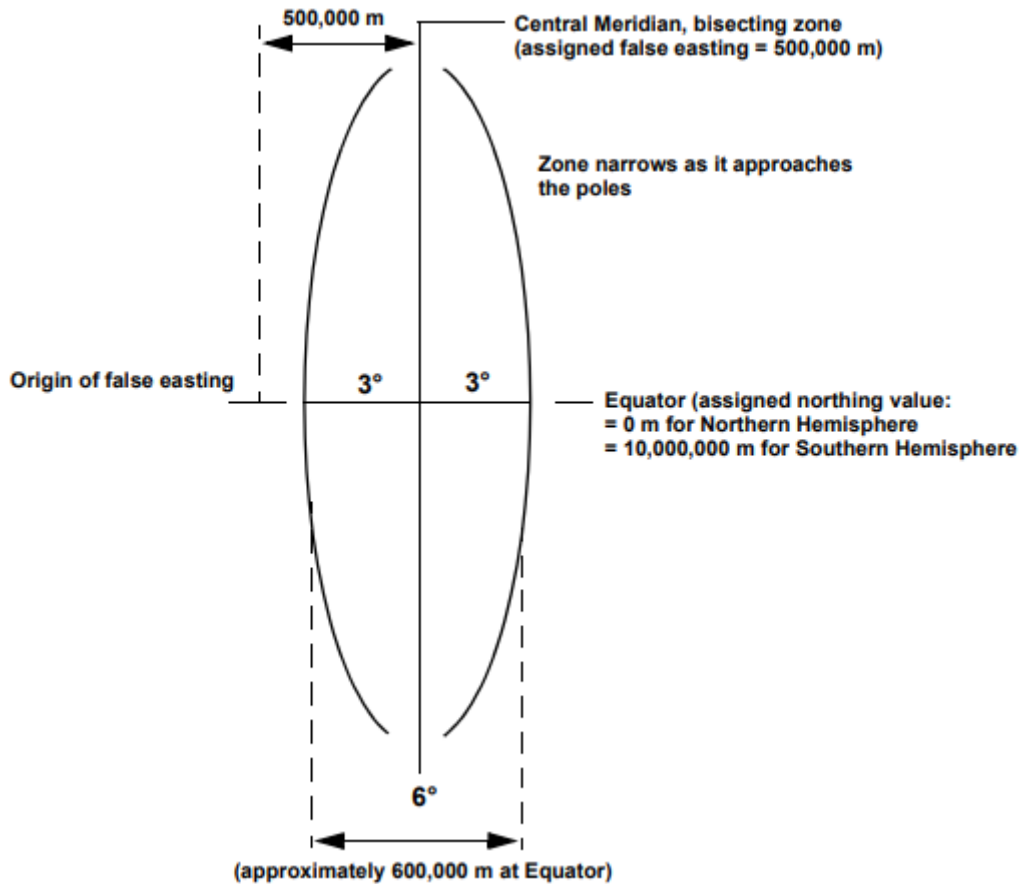
Figure 2.7: The UTM Zone Configuration (Baker Hughes, 1998).

2.3.3 Field Coordinates

The UTM zoning system can also be used to define the location of points on a well path. Those points are known as global coordinates. It is not the normal practice to use global coordinates, and the local field coordinates are used instead. As normally called the Rotary Table, the rig drilling floor is set as the origin point and receives a coordinate of 0 m. The Local Northing, Easting, and Vertical coordinates are calculated as a deviation or separation in meters from this origin point (right-hand reference).

When drilling a well using a Drilling Template, where multiple wells are drilled side by side and separated by a steel frame, the origin coordinate is standard set at the middle slot, and the other slots have a local northing and easting deviation from it. This referencing procedure is important when comparing the well position, especially for anti-collision analysis.

On this thesis, the wellhead of the Reference well was set as the local origin point and the offset wellheads were separated using predetermined distances in meters Northing and Easting from the Reference well. The calculating methods will presented at the section 2.4.3.
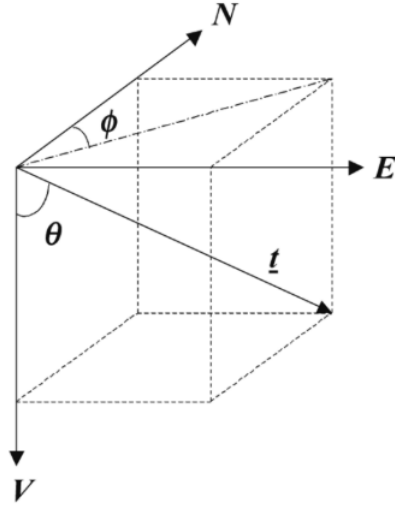
Figure 2.8: The Field Coordinates where t is the Unit Direction Vector. The angle ϕ and θ are the Azimuth and Inclination, respectively (Sawaryn & Thorogood, 2005).

2.3.4   Borehole Coordinates

The borehole coordinates are represented by highside (h), rightside (r_{sid}) and tangent (t) unit vectors of the respective well path point. The combination of those vectors give the direction vector of the well path and equations are (Sawaryn & Thorogood, 2005):

$$h = \begin{bmatrix} \cos I \cos A \\ \cos I \sin A \\ -\sin I \end{bmatrix} \tag{2.1}$$

$$r_{sid} = \begin{bmatrix} -\sin A \\ \cos A \\ 0 \end{bmatrix} \tag{2.2}$$

$$t = \begin{bmatrix} \sin I \cos A \\ \sin I \sin A \\ \cos I \end{bmatrix} \tag{2.3}$$

Where:

h is the unit highside vector of the borehole coordinates

r_{sid} is the unit rightside vector of the borehole coordinates

t is the unit direction vector of the borehole coordinates

12
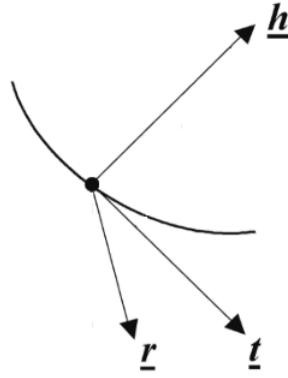
Figure 2.9: The Borehole Coordinates (Sawaryn & Thorogood, 2005).

2.3.5 Magnetic Declination and Grid Convergence

A magnetic surveying tool measures the direction of the borehole in relation to the Magnetic North. The angle between the Magnetic North and the True North is called Magnetic Declination, and it is used to correct from the Magnetic Azimuth to the True Azimuth.

By convention, when the Magnetic North vector is located to the left of the True North vector, it receives the name of West Declination Correction, and it is assigned a negative sign. When the Magnetic North is to the right, the angle receives the name of East Declination Correction, and it is assigned a positive sign.

As already mentioned, the Universal Transverse Mercator (UTM) is a technique that projects the Earth's curved surface onto a flat surface, creating a rectangular grid system. The grid lines going towards the North are called Grid North. In order to convert True North to Grid North, the angle between both vectors needs to be measured. This angle is called Grid Convergence. Analogously to the Magnetic Declination, the angle is called West Convergence Correction when to the left of the True North (negative sign) and East Convergence Correction when to the right (positive sign).

Depending on the company or location regulations, the borehole can be referenced by either True North or Grid North. If the True North is used as the reference north, then only the declination correction is necessary. If the Grid North is the reference North, then a combination of both declination and convergence corrections is necessary. In order to convert the magnetic Azimuth to the grid azimuth, the convergence correction needs to be subtracted from the declination. This correction is called the Grid Correction, and the resultant value is added to the measured magnetic Azimuth.
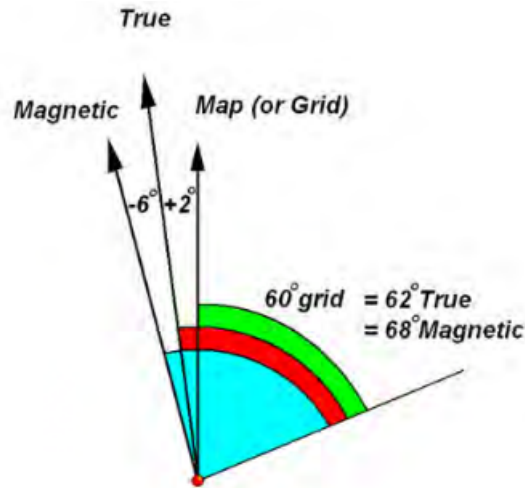
Figure 2.10: The Grid Correction Example (Jamieson et al., 2007).

2.4 Directional Survey

The survey is a measurement of the location at a specific point of the well path taken by sensors placed downhole. There are mainly two types of measurements: magnetic and gyroscopic. After taking, the measurements are corrected and used to calculate the well path's correct location in the local field and global coordinates. The purposes of the directional surveys are (PetroWiki, n.d.):

- Determine the exact location of the wellbore.

- Monitor the directional performance to ensure the target will be reached.

- To orient the deflection tool for well path navigation.

- Monitor the proximity with nearby wells and avoiding a collision.

- To perform a geological mapping of the formation by determining the True Vertical Depth (TVD).

- Monitor the Dogleg Severity of the well path, which is the measure of the change in the inclination and/or direction of the good path.

- Fulfill legal requirements within the regulatory agencies.

2.4.1 Survey Reference

The survey is a measurement of the inclination and Azimuth at a specific depth.

- **Depth References**: The origin point of the depth reference is normally the rig drilling floor, called Rotary Table. There are two types of depths:

  - **Measured Depth (MD)**: is the distance measured along the well path from the surface reference point to the trajectory station. It is usually measured by the total length of the pipe below the rotary table.

  - **Total Vertical Depth (TVD)**: The total vertical distance from the reference

14

or origin depth to the survey point. The combination of the other measurements calculates it.

- **Inclination**: is the angle between the local gravity vector and the direction vector of the wellbore. By convention, 0° inclination is purely vertical, and 90° inclination is horizontal.

- **Azimuth**: The Azimuth is the measurement of the wellbore's direction. There are in total of 3 azimuths.

  - **Magnetic Azimuth**: is the Magnetic North's measurement at a specific location. The magnetic Azimuth is measured by the magnetometer and accelerometer sensors placed inside magnetic surveying tools. Although the magnetic tools measure the magnetic Azimuth, the final wellbore coordinate is converted either to True Azimuth or Grid Azimuth.

  - **True Azimuth**: is the direction of the geographic North, which lies on Earth's rotation axis. The True North is used as the official reference north in certain locations.

  - **Grid Azimuth**: The direction of the grid lines of the projection of the Earth's curved surface into a flat surface. The Grid North is used as the official reference north in certain locations.

2.4.2 Survey Tools

As already mentioned, the directional surveying technique measures the inclination and Azimuth using directional sensors. The sensor's types can be divided into magnetic tools that measure Earth's Magnetic North direction and the gyroscopic tools that use a gyro instrument to measure the angle between the wellbore direction and a reference landmark.

MWD Tools

The Measurement While Drilling (MWD) tools are instruments made of non-magnetic material containing a sensor package that includes three magnetometers and three accelerometers that, together, calculate the Inclination and the Azimuth of the wellbore.

The data is often measured in raw and stored into a hard disk internal to the MWD tool. The data is also transmitted to the surface, commonly using a mud pulse telemetry technology. The data is processed with corrections and conversions applied at the surface, providing the correct survey measurements.

The three accelerometers are mounted orthogonally to each other, with the z-axis often installed along the pipe's body. They measure the strength of Earth's gravitational field along the axis. The data is converted and corrected at the surface, generating the Inclination angle.

The three magnetometers, as the accelerometers, are also mounted orthogonally to each other. They measure the Magnetic North's direction and, together with the accelerometers, are used to calculate the Magnetic Azimuth of the wellbore. The data is then corrected to either True Azimuth or Grid Azimuth, depending on the local or company's policy. The inclination and magnetic azimuth equations are given below:

$$Inc = cos^{-1}(\frac{G_z}{\sqrt{G_x^2 + G_y^2 + G_z^2}}) \tag{2.4}$$

$$Azi_{mag} = tan^{-1}(\frac{(G_x B_y - G_y B_x)\sqrt{G_x^2 + G_y^2 + G_z^2}}{B_z(G_x^2 + G_y^2) - G_z(G_x B_x + G_y B_y)}) \tag{2.5}$$

Where:

G_x, G_y and G_z are the accelerometer measurements in the x, y and z, with the z axis is along the body of the tool.

B_x, B_y and B_z are the magnetometer measurements in the x, y and z, with the z axis is along the body of the tool.
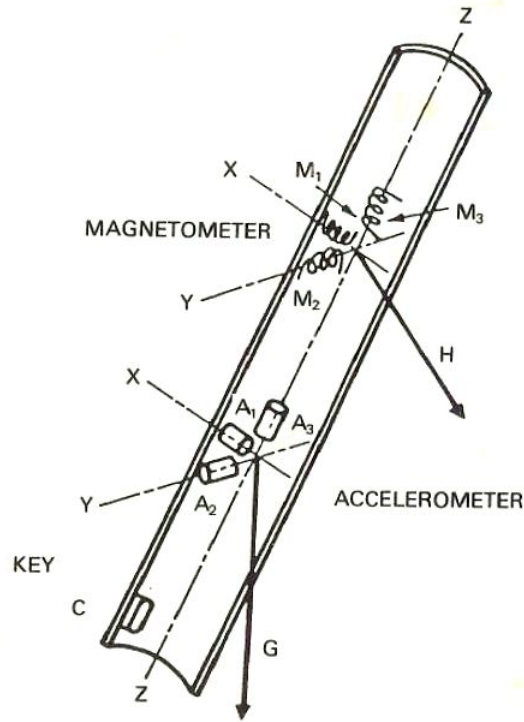
Figure 2.11: Example of the MWD Tools Mounted Orthogonally to Each Other (Choudhary, 2011).

The MWD tools error models and corrections were the only surveying tool considered throughout this thesis. The MWD tools are not free of problems, and the main ones are described below.

1. **Magnetic Interference**
   One of the issues of magnetic technology is magnetic interference. The magnetic measurements are affected by nearby magnetic fields, and the MWD tools are not free of the problem. The total magnetic force acting on the MWD tool will be the vector sum of all magnetic fields created by all sources of magnetism in the area (Baker Hughes, 1998). The Azimuth calculated by the tool will no longer represent the accurate Magnetic North direction. There are many causes of magnetic interference:

- **Drill String Magnetization**: with most components made of metal, the drill string can become permanent or induced magnetized when moved or rotated downhole. In order the reduce the effects of this source of magnetic field, a non-magnetic collar needs to be placed before and after the magnetometers to isolate the sensors from the interference.

- **Nearby Metal Structures and Downhole Junk**: the magnetic interference can be induced by nearby metal structures, like the rig (shallow depths) and casing from close by cased wells. Another source of interference is the abandoned junk material downhole, like old drill strings, etc.

- **Magnetic Solar Storms**: the sun is constantly sending magnetic shock waves (solar winds) that cause temporary disturbance on Earth's magnetic field. From time to time, the magnetic waves are strong enough to affect the magnetic measurements of the MWD sensors downhole. Once the strength of the storm is known, it can be post-effect corrected by specialized software. This type of magnetic interference is quite often in high latitude regions (i.e., Norway).

2. **Azimuth Error**
The MWD tools respond to the local magnetic field's horizontal component, which can be affected by the drill string magnetization along the tool's body. This situation affects the east and west component of the field, and it increases with the inclination and proximity to 90° (east) and 270° azimuths. The maximum error is at 90° or 270° Azimuth with 90° of inclination.

Gyroscopic Tools

The Gyroscope Survey tool is a device that measures the direction of the wellbore by using a spinning gyro, operating on the principle of the conservation of the angular momentum. There mainly four types of Gyroscopic tools: Free Gyro, Rate or North Seeking Gyro, Ring Laser Gyro, and Inertial Grade Gyro (Ajetunmobi, 2012).

Since it does not use magnetic sensors, it is not affected by magnetic interferences as the MWD tools, and it is often used in areas where the MWD measurements are not suitable due to high magnetic interference (i.e., Casing Proximity). It can be set to measure either the True or Grid North directly.

This survey tool and its error models were not taken into consideration for building the position uncertainty model in this work.

2.4.3   Survey Calculation Methods

The Directional Survey is a measure of the inclination and azimuth of the wellbore at certain measured depth. In order to define the location of the survey point in space, it is necessary to calculate the point into NEV coordinate system (Figure 2.8). The location of a point on a 3D curve representing the center line of a well path can be determined by a position vector $\vec{p}(s)$ that is function of the distance measure along the curve from the origin (s).

$$\vec{p}(s) = \begin{bmatrix} N \\ E \\ V \end{bmatrix} = N(s)\vec{i} + E(s)\vec{j} + V(s)\vec{k} \qquad (2.6)$$

Where:

N, E and V are the North, East and Vertical coordinate components of the position vector $\vec{p}$.

$\vec{i}, \vec{j}$ and $\vec{k}$ are unit vectors in the x, y and z direction, respectively.

The unit directional vector $\vec{t}(s)$ of the survey point can be calculated by the inclination and azimuth measured by the accelerometer and magnetometer sensors. The equation of the unit vector $\vec{t}(s)$ is:

$$\vec{t}(s) = \frac{d\vec{p}(s)}{ds} = (\sin I \cos A)\vec{i} + (\sin I \sin A)\vec{j} + (\cos I)\vec{k} \tag{2.7}$$

Where:

I is the Inclination at survey station.

A is the Azimuth at the survey station.

s is the distance measure along the curve from the origin.

It is also important to determine the wellbore curvature. The curvature is the second derivative of position vector $\vec{p}(s)$ and equal to the multiplication between the radius of curvature $\kappa(s)$ and the unit normal vector $\vec{n}$ of the survey point.

$$\vec{K}(s) = \frac{d^2\vec{p}}{ds^2} = \frac{d^2 N(s)}{ds^2}\vec{i} + \frac{d^2 E(s)}{ds^2}\vec{j} + \frac{d^2 V(s)}{ds^2}\vec{k} = \kappa(s)\vec{n} \tag{2.8}$$

Where:

$\vec{K}$ is the wellbore curvature vector.

κ is the magnitude of the wellbore curvature.

$\vec{n}$ is the vector normal to point $\vec{p}$.

The κ is the magnitude of the wellbore curvature which is often expressed in 1/m or 1/ft. It provides information about the rate of overall change in the angle due to simultaneous changes in hole inclination and azimuth along the well path (Mitchell & Miska, 2016). From calculus, the curvature of a 3D curve in NEV coordinates can be expressed as:

$$\kappa(s) = \sqrt{\left(\frac{d^2 N}{ds^2}\right)^2 + \left(\frac{d^2 E}{ds^2}\right)^2 + \left(\frac{d^2 V}{ds^2}\right)^2} \tag{2.9}$$
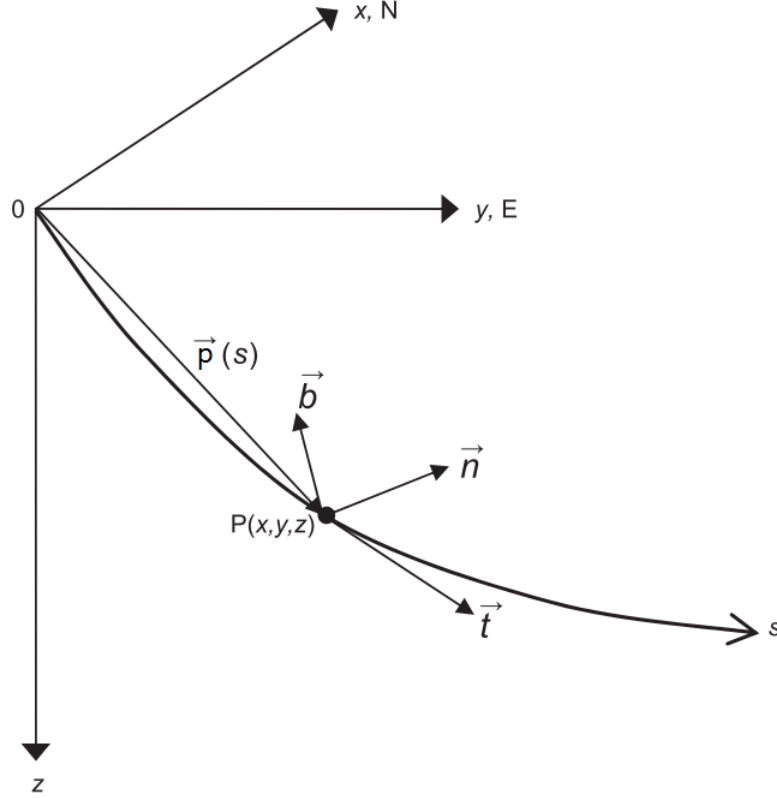
Figure 2.12: A Segment of a Well Path with Arbitrary point P at the Distance $\vec{p}$ from the origin (Mitchell & Miska, 2016).

As described by Mitchell and Miska (2016), the wellbore curvature is the rate of change of the overall angle along the trajectory. Therefore the overall angle change β (Dogleg) (in radian) between two neighboring points on the trajectory located Δs apart can be obtained by integrating the curvature along the trajectory:

$$\beta = \int_0^{\Delta s} \kappa(s)\, ds \qquad (2.10)$$

Where:

β is the dogleg in radian between two points along the well path.

Also, the angle β can be defined as the angle between two points on the well trajectory. To put it in simple terms, the β is the angle between the two unit direction vectors of each arbitrary points. So, β (in radian) can be found by the equation:

$$\beta = \arccos(\vec{t_1} \cdot \vec{t_2}) = \arccos\left[\sin I_1 \sin I_2 \cos(A_1 - A_2) + \cos I_1 \cos I_2\right] \qquad (2.11)$$

The Dogleg can also be calculated using Lubinski's equation, which is independent of the survey calculation methods presented next. Lubinski's dogleg equation was used to the dogleg severity throughout this thesis.

19

$$\beta = 2 \arcsin \sqrt{\sin^2 \left(\frac{I_2 - I_1}{2} \right) + \sin I_1 \sin I_2 \sin^2 \left(\frac{A_2 - A_1}{2} \right)} \qquad (2.12)$$

In the daily directional drilling, the rate of change in angle is used more often than the Dogleg β and it is expressed in °/30 m or °/100 ft. The rate of change is called Dogleg Severity and it can be found by the equation:

$$\text{DLS} = \frac{180}{\pi} \beta f \ , \quad \text{for } f = 30 \text{ m or } f = 100 \text{ ft} \qquad (2.13)$$

There many different methods for calculating the directional survey, with the most common ones are the Tangential, Average Angle, Balanced Tangential, Radius of Curvature, and Minimum Curvature Methods.

Tangential Method

This method assumes the trajectory between two surveys is a tangent. It only takes into consideration the next survey position when calculating the NEV coordinates. When calculating the Tangential method, it is the least accurate of the methods, and because of that is not recommended to be used.

$$\vec{p_2} = \vec{p_1} + \vec{t_2} \Delta s \ , \quad \text{where } \Delta s = \text{MD}_2 - \text{MD}_1 \qquad (2.14)$$

Averaged Angle Method

The Averaged Angle method assumes each course length is a tangent, consequentially, assumes the inclination and azimuth angles over a course length Δs are constant and equal to the average value of the respective angles for both trajectory stations.

$$\vec{p_2} = \vec{p_1} + (\vec{t_{av}}) \Delta s \ , \quad \text{where} \quad \begin{cases} t_{av} = \begin{bmatrix} \sin \overline{I} \cos \overline{A} \\ \sin \overline{I} \sin \overline{A} \\ \cos \overline{I} \end{bmatrix} \\ \overline{I} = \dfrac{I_1 + I_2}{2} \\ \overline{A} = \dfrac{A_1 + A_2}{2} \end{cases} \qquad (2.15)$$

The method produces a similar output as the Tangential Method, but it has a few pitfalls, especially when the angles are close to 0 and 2π or when the well is close to vertical where the azimuths are undefined (Mitchell & Miska, 2016). As the Tangential, this method is not considered to be accurate enough and should be avoided.

Balanced Tangential Method

The Balance Tangential Method assumes that two straight segments of equal lengths can determine the actual well path. The method is similar to the Tangential method, but

it considers both trajectory stations, averaging both values. It is more accurate than the Tangential and Averaged angle producing similar results as the Minimum Curvature Method.

$$\vec{p_2} = \vec{p_1} + \frac{\vec{t_1} + \vec{t_2}}{2}\Delta s \tag{2.16}$$

Radius of Curvature Method

The Radius of Curvature Method is more accurate than the other three methods presented so far. It assumes the wellbore course is a 3D curve with a spherical arc passing through both upper and lower trajectory stations. If the rate of change in inclination can be defined by the build rate B and the rate of change in the horizontal component defined by horizontal turn H, the equations for both rates of change are (Mitchell & Miska, 2016):

$$B = \frac{dI}{ds} \tag{2.17}$$

$$H = \frac{1}{sinI}\frac{dA}{ds} \tag{2.18}$$

Where:

B is the rate of change in inclination, also known as build rate.

H is the rate of change in the horizontal component, also known as horizontal turn rate.

As defined by Mitchell and Miska (2016) the Radius of Curvature method considers that both B and H are constants. With that in mind, the equations for each NEV coordinate can be found by:

$$
\begin{aligned}
N_2 &= N_1 + \frac{1}{H}\int_{A_1}^{A_2} \cos A \, dA = N_1 + \frac{\sin A_2 - \sin A_1}{H} \\
E_2 &= E_1 + \frac{1}{H}\int_{A_1}^{A_2} \sin A \, dA = E_1 + \frac{\cos A_1 - \cos A_2}{H} \\
V_2 &= V_1 + \frac{1}{B}\int_{I_1}^{I_2} \cos I \, dI = E_1 + \frac{\cos I_2 - \cos I_1}{B}
\end{aligned}
\tag{2.19}
$$

One of the issues with this method is that even if the Build and Horizontal rates are constant, the wellbore curvature should not be constant between the two stations because the inclination varies between stations (Mitchell & Miska, 2016).

Minimum Curvature Method

Like the Radius of Curvature Method, the Minimum Curvature Method assumes that the trajectory is a smooth 3D curve over the surface of a sphere with the two trajectory stations located in the same plane. The method uses the same equations as in the Balanced

21

Tangential Method with the two vector points smoothed onto the wellbore curve by using a ratio factor defined by the curvature (Dogleg) of the wellbore (Mitchell & Miska, 2016). It results in more accurate calculations and therefore is the most adopted method in well planning. Sawaryn and Thorogood (2005) defined the equations for calculating the $\vec{p}$ as:

$$\vec{p_2} = \vec{p_1} + \frac{\Delta s}{2} f(\beta)(\vec{t_1} + \vec{t_2}) \ , \tag{2.20}$$

Where

$$f(\beta) = \frac{\tan\left(\frac{\beta}{2}\right)}{\frac{\beta}{2}} \ , \text{ for } \quad \beta \geq 0.02$$

$$f(\beta) \approx 1 + \frac{\beta^2}{12}\{1 + \frac{\beta^2}{10}[1 + \frac{\beta^2}{168}(1 + \frac{31\beta^2}{18})]\} \ , \text{ for } \quad \beta < 0.02$$

Where:

$f(\beta)$ is a function of dogleg severity.

β is the dogleg in radian between two points along the well path.
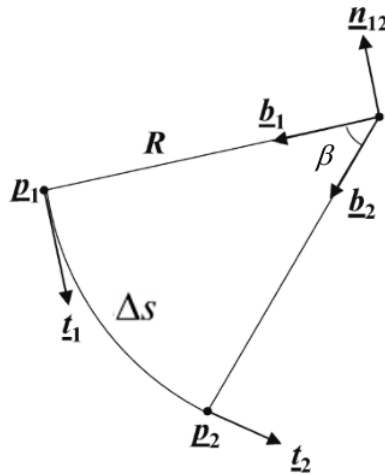
Figure 2.13: The Geometry of the Minimum Curvature Between Two Adjacent Survey Points (Sawaryn & Thorogood, 2005).

Chapter 3

The Error Model

3.1 Introduction

All systems that rely on taking measurements are susceptible to errors and uncertainties. The Well Construction subject is no different, and the survey measurements are not a 100% accurate. Determining how accurate a survey measurement is an important subject, especially for Anti-Collision Analysis and Target Sizing (Jamieson et al., 2007). Many factors can contribute to this situation, and an error model needs to be defined to determine the position uncertainty of the well path at a specific depth.

There is no *de facto* industry-standard error model, and it is desirable to apply a consistent and predictable set. Through the years, many different models were presented, and Walstrom et al. (1969) was one of the first to introduce the concept of an ellipse of uncertainty to describe the position uncertainty. This ellipse was calculated using only the random error model in which the size was smaller than it really was (Wolff et al., 1981).

In 1981, the error model from Wolff et al. (1981) was presented. It used a systematic error model and not compensating for the random error type. The errors were added in a linear summation making the error uncertainty bigger than the one presented by Walstrom (Muhammadali, 2017). The model presented by Wolff et al. (1981) was the first to be extensively used by many different companies worldwide.

Later, The Industry Steering Committee on Wellbore Survey Accuracy (ISCWSA), also known as the SPE Wellbore Positioning Technical Section (WPTS), developed an error model based on the works from Williamson (2000) for the Measurement While Drilling (MWD) surveying tool, the article presented by Torkildsen et al. (2008), where it describes the position accuracy for the Gyroscopic surveying tools, and finally, by Brooks and Wilson (2005) work, where the depth uncertainties were quantified. The model developed by ISCWSA suffered many revisions through the years and combined different types of error to quantify the position uncertainty. This model was the model selected and implemented in this thesis.

The model has its limitations, requiring that survey tool be rigorously calibrated, with a maximum of 30 m. (or 100 ft.) interval between surveys. The model also assumes that the measurements B_t (Total Magnetic Field), G_t (Total Gravity Field), Dip (Magnetic Inclination) and gyro drifts suffered a rigorous quality check on every survey, and the

taking surveys in a clean magnetic environment without human errors, which the model cannot handle.

As already mentioned, ISCWSA's model describes the different physical phenomena contributing to the borehole uncertainty. Those phenomena are called Error Sources, and they vary with the type of the Surveying Tool selected. Although the model provided the error sources for both MWD and Gyroscopic tools, this thesis concentrates its attention on the MWD errors only.

Each error source identified has its error magnitude, which is the standard deviation of the error determined by the tests conducted, and a set of weighting functions that mathematically describe how the errors affect the survey measurements (ISCWSA, 2017a). Finally, each error source has a propagation mode that will determine how those errors will be accumulated or combined over depth. An Ellipsoid of Uncertainty can statistically and geometrically describe the accumulation of the uncertainty for a particular survey point since it is a 3-dimensional problem.

3.2 MWD Error Sources

For each surveying tool, a set of error sources needs to be identified. The surveying tools described by the ISCWSA model are the MWD and Gyroscopic tools, but in this work, only the MWD tool errors will be considered. The list of error sources provided by ISCWSA is considered a basic set. In the real world, the companies' different tools developed through the years will have their own set of errors that need to be described by its providers in detail to define the position uncertainty model with the necessary accuracy.

Examples of error sources are misalignment of the survey tool about the center of the borehole, sensor errors after calibrating the tool, the pipe's stretch in the hole when applying weight to the string, and many others. The full list of the error sources provided by ISCWSA and implemented in this work can be check in the Appendix A.

3.2.1 Error Magnitude and Weighting Functions

The Error Magnitudes are defined as the standard deviation (1-σ) of a survey data under normal operating conditions. The magnitude can be drastically reduced if the In-Field Referencing (IFR) measurements are used to determine the magnetic field in the area instead of the standard BGGM model (Jamieson et al., 2007). The full list of error magnitudes can be checked in the table A.1 in Appendix A.

The Weighting Functions of each error source is a mathematical description of how that particular error affects the survey Measured Depth, Inclination and Azimuth. When a survey is taken, the Magnetic Azimuth and the Inclination are calculated using the equations (2.5) and (2.4).

$$Inc = cos^{-1}(\frac{G_z}{\sqrt{G_x^2 + G_y^2 + G_z^2}}) \qquad (2.4)$$

$$Azi_{mag} = tan^{-1}(\frac{(G_x B_y - G_y B_x)\sqrt{G_x^2 + G_y^2 + G_z^2}}{B_z(G_x^2 + G_y^2) - G_z(G_x B_x + G_y B_y)}) \qquad (2.5)$$

The Weighting Functions are then derived by taking the partial derivatives from those equations concerning the error source (Jamieson et al., 2007). When the well path is vertical, certain error sources do not behave the same way, and their weighting functions have to reflect those changes. Those error sources are known as Singular, and another set of weighting functions are used in this case. The full list of weighting functions and singularities provided by ISCWSA can be check in the table A.2 in the Appendix A.

3.2.2 Types of Error and Propagation Mode

The Errors can be classified as three different basic types (Muhammadali, 2017): Random, Systematic, and Gross. The type of error determines how the errors will be accumulated along the well path, and it is of great importance to understand the nature of each error listed.

- **Random**: The Random errors as the namesake occur irregularly. These can happen due to random and difficult to predict fluctuations in the experimental or operational conditions. Thus, it is imperative to take many samples as possible to reduce its effects on the measurements. The contribution of the error sources is statistically independent, with values being positive or negative errors.

- **Systematic**: The Systematic type is the error that consistently deviates the measurements from its actual value. It is expected from an error source of this type to have a predictable deviation from survey station to survey station. An example of the systematic error source is the SAG error, which defines the directional sensor's misalignment in relation to the borehole axis, which is predictable and quantifiable.

- **Gross**: The Gross error is caused by human mistake or equipment failure. Examples of errors are wrong pipe tally, the wrong insert of values into the surface system. The ISCWSA model does not take into consideration the Gross Errors.

Each error source has a Propagation Mode that defines how errors are correlated from survey station to survey station or well to well within a field, and consequentially how those errors will be accumulated (Jamieson et al., 2007). Due to its nature, it can be positive or negative for the Random errors creating a canceling effect. In order to consider those errors, their contributions must be Root-of-Sum-of-Squares (RSS) together. The Systematic error, on the other hand, can be accumulated with a simple linear summation.

3.3 Evaluation of Position Uncertainty

Once the all error sources are identified and its effects on each of the survey parameters (MD, Inc and Azi) are defined, the position uncertainty can be evaluated. The equation used to evaluate was given by Jamieson et al. (2007) and it is defined as:

$$e_{i,k} = \sigma_i \left(\frac{d\Delta r_k}{dp_k} + \frac{d\Delta r_{k+1}}{dp_k} \right) \frac{\partial p_k}{\partial \varepsilon_i} \qquad (3.1)$$

where:

$e_{i,k}$ is error size due to i^{th} error source at the kth survey station. It's a (3×1) matrix in the NEV coordinates.

σ_i is the magnitude of the ith error.

$\frac{\partial p_k}{\partial \varepsilon_i}$ is the weighting funtion (3×1) matrix of the ith error source

$\frac{d\Delta r_k}{dp_k}$ is the effect of the errors in the survey measurements (MD, Inc and Azi) at the survey position from $(k-1)$ to k. It is (3×3) matrix in the NEV coordinates.

$\frac{d\Delta r_{k+1}}{dp_k}$ is the effect of the errors in the survey measurements (MD, Inc and Azi) at the survey position from k to $(k+1)$. It is (3×3) matrix in the NEV coordinates.

As standard procedure, the wellbore coordinates in NEV are usually calculated by using the minimum curvature method, which was described in the section 2.4.3. In order to simplify the equations for $\frac{d\Delta r_k}{dp_k}$ and $\frac{d\Delta r_k}{dp_{k+1}}$, the balanced tangential method, described in the section 2.4.3, was used to calculate the terms in NEV coordinates without a significant loss of accuracy in the uncertainty results (Jamieson et al., 2007).

The term $\frac{d\Delta r_k}{dp_k}$ can be calculated as:

$$\frac{d\Delta r_k}{dp_k} = \frac{1}{2}\begin{bmatrix} \sin(I_{k-1})\cos(A_{k-1}) + \sin(I_k)\cos(A_k) & (\text{MD}_k - \text{MD}_{k-1})\cos(I_k)\cos(A_k & -(\text{MD}_k - \text{MD}_{k-1})\sin(I_k)\sin(A_k) \\ \sin(I_{k-1})\sin(A_{k-1}) + \sin(I_k)\sin(A_k) & (\text{MD}_k - \text{MD}_{k-1})\cos(I_k)\sin(A_k & (\text{MD}_k - \text{MD}_{k-1})\sin(I_k)\cos(A_k) \\ \cos(I_{k-1}) + \cos(I_k) & -(\text{MD}_k - \text{MD}_{k-1})\sin(I_k) & 0 \end{bmatrix} \quad (3.2)$$

and the term $\frac{d\Delta r_{k+1}}{dp_k}$ can be calculated by the equation:

$$\frac{d\Delta r_{k+1}}{dp_k} = \frac{1}{2}\begin{bmatrix} -\sin(I_k)\cos(A_k) - \sin(I_{k+1})cos(A_{k+1}) & (\text{MD}_{k+1} - \text{MD}_k)cos(I_k)\cos(A_k & -(\text{MD}_{k+1} - \text{MD}_k)\sin(I_k)\sin(A_k) \\ -\sin(I_k)sin(A_k) - \sin(I_{k+1})\sin(A_{k+1}) & (\text{MD}_{k+1} - \text{MD}_k)\cos(I_k)\sin(A_k & (\text{MD}_{k+1} - \text{MD}_k)\sin(I_k)\cos(A_k) \\ -\cos(I_k) - \cos(I_{k+1}) & -(\text{MD}_{k+1} - \text{MD}_k)\sin(I_k) & 0 \end{bmatrix} \quad (3.3)$$

Where:

MD is the Measured Depth

I is the Inclination

A is the Azimuth

The error sizes e is then calculated for all survey stations by adding the error in the survey measurements for a given station k to the error at survey station $k-1$ that precedes it and to the error at the survey station $k+1$ that follows it. When the last survey station is reached, adding the error in the survey measurements at station k to the next station $k+1$ is not possible and the error size e equation is reduced to:

$$e_{i,k}^* = \sigma_i \frac{d\Delta r_k}{dp_k} \frac{\partial p_k}{\partial \varepsilon_i} \quad (3.4)$$

3.3.1 Regular and Singular Weighting Functions

As already mentioned, the weighting functions are mathematical expressions that describe how the specific error source affects each of the survey measurements. The weighting functions $\frac{\partial p_k}{\partial \varepsilon_i}$ are a (3×1) matrix in NEV axes that is used to calculate the error size e in the expressions (3.1) and (3.4).

$$\frac{\partial p_k}{\partial \varepsilon_i} = \begin{bmatrix} \frac{\partial \text{MD}_i}{\partial \varepsilon_i} \\ \frac{\partial \text{Inc}_i}{\partial \varepsilon_i} \\ \frac{\partial \text{Azi}_i}{\partial \varepsilon_i} \end{bmatrix} \tag{3.5}$$

However, when the well path is vertical, the behavior of the error source changes. Those error sources that behave differently are called Singular, and their Weighting Functions will change when the inclination of the well path is close to zero. The expression for calculating the error size will also changed, with the terms $(\frac{d\Delta r_k}{dp_k} + \frac{d\Delta r_{k+1}}{dp_k})$ and $\frac{d\Delta r_k}{dp_k}$ being reduced to $\frac{(\text{MD}_{k+1} - \text{MD}_{k-1})}{2}$ and $\frac{(\text{MD}_k - \text{MD}_{k-1})}{2}$, respectively. The new expressions for e and $e*$ are:

$$e_{i,k} = \sigma_i \frac{(\text{MD}_{k+1} - \text{MD}_{k-1})}{2} \left(\frac{\partial p_k}{\partial \varepsilon_i} \right)_{sing} \tag{3.6}$$

$$e_{i,k}^* = \sigma_i \frac{(\text{MD}_k - \text{MD}_{k-1})}{2} \left(\frac{\partial p_k}{\partial \varepsilon_i} \right)_{sing} \tag{3.7}$$

The full list of weighting functions and singular error sources can be found in the table A.2 and A.3 in the Appendix A.

3.4 Propagation of the Error and the Covariance Matrix

After calculating each error source's contributions, the error sizes need to be accumulated or added together. Knowing how the errors are related to each other at each survey station is extremely important and will help define their propagation mode.

In case the propagation mode of a particular error is random, meaning the error source is statistically independent of the other error sources, the values can take the negative or positive form. When those terms are added together, a canceling effect can reduce the contribution of those errors in the total error. The Root-of-Sum-of-Squares (RSS) method is more appropriated than a linear summation to mitigate the situation.

$$e_{total} = \sqrt{e_1^2 + e_2^2} \tag{3.8}$$

If the error has a systematic propagation mode, the errors between stations correlate to each other, and the canceling effect is not observed. In this case, the direct linear summation can be performed to find the total error e_{total}.

$$e_{total} = e_1 + e_2 \tag{3.9}$$

The variance of a set of data is defined as the measure of the variation or spread of the data, and its mathematical definition is the square of the standard deviation $\text{Var}(X) = \sigma^2(x)$ (Johnson, 2017). If the total error e_{total} can be defined as the standard deviation of the position in NEV axes, the variance of position error is e_{total}^2. When squaring the equations (3.8) and (3.9) the respective resultant equations are:

$$e_{total}^2 = e_1^2 + e_2^2 \tag{3.10}$$

$$e_{total}^2 = (e_1 + e_2)^2 \tag{3.11}$$

For the generalized summation of two or more errors and taking in consideration to the fact that the error sizes e are (3×1) vectors in NEV axes, the variance e_{total}^2 is can be found by the vector relation $e_i e_i^T$. Respectively, the equations (3.10) and (3.11) become:

$$E_{total} = \sum e_{i,k} \sum e_{i,k}^T = \sum e_{i,k} e_{i,k}^T \tag{3.12}$$

Where:

E_{total} is the (3×3) variance-covariance matrix with the diagonal values equal to the variance e_{total}^2.

$e_{i,k}$ is the (3×1) error size vector of the ith error source at the kth survey station.

$e_{i,k}^T$ is the (1×3) transposed vector of $e_{i,k}$.

The Covariance Matrix, also known as Variance-Covariance Matrix, is a symmetric and positive semi-definite matrix that expresses patterns of variability and covariation across the set of data for two or more variables (Cattell, 1988). The diagonal terms of the matrix are the variance $\text{Var}(X) = \sigma^2(x)$ and the non-diagonal terms are the covariance $\text{Cov}(X,Y)$. Covariance is a measure of the direction and strength of the association of two or more variables/data sets.

$$COV = \begin{bmatrix} \sigma_x^2 & Cov(x,y) & Cov(x,z) \\ Cov(x,y) & \sigma_y^2 & Cov(y,z) \\ Cov(x,z) & Cov(y,z) & \sigma_z^2 \end{bmatrix} \tag{3.13}$$

When considering the error model until now described, it is necessary to considered the summations of both Random and Systematic errors for each error source and each survey station. The overall summation of all those terms that defines the covariance matrix as mentioned by Jamieson et al. (2007) is:

$$COV_k^{survey} = \sum COV_{i,k}^{rand} + \sum COV_{i,k}^{sys} \tag{3.14}$$

Where the contribution of the random errors are given by the equation:

$$COV_{i,k}^{rand} = \sum_{k=1}^{K-1} (e_{i,k})(e_{i,k})^T + (e_{i,k}^*)(e_{i,k}^*)^T \tag{3.15}$$

And the contribution of the systematic errors are:

$$COV_{i,k}^{syst} = (\sum_{k=1}^{K} e_{i,k} + e_{i,k}^*)(\sum_{k=1}^{K} e_{i,k} + e_{i,k}^*)^T \tag{3.16}$$

The final Covariance Matrix for the kth survey station is a (3×3) matrix in the NEV axes given by the equation (ISCWSA, 2017a):

$$COV_{NEV,k} = \begin{bmatrix} \sigma_N^2 & Cov(N,E) & Cov(N,V) \\ Cov(N,E) & \sigma_E^2 & Cov(E,V) \\ Cov(N,V) & Cov(E,V) & \sigma_V^2 \end{bmatrix} \tag{3.17}$$

3.5   Scaling Factor k and Confidence Level

The scaling factor k can be found by the inverse cumulative distribution function of the chi-square distribution with a specified degree of freedom, for a certain probability. The chi-square (χ^2) distribution is obtained from the values of the ratio of the sample variance and population variance multiplied by the degrees of freedom. This occurs when the population is normally distributed with population variance σ^2 (Jones, n.d.). As already mentioned, the scaling factor selected was $k = 3.058$, that gives a confidence level of 97.5%. The factor shall be used to define the size of the Ellipsoid and Cylinder of Uncertainty principal axes.

Table 3.1: The Cumulative Distribution of the Chi-Square Distribution for Different Degrees of Freedom.

| degrees | Confidence Level | | | | | |
| | Standard Deviation | | | | | |
of freedom	±1	±2	±2.878	±3	±3.058	±3.5
1	68.27%	95.45%	99.60%	99.73%	99.78%	99.95%
2	39.35%	86.47%	98.41%	98.89%	99.07%	99.78%
3	19.87%	73.85%	95.95%	97.07%	97.50%	99.34%

Table 3.2: The Inverse Cumulative Distribution Function of the Chi-Square Distribution for Different Degrees of Freedom.

degrees of freedom	Scaling Factor k					
	Confidence Level					
	68.27%	90.00%	95.95%	97.07%	97.50%	99.34%
1	1.0000	1.6449	2.0486	2.1794	2.2414	2.7164
2	1.5152	2.1460	2.5324	2.6571	2.7162	3.1688
3	1.8780	2.5003	2.8781	3.0000	3.0575	3.4988

3.6   Ellipsoid of Uncertainty

The Covariance Matrix can be described graphically as an ellipsoid at a particular survey station (ISCWSA, 2017a). The diagonal components of the matrix σ_N^2, σ_E^2 and σ_V^2 are the variances in the North, East and Vertical axis, respectively. The other Cov terms describe the rotation of the ellipsoid for each principle axes. The general quadratic equation of an Ellipsoid is (Wikipedia, n.d.):

$$E = \{x | (x - c)^T A (x - c) = 1\} \tag{3.18}$$

where:

x is a vector representing the $[x, y, z]$ coordinate system.

c is the center of the ellipsoid.

A is a positive definite matrix.

As defined by its quadratic equation (3.18), the eigenvectors of A define the rotation of the principal axes of the ellipsoid. The principal axes radii are defined as the inverse of the square roots of eigenvalues of A (Friendly et al., 2011), $1/\sqrt{\lambda_i}$ for $i = 1, 2$ and 3. For a positive definite matrix A, the eigenvectors of A and A^{-1} are equal while the eigenvalues of A^{-1} are $\frac{1}{\lambda_i}$. Analogously, the the principal axis radii of a Ellipsoid for A^{-1} is $\sqrt{\lambda_i}$.

Since the Covariance Matrix is a positive semi-definite matrix which presents the same eigenvectors and eigenvalues properties as a positive semi-definite matrix described above, and assuming the positional error is a normal distribution, an Statistical Ellipsoid centered at c can be expressed by the equation (Friendly et al., 2011):

$$E = \{r | (r - c)^T COV^{-1} (r - c) = k^2\} \tag{3.19}$$

where:

COV^{-1} is the inverse of the Covariance Matrix.

r is a vector representing the NEV coordinate system.

k is the dimensionless scaling factor that represents the confidence level of the uncertainty.

c is the center of the ellipsoid at the survey station.

Taken the definition above, the principal radii size of the statistical ellipsoid for COV_{NEV}^{-1}, centered at the point in space c is $R_i = k\sqrt{\lambda_i}$, where k is dimensionless scaling factor defined by the degrees of freedom and the confidence level of the uncertainty data. Also, the rotation of the Ellipsoid of Uncertainty is defined by the eigenvectors of COV_{NEV}^{-1}. Below an example of an Ellipsoid calculated by the Covariance Matrix of the positional uncertainty.
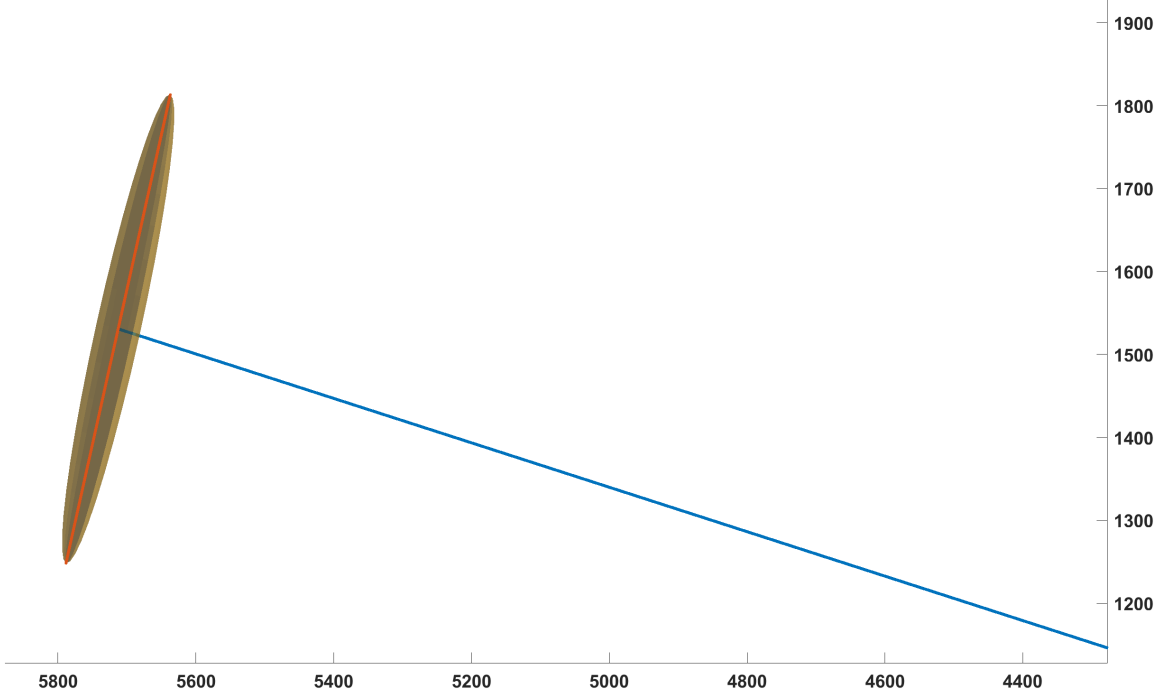
Figure 3.1: An example of ellipsoid of uncertainty

3.7 Twisted Elliptic Cylinder of Uncertainty

A series of ellipsoids of uncertainty along the well path with the center at the survey stations can form a surface that envelops the ellipsoids. The resultant surface is a twisted elliptic cylinder with principal radii size and posture defined by the rotation and the ellipsoids' principal radii size. This surface is very complicated with a 3D twisted curve and an elliptic cross-section, making it very hard to describe it mathematically.

In the works from Liu (2019), the equations to find the cylinder were defined. If the cross-section of the Twisted Elliptic Cylinder of Uncertainty (TECoU) represented by an ellipse can be found, the twisted cylinder surface can be found as well. The transformation matrix B, that transforms between the NEV coordinating system to $[x, y, z]$ coordinating system, can be used to define the ellipsoid, then the new equation becomes:

$$\sum_{i=1}^{3} \left(\frac{\vec{B}_i \vec{x}}{R_i} \right)^2 = 1, \quad \text{where:} \quad \begin{cases} \vec{B}_i & = [B_{i,1}, B_{i,2}, B_{i,3}] \\ \vec{x} & = [x, y, z] \\ R_i & = k\sqrt{\lambda_i} \end{cases} \tag{3.20}$$

The transformation matrix B can be found from the relation between the eigenvector of COV_{NEV} and the transformation matrix T, which transforms the ellipsoid from the $[x, y, z]$ coordinating system to NEV coordinating system.

$$B = H^T T, \qquad (3.21)$$

Where:

B is the transformation matrix of COV_{NEV} that transforms between the NEV coordinating system to $[x, y, z]$ coordinating system.

H is the Eigenvectors of COV_{NEV}.

T is the transformation matrix that transforms from the $[x, y, z]$ coordinating system to NEV coordinating system.

The equation that defines the transformation matrix T is:

$$T = \begin{pmatrix} \cos(I)\cos(A) & -\sin(A) & \sin(I)\cos(A) \\ \cos(I)\sin(A) & \cos(A) & \sin(I)\sin(A) \\ -\sin(I) & 0 & \cos(I) \end{pmatrix} \qquad (3.22)$$

Where:

I is the Inclination at survey station.

A is the Azimuth at the survey station.

s is the distance measure along the curve from the origin.

As pointed by Liu (2019), the projection curve equation of the tangent curve between the elliptic cylinder surface and the ellipsoid on the plane xy is:

$$\begin{bmatrix} x \\ y \end{bmatrix}^T F \begin{bmatrix} x \\ y \end{bmatrix} = 1 \qquad (3.23)$$

Where F is a (2×2) matrix with its terms defined as:

$$F_{1,1} = \sum_{i=1}^{3} \left(\frac{D_{i,1}}{R_i} \right)^2, \quad F_{1,2} = F_{2,1} = \sum_{i=1}^{3} \left(\frac{D_{i,1} D_{i,2}}{R_i} \right), \quad F_{2,2} = \sum_{i=1}^{3} \left(\frac{D_{i,2}}{R_i} \right)^2$$

Where the term $D_{i,j}$ are defined as:

$$D_{i,j} = B_{i,j} - B_{i,3} C_j, \text{ for } \begin{cases} i = 1, 2, 3 \\ j = 1, 2 \end{cases}$$

and C_j:

$$C_1 = \frac{\sum_{i=1}^{3} \frac{B_{i,1}B_{i,3}}{R_i^2}}{\sum_{i=1}^{3} \left(\frac{B_{i,3}}{R_i}\right)^2}, \quad C_2 = \frac{\sum_{i=1}^{3} \frac{B_{i,2}B_{i,3}}{R_i^2}}{\sum_{i=1}^{3} \left(\frac{B_{i,3}}{R_i}\right)^2}$$

If the matrix $G = F^{-1}$, as mentioned by Liu (2019) the radius of the principal axes and the rotation angle of the cross section ellipse of the error elliptic cylinder, which are similar to the ellipses of uncertainty principal axes equations are:

$$R_{cyl,1} = \sqrt{G_{1,1}\cos^2\theta + G_{1,2}\sin 2\theta + G_{2,2}\sin^2\theta}$$
$$R_{cyl,2} = \sqrt{G_{1,1}\sin^2\theta - G_{1,2}\sin 2\theta + G_{2,2}\cos^2\theta} \tag{3.24}$$
$$\theta = \frac{1}{2}\tan^{-1}\left(\frac{2G_{1,2}}{G_{1,1} - G_{2,2}}\right)$$

Below an example of the Twisted Elliptic Cylinder of Uncertainty (TECoU) derived by the equations above.
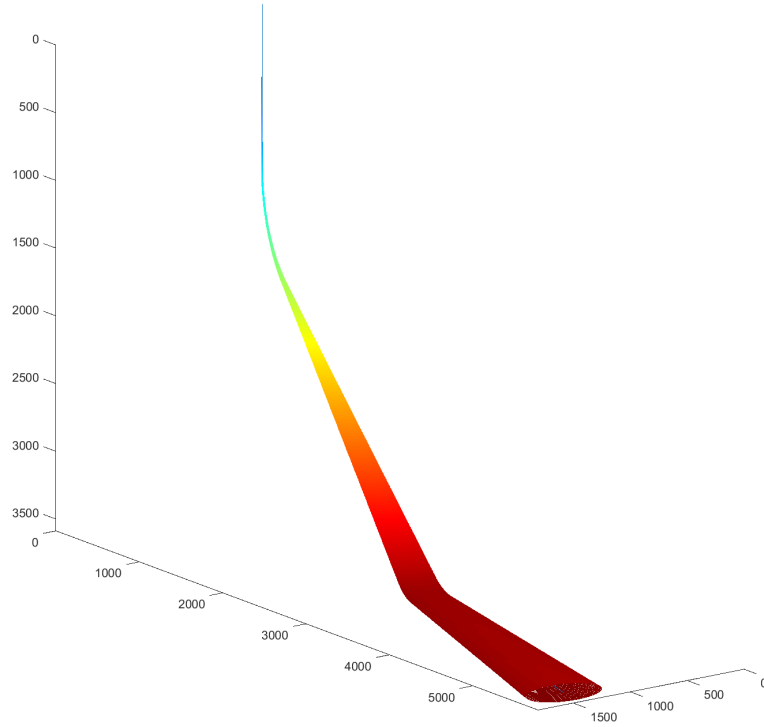
Figure 3.2: An example of a cylinder plotted using the Liu (2019) method.

The cylinder surface was found using the basic elliptic cylinder parametric equations:

$$\begin{aligned} x &= R_{cyl,2}cos\phi \\ y &= R_{cyl,1}sin\phi, \quad \text{where} \quad \begin{cases} \phi \in [0, 2\pi] \\ v \in [0, \Delta\text{MD}], \text{ for a very small } \Delta\text{MD} \end{cases} \\ z &= v \end{aligned} \tag{3.25}$$

The Elliptic Cylinder surface is found for the $[x, y, z]$ coordinate system. To change the coordinating system to NEV coordinate system, the transformation matrix T needs to be multiplied to $[x, y, z]$ cylinder coordinates. The new parametric equations of the TECoU are:

$$
\begin{aligned}
N &= Tx \\
E &= Ty \\
V &= Tz
\end{aligned}
\tag{3.26}
$$

Chapter 4

Anti-Collision

4.1 Anti-Collision Analysis

In congested fields (i.e., Troll Field), a collision between two wells can be a severe problem, especially if those wellbores are oil producers. New discoveries are also in areas that were not viable economically until a few years ago, increasing the importance of extending and improving the production by increasing the number of available slots without the expense of significant additions to infrastructure (Poedjono et al., 2009). For those reasons, an accurate anti-collision analysis must be performed.

The anti-collision analysis identifies the position of a planned well path in relation to other nearby wells. It determines if the same wellbore can be drilled safely without colliding with others. The anti-collision plan starts by determining the accurate position of all wellbores in the area and ends with plans for drilling paths for future wells (Rocha et al., 2011).

Many different companies have currently created their anti-collision analysis or process, making the standardization very difficult. There are also mathematical and computational difficulties due to the nature of the 3D problem of the anti-collision analysis, making it harder to apply the available solutions. The thorny issue requires a simple representation that all the drilling process actors can understand and use (Sawaryn et al., 2018). The Industry Steering Committee on Wellbore Survey Accuracy (ISCWSA), also known as SPE Wellbore Positioning Technical Section (WPTS), was created not only to address the use and accuracy of the directional instruments but also the issues related to anti-collision, well interception, and industry education. They have been working through the years to promote the standardization of the anti-collision analysis since then.

This work implements the WPTS recommended procedures and equations and tries to bring an Twisted Elliptic Cylinder of Uncertainty as an alternative method to calculate the safety factor and compare the results the traditional Ellipsoid of Uncertainty.

4.2 Scanning Methods

Several scanning methods were presented in the past few years. The most common and widely used methods are the Traveling Cylinder (Normal Plane method), the Horizontal Plane method, and the Minimum Curvature (Closest 3D Approach method).

As mentioned by Mansouri et al. (2020), the output from the proximity or scanning analysis involve four key measurements:

- Center to Center Distance (C-C) distance

- The Directional Uncertainty Distance σ_D

- The Separation Factor

- The Minimum Allowable Separation Distance (MASD)

The C-C distance is the distance between a measured point (survey point) in the reference well to a point in a specific Offset well nearby. The distance will have different outputs depending on the selected scanning method.

Finding the directional uncertainty distance, σ_D, will also be impacted by the scanning method selected since it is calculated by the distance between the geometry representation of the position uncertain. As already mentioned in the chapter 3, the position uncertainty is represented by an Ellipsoid of Uncertainty. In this work, the Twisted Elliptic Cylinder of Uncertainty will be presented as an alternative to the ellipsoid.

4.2.1 Traveling Cylinder

The Traveling Cylinder Method was introduced to the industry a long time ago by Thorogood et al. (1990), and it is still widely used. The method is a graphic representation of the well separation in the form of a diagram that helps the Directional Drillers to identify the potential collision risks. It consists of an orthogonal circular plane around the well path and checks for nearby offset wells that intersects the plane, as in a radar.
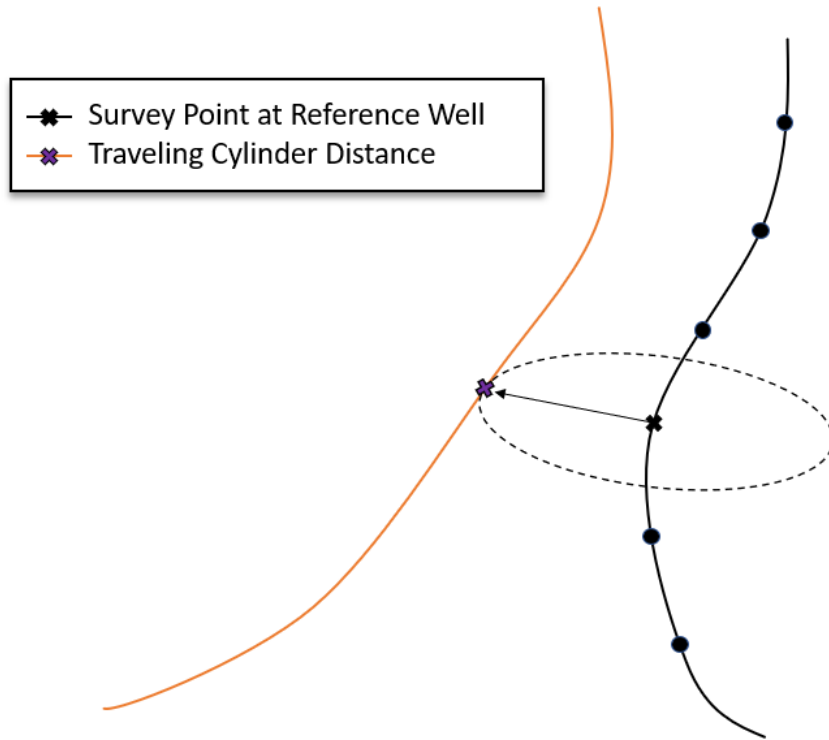
Figure 4.1: Example of Traveling Cylinder Scanning Method.
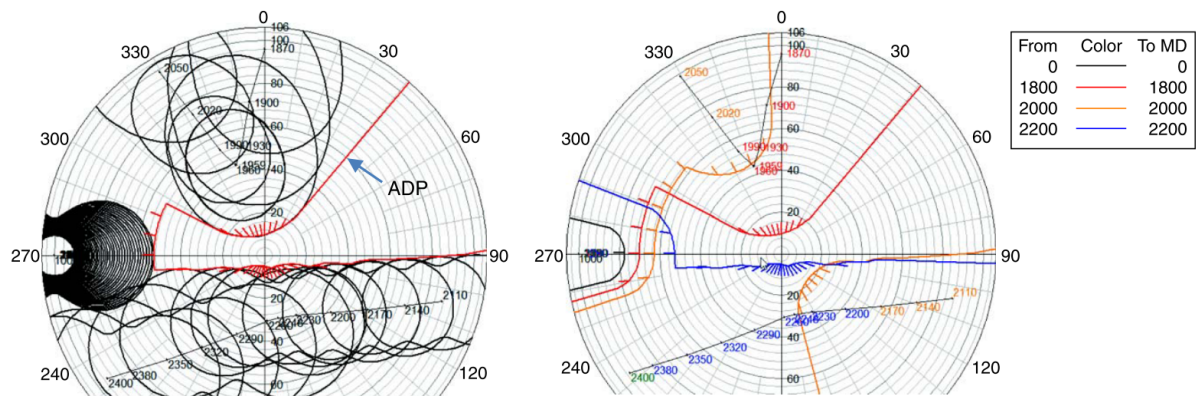
Figure 4.2: Example of the Traveling Cylinder Diagram (Sawaryn et al., 2019)

The method is a simple and straightforward way to represent the relative positions and rates of convergence of other wells with respect to the plan under consideration (Thorogood et al., 1990). However, it also has limitations being more effective if the offset wells under investigation are close to parallel regarding the reference well. It is not recommended to be used in situations where the offset well is near-orthogonal or end-to-end approach (Sawaryn et al., 2018), and it will not always find the closest distance in those situations. The Traveling Cylinder is not being considered in this thesis.

4.2.2 Horizontal Distance

The Horizontal Plane Scanning method is a simple method that finds the closest distance between the reference and offset well in the horizontal or orthogonal plane in relation to the TVD, independent of both wells' well paths. It is the least used method, and it has similar limitations as in the Traveling Cylinder scanning method. The Horizontal Plane scanning method is not being considered in this thesis.
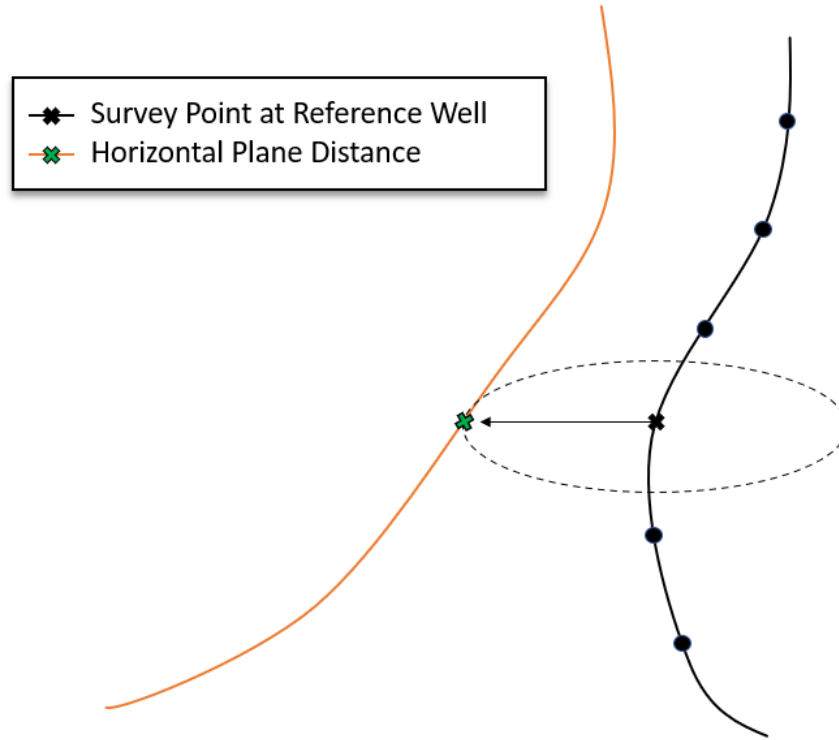
Figure 4.3: Example of Horizontal Plane Scanning Method.

4.2.3 Minimum Distance (Closest 3D Approach)

The Minimum Distance or Closest 3D Approach Scanning Method is the most conservative of all three methods. If a sphere with its origin at the survey point in the reference well start to expand until it touches the offset well, the minimum distance would be the sphere's radius (Figure 4.4).
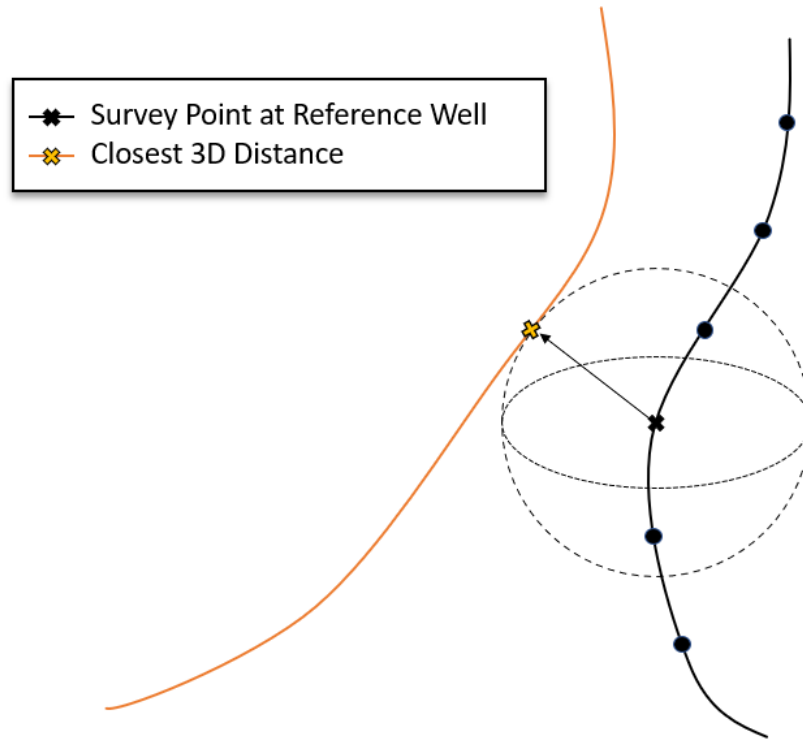
Figure 4.4: Example of Minimum Distance Scanning Method.

This method will always locate in the offset well the closest tridimensional point to the reference well regardless of the relative position between wells. When comparing the minimum distance method to the other two presented, it will also find the shortest distance for any given scenario. Figure 4.5 shows a comparison between all three methods.

It is recommended to use side by side the Traveling Cylinder Diagram and analysis together with the 3D closest distance to give a different and more accurate perspective to the user. It is also recommended to use the Minimum Distance as the scanning method to calculate the C-C in the definitive anti-collision report (Jamieson et al., 2007). This thesis uses the Minimum Distance to calculate the C-C distance and the Directional Uncertainty Distance, which are used to determine the separation factors.
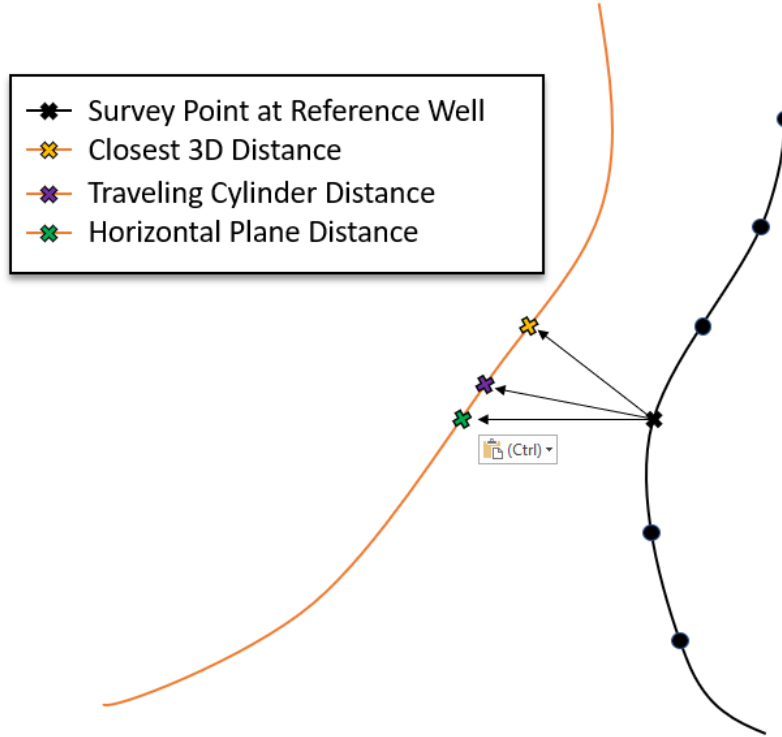
Figure 4.5: A Comparison Between the Different Scanning Methods.

4.3 Directional Uncertainty Calculation Methods

The Directional Uncertainty σ_D acts along the vector $\vec{r}$ (C-C vector) that connects the point in the reference well and the point found by the selected scanning method in the offset well (C-C line). The value can be found by combining the two individual directional uncertainties along $\vec{r}$ of each point 1 (reference well) and 2 (offset well), $\sigma_1(r)$ and $\sigma_2(r)$, respectively.

There are a few always to calculate those individual uncertainties, $\sigma_1(r)$ and $\sigma_2(r)$. In the paper from Bang et al. (2020), the Pedal-Curve Radius, the Ellipsoid Radius, and method that combines both covariance matrices from the reference and offset well were presented. The methods of adding up those uncertainties to find σ_D were also presented: The Linear Summation and the Root-of-Sum-of-Squares (RSS) method.

Since the safety factors used in this work are heavily dependent on finding the correct term σ_D, it is crucial the determine the most accurate procedure to calculate it. As mentioned by Bang et al. (2020), the correct way to calculate the term is by calculating the individual uncertainties by using the Pedal-Curve Method and combining them by using the Root-of-Sum-of-Squares (RSS). These methods described before will compare the two first and most used methods, the Pedal Radius, and the Surface-vector methods.

Combining both covariance matrices produces the same results as the Pedal-Curve or Ellipsoid Radius methods. It will be presented in more detail when mentioning the Separation Factor equation from Equinor in section 4.4.

4.3.1 Pedal-Curve Radius Method

The Pedal Radius is defined as the orthogonal intersection between the C-C line and a line tangent to the ellipsoid. It can also be referred to as the ellipsoid's projected dimension onto the C-C line. Although it is the default method for most well-planning software (ISCWSA, 2013), it is also the most conservative option for calculating the safety factor.
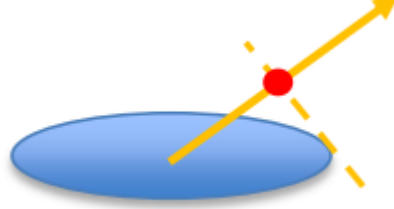
Figure 4.6: The pedal curve represented by the intersection of the dashed tangential to the ellipsoid line to the C-C line (Bang & Nyrnes, 2015)

.

The method for calculating the pedal curve radius was presented by Bang et al. (2020) and root squared of the multiplication between the covariance matrix and the unit tangent vector of $\vec{r}$. The $\sigma_1(r)$ and $\sigma_2(r)$ are the individual directional uncertainties for the Reference and the Offset well, respectively. The $\sigma_j(r)$ terms calculated from equation (4.1) are for 1σ (1 standard deviation). They are used to calculate the Directional Uncertainty σ_D of the Separation Factor equation.

$$\sigma_j(r) = \sqrt{u_{r,j}^T (COV_{NEV,j}) u_{r,j}} \quad , \quad \text{where} \quad \begin{cases} \text{for } j = 1, 2 \\ u_{r,1} = \dfrac{\vec{p}_{min} - \vec{p}_0}{||(\vec{p}_{min} - \vec{p}_0)||} \\ u_{r,2} = \dfrac{\vec{p}_0 - \vec{p}_{min}}{||(\vec{p}_0 - \vec{p}_{min})||} \end{cases} \quad (4.1)$$

Where:

$COV_{NEV,j}$ is the covariance matrix of the specific point in the Reference or Offset well.

$\vec{u}_{r,j}$ is the unit tangent vector of $\vec{r}$, with a direction from reference to the offset well if $j = 1$ and with a direction from the offset point to the reference well if $j = 2$.

$\vec{p}_0$ is the survey point in the Reference wellbore.

$\vec{p}_{min}$ is the closest point to $\vec{p}_0$ in the Offset well.

In this thesis, the Pedal Radius was also calculated manually by finding the projection of the ellipsoid onto the C-C line. For a given vector $\vec{r} = \vec{p}_0 + t\vec{v}$ (4.2) that defines C-C line from a survey point, $\vec{p}_0$, in the reference well, to a point, $\vec{p}_{min}$, in the offset well, there is a plane that is orthogonal to and intersects $\vec{r}$ at the point $\vec{r}_{ped}$. The plane is tangent to the ellipsoid at the point $\vec{p}_a$. This point $\vec{r}_{ped}$ is given by the coefficient $t = t_{max}$ from the equation (4.3), which is the maximum t coefficient that satisfies the condition.

$$\vec{r} = \vec{p}_0 + t\vec{v}, \quad \text{where} \quad \{\vec{v} = (\vec{p}_{min} - \vec{p}_0) \tag{4.2}$$

Where:

$\vec{v}$ is the directional vector of $\vec{r}$ from the vector $\vec{p}_0$ to $\vec{p}_{min}$.

$\vec{p}_0$ is the survey point in the Reference wellbore.

$\vec{p}_{min}$ is the closest point to $\vec{p}_0$ in the reference well.

t is the vector coefficient where $0 \leq t \leq 1$

Numerically, the pedal curve radius can be find as the maximum value of $t = t_{max}$ where:

$$t_{max} = \frac{\vec{v} \cdot (\vec{p}_a - \vec{p}_0)}{||\vec{v}||^2} \tag{4.3}$$

Where:

t_{max} is the maximum coefficient of $\vec{r}$ that satisfies the condition for finding $\vec{r}_{ped}$. It generates the vector point $\vec{r}_{ped} = \vec{p}_0 + t_{max}\vec{v}$, and it is perpendicular to a plane that contains $\vec{r}_{ped}$ and $\vec{p}_a$ with a normal $\vec{v}$

$\vec{v}$ is the direction of $\vec{r}$

$\vec{p}_a$ is a point in the ellipsoid that is touched by the plane.

The pedal curve radius of the ellipsoid for both Reference and Offset well is given, respectively, by the equations:

$$\sigma_1(r) = ||\vec{r}_{ped,1} - \vec{p}_0|| \tag{4.4}$$
$$\sigma_2(r) = ||\vec{r}_{ped,2} - \vec{p}_{min}|| \tag{4.5}$$

For the numerically calculated pedal radius, the terms $\sigma_1(r)$ and $\sigma_2(r)$ already consider the scaling factor k in the final values.

4.3.2 Surface-Vector Method

The Surface-Vector Method calculates the individual directional uncertainties $\sigma_1(r)$ and $\sigma_2(r)$ from the respective points in the reference and offset well to the point where the C-C line intersects the surface of the geometric representation of the position uncertainty. The basic geometrical representation of the uncertainty in the 3D environment, as already mentioned, is the ellipsoid. Also, the Twisted Elliptic Cylinder is presented in this work as an alternative geometrical representation. For each of those surfaces, there are different methodologies to find the directional uncertainty distances.
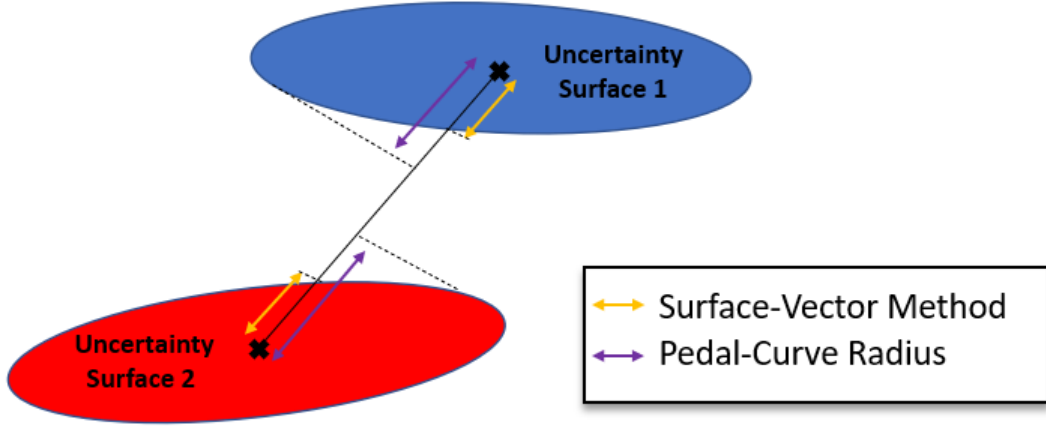
Figure 4.7: A Example of the Surface-Vector Method and a Comparison with the Pedal-Curve Radius Method.

Ellipsoid Radius

The Ellipsoid Radius method is the radius of the ellipsoid along the C-C line or the distance from the point the well path to the point in the Ellipsoid Surface where the C-C line intersects it. It underestimates the uncertainty for some relative orientation of the ellipsoids. Because of it, the Ellipsoid Radius is not currently implemented in any commercial application.

The equation (4.6) for finding the directional uncertainties $\sigma_1(r)$ and $\sigma_2(r)$ was presented by Bang et al. (2020). Since the Ellipsoid Radius and the Cylinder Surface Radius share some similarities, the Ellipsoid Radius was used to compare and investigate the differences between both methods.

$$\sigma_j(r) = \frac{1}{\sqrt{u_{r,j}^T (COV_{(NEV,j)}^{-1}) u_{r,j}}} \quad , \quad \text{where} \quad \begin{cases} \text{for } j = 1, 2 \\ u_{r,1} = \dfrac{\vec{p}_{min} - \vec{p}_0}{||(\vec{p}_{min} - \vec{p}_0)||} \\ u_{r,2} = \dfrac{\vec{p}_0 - \vec{p}_{min}}{||(\vec{p}_0 - \vec{p}_{min})||} \end{cases} \quad (4.6)$$

Cylinder Surface Radius

The Cylinder Surface Radius is defined as the line along the C-C that connects the well path to the point where the C-C line intersects the surface of the cylinder. The Twisted Elliptic Cylinder was described by Liu (2019), and the detailed calculation method can be found in section 3.7.

The surface of the Twisted Elliptic Cylinder of Uncertainty is a very intricate surface, where the size of its principal radii and the posture are changing with the MD. Because of that, it was decided to find the point on $\vec{r}$ that "touches" the surface of the cylinder

numerically. This point that touches the Cylinder Surface is called $\vec{p_c}$ and it is given by the equation:

$$\vec{p_c} = p_0 + t_c\vec{v}, \quad \text{where} \quad \{\vec{v} = \vec{p}_{min} - \vec{p_0} \tag{4.7}$$

And,

t_c is a scalar coefficient of the line $\vec{r}$ that gives the cylinder radius for $t = t_c \in [0, 1]$

$\vec{v}$ is the directional vector of the C-C vector $\vec{r}$.

The directional vector $\vec{v_c}$ of any given line with the origin at $\vec{p_0}$ and it goes to a point at the surface of the cylinder $\vec{p_s}$ is given by the equation:

$$\vec{v_c} = \vec{p_s} - \vec{p_0} \tag{4.8}$$

Where:

$\vec{v_c}$ is the directional vector of any given line with the origin at $\vec{p_0}$ and going to a point at the cylinder surface $\vec{p_s}$.

$\vec{p_0}$ is a point in the well path.

$\vec{p_s}$ is a point at the surface of the cylinder.

The point that the C-C vector line intersects the surface of the cylinder $\vec{p_c}$ is found when the unit directional vector of $\vec{v_c}$, $\vec{u_c}$ is equal to the unit directional vector of C-C vector line $\vec{r}$, $\vec{u}$. From the definition of the dot product between two vectors $\vec{a} \cdot \vec{b} = ||\vec{a}||||\vec{b}|| \cos\theta$, where θ is the angle between the vectors $\vec{a}$ and $\vec{b}$, it can be also defined that dot product of a $\vec{a}$ for itself is $\vec{a} \cdot \vec{a} = ||\vec{a}||^2$ since the angle θ between itself is 0°. If $\vec{u_c} = \vec{u}$ is safe to assume that the angle between these two vectors is 0°. The point $\vec{p_s}$ will be equal to $\vec{p_c}$ only if the condition below is met:

$$\cos 0° = \frac{\vec{u_c} \cdot \vec{u}}{||\vec{u_c}||||\vec{u}||} \quad \rightarrow \quad \cos^{-1}(\vec{u_c} \cdot \vec{u}) \approx 0, \quad \text{where} \quad \begin{cases} \vec{u_c} = \dfrac{\vec{v_c}}{||\vec{v_c}||} \\ \vec{u} = \dfrac{\vec{v}}{||\vec{v}||} \end{cases} \tag{4.9}$$

The Cylinder Surface Radius for both Reference and Offset well is given, respectively, by the equations:

$$\sigma_1(r) = ||\vec{p}_{c,1} - p_0|| \tag{4.10}$$
$$\sigma_2(r) = ||\vec{p}_{c,2} - p_{min}|| \tag{4.11}$$

For the numerically calculated pedal radius, the terms $\sigma_1(r)$ and $\sigma_2(r)$ already consider the scaling factor k in the final values. The Figure below shows a comparison between the pedal radius, the ellipsoid radius, and the cylinder surface radius methods.
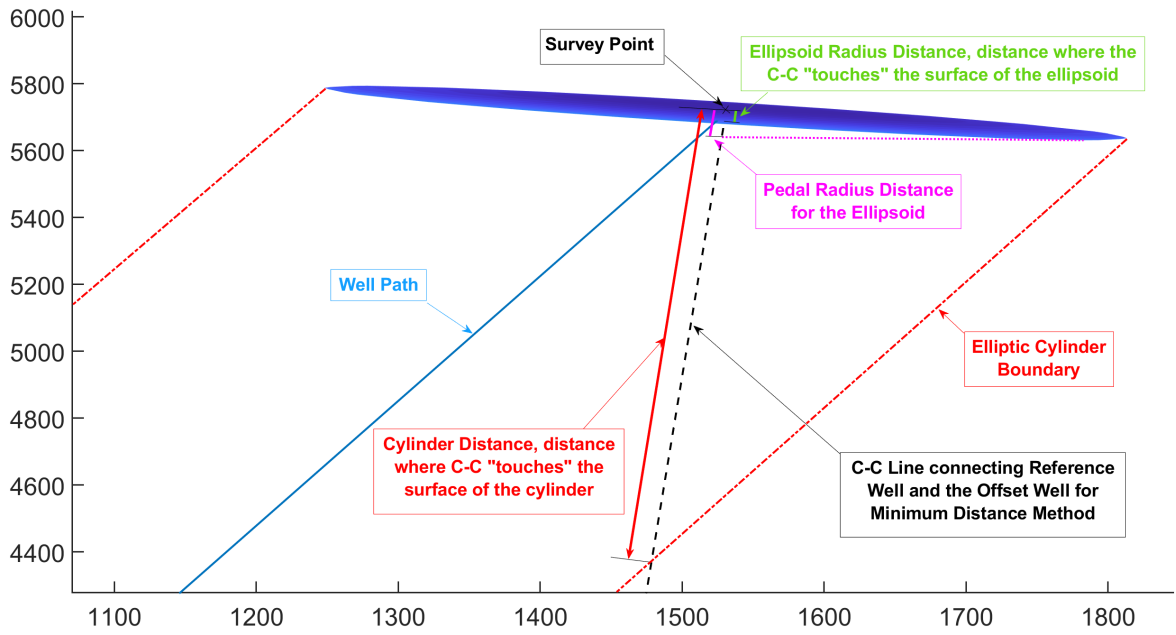
Figure 4.8: Comparison between the Ellipsoid Radius distance, Pedal Radius Distance and the Cylinder Distance.
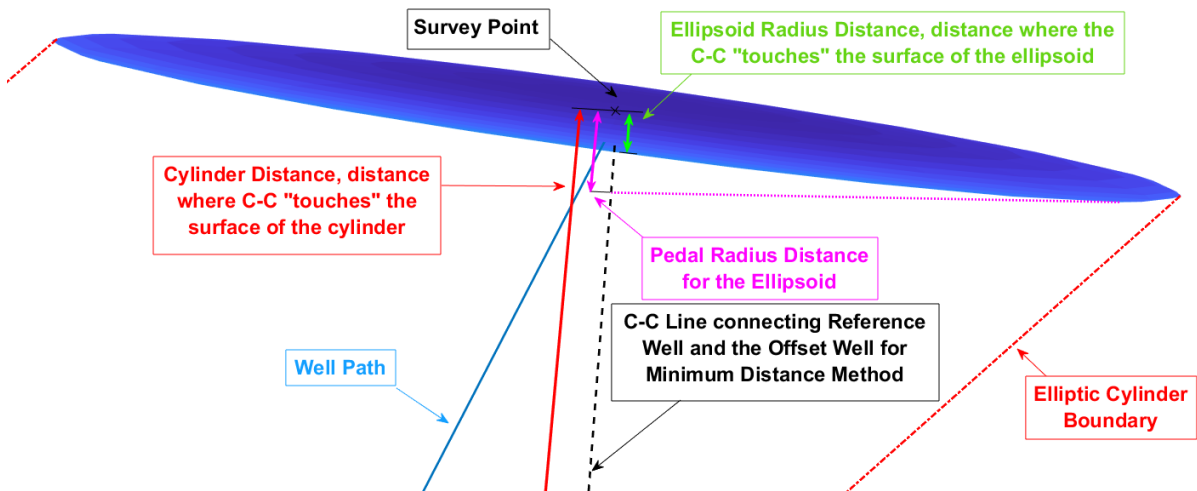
Figure 4.9: A Zoom View of the Figure 4.8 showing the comparision between the Ellipsoid Radius distance, Pedal Radius Distance and the Cylinder Distance.

4.3.3 Scalar Expansion Method

The Scalar Expansion Method calculates the amount of contraction or expansion is necessary for both ellipsoids of uncertainty to touch each other. This scalar factor produces by this method is the separation factor, and it outputs similar results than the other two basic methods without being too optimistic or pessimistic (Jamieson et al., 2007). The method was not used in this thesis.
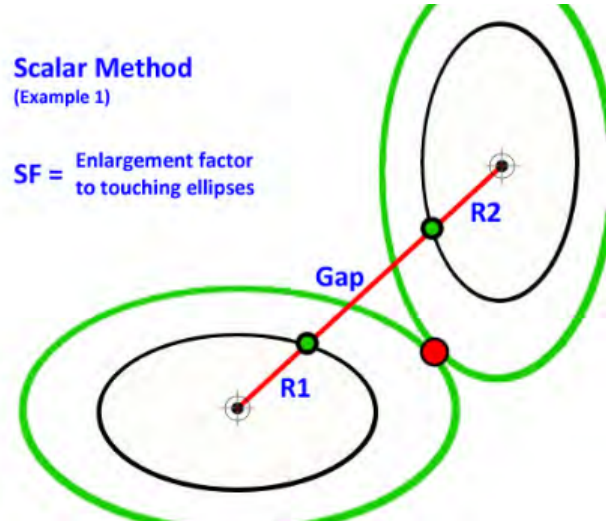
Figure 4.10: A illustration of the Scalar Expansion Method from Jamieson et al. (2007).

4.4 Separation Factors

The Separation Factor is a concept widely used by the industry to determine if the distance between two wellbores is safe. Unfortunately, despite many efforts, there is not a standard way to calculate the value. Different companies worldwide are using different versions of the term, creating not only confusion to determine the safety of the drilling operation but also to catastrophic results.

This work compares three different equations used in the field, and those equations are all based on the ratio-type Safety Factor. Although, as mentioned, different types are used, the ratio-type factor is the type of equation recommended by ISCWSA/WPTS as the most accurate and because it represents a close relationship between the safety factor and the probability of well crossing (Bang et al., 2020).

The ratio-type is commonly a ratio between the wellbores C-C distance and the directional uncertainties, as shown in the equation below.

$$SF_{basic} = \frac{D}{k\sigma_D} \tag{4.12}$$

Where:

C-C distance between the points in the reference and offset wells.

k is the dimensionless scaling factor defined by the confidence level of the measurements.

σ_D is the directional uncertainty.

Since most of the Safety Factor equations the Directional Uncertainty σ_D is calculated for 1σ, it is necessary to multiply the uncertainty by the scaling factor k, which represents the confidence level of the data. As it will be demonstrated in the next sections, when calculating the Pedal-Curve Radius for the Ellipsoid and the Cylinder Surface Radius numerically, the resultants σ_1 and σ_2 already take into consideration the confidence level

used. The terms $\sigma_1(r)$ and $\sigma_2(r)$ need to be divided by the scaling factor k_{num} used to calculate the uncertainty's geometrical representation.

$$\sigma_j(r)_{num} = \frac{\sigma_j(r)}{k_{num}} \tag{4.13}$$

where:

$\sigma_j(r)_{num}$ is the individual directional uncertainties for 1σ. The term $\sigma_j(r)$ and $\sigma_2(r)$ was calculated by the equations (4.4) and (4.5) for the Ellipsoid Pedal Radius, and equations (4.10) and (4.11) for the Cylinder Surface Radius.

k_{num} is the scaling factor used to build the Ellipsoid and the Twisted Elliptic Cylinder of Uncertainty.

The new terms for 1 standard deviation $\sigma_1(r)_{num}$ and $\sigma_2(r)_{num}$ are finally used to calculated the term σ_D of in the equation (4.12).

A collision between wellbores, as already mentioned, can be determined by the calculated safety factor value. If the value is equal or less than SF_{critic}, a technical or *de facto* collision has happened. In the article Bang et al. (2020) recommend a $SF_{critic} = 1$ to be used, although many companies have adopted through the years a stop drilling criterion of $SF \leq 1.25$, or even $SF \leq 1.5$ for the most conservative ones. Technical collision is when the Ellipsoid of Uncertainties from both references and offset well are touching or overlapping each other. However, there is no parameter (high torque, losses of mud, etc.) indicating they have collided.

Determining the factor σ_D is an important task and, as presented by Bang et al. (2020), there are mainly two ways to combine the individual directional uncertainties $\sigma_1(r)$ and $\sigma_2(r)$: Linear Summation or a Root-of-Sum-of-Squares (RSS) methods. The Linear Summation method is when therms $\sigma_1(r)$ and $\sigma_2(r)$ are added up together, $\sigma_D = \sigma_1(r) + \sigma_2(r)$, while the term σ_D when using the RSS method is $\sigma_D = \sqrt{\sigma_1^2(r) + \sigma_2^2(r)}$. Except for the Simplified Separation Factor the σ_D was always calculated by the RSS method since is the method recommended by Bang et al. (2020).

The three equations selected by this thesis to calculate the Separation Factor were the Simplified, ISCWSA, and Equinor's. They shall be presented in more detail in the next sections.

4.4.1 Simplified Separation Factor Equation

The Simplified Separation Factor is the general safety factor equation (4.12). It has been used extensively by many companies and planning software, and it was recently recommended by the article Mansouri et al. (2020). It does not take into consideration the radius of the wellbore.

$$SF_{simplified} = \frac{D}{k\sigma_D}, \quad \text{where} \quad \sigma_D = \sigma_1(r) + \sigma_2(r) \tag{4.14}$$

The Simplified Safety Factor is the least stable of the equations selected, with the safety factor close to infinite due to the small directional uncertainty at shallow depths. Another difference between the other two equations is regarding how the term σ_D is calculated. It uses a linear summation of the term σ_1 and σ_2 instead of the recommended by Bang et al. (2020) RSS method. As pointed out in the same article, the linear summation method to combine the individual uncertainty produces pessimistic (smaller) safety factor results.

For the numerically calculated individual directional uncertainties, the term σ_D becomes $\sigma_D = \frac{\sigma_1(r)+\sigma_2(r)}{k_{num}=3.058}$, where k_{num} is the scaling factor used to calculate the tridimensional surfaces.

4.4.2   Equinor's Safety Factor Equation

Equinor, a Norwegian state-owned energy company, uses a slightly different version of the separation factor equation. The primary safety factor ratio was modified to incorporate the radius of both Reference and Offset wellbores. When the wells are near, it is misleading and potentially dangerous, not include these dimensions (well radius) (ISCWSA, 2013).

$$SF_{equinor} = \frac{D - R_r - R_o}{k\sigma_D}, \quad \text{for} \quad k = 2.878 \tag{4.15}$$

with:

$$\sigma_D = \sqrt{u_r^T(COV_{(NEV,1)} + COV_{(NEV,2)})u_r}, \quad \text{for} \quad u_r = \frac{\vec{p}_{min} - \vec{p}_0}{||(\vec{p}_{min} - \vec{p}_0)||} \tag{4.16}$$

where:

D is the distance C-C between the reference and offset wells.

R_r and R_o are the wellbore radius for the reference and offset wells.

k is the scaling factor determined by the confidence level used in the calculations.

$\vec{u}_r$ is the unit tangent vector of $\vec{r}$, with a direction from reference well to the offset well.

$\vec{p}_0$ is the survey point in the reference well.

$\vec{p}_{min}$ is the offset well closest point to the reference well.

The Directional Uncertainty σ_D is calculated by combining the individual covariance matrices of the points in the Reference and Offset well. According to Bang et al. (2020), the combination procedure produces the same results as the σ_D calculated by the individual uncertainties and RSS summation.

Also, the scaling factor used in real operations by Equinor is quite low when compared with the recommended and more conservative value used by ISCWSA / WPTS. While SPE Technical Section recommends a scaling factor of $k = 3.5$, which represents a confidence level of 99.34%, Equinor uses a most optimistic value $k = 2.878$, confidence level 95.95%. The Ellipsoid of Uncertainty and the Twisted Elliptic Cylinder were calculated for a confidence level of 97.50%.

When calculating the safety factor for the numerically calculated pedal-curve radius and the cylinder surface radius using the Equinor equation, the term σ_D had to be changed.

Since the combination of covariance matrix as in the equation (4.16) produces the same results as if the term was calculated by the individual uncertainties and combining using the RSS summation method, σ_D used was the same as the equation (4.18).

4.4.3 ISCWSA/WPTS Separation Factor Equation

The Separation Factor presented by ISCWSA/WTPS, is the most robust when comparing with the other two equations. The equation (4.17) was presented in the article Sawaryn et al. (2019) in a effort to standardize the anti-collision analysis across the different companies. The WPTS believes that the standardization will clarify the expectations and requirements and support consistency between operators, service providers, and regulators and increase planning and operational efficiencies and reduce the burden of training (Sawaryn et al., 2019).

$$SF_{wpts} = \frac{D - R_r - R_o - S_m}{k\sqrt{\sigma_D^2 + \sigma_{pa}^2}}, \quad \text{for} \quad k = 3.5 \tag{4.17}$$

with:

$$\sigma_D = \sqrt{\sigma_1(r)^2 + \sigma_2(r)^2} \tag{4.18}$$

where:

D is the distance C-C between the reference and offset wells.

R_r and R_o are the wellbore radius for the reference and offset wells.

S_m is the surface margin that increases the effective radius of the offset well.

k is the scaling factor determined by the confidence level used in the calculations.

σ_{pa} is the uncertainty in the projection ahead of the current survey station.

$\sigma_1(r)$ and $\sigma_2(r)$ are the individual directional uncertainties for the reference and offset well, respectively.

The terms S_m and the σ_{pa} are additions to the generic safety factor equation (4.12). The safety margin S_m defines the minimum acceptable separation during the wells' design while the project-ahead uncertainty σ_{pa} is partially correlated with the projection from the survey depth to a distance beyond the bit. The recommended values by Sawaryn et al. (2019) are $S_m = 0.3$ m and $\sigma_{pa} = 0.5$ m and they have much more impact on shallow depths where the significance of the parameters is increased.

The confidence level of 99.34% selected by ISCWSA is considered very conservative. The scaling factor is $k = 3.5$, produce a bigger Ellipsoid or Cylinder of Uncertainty than the one used by Equinor. The scaling factor used in the equation (4.17) when comparing the results based on the numerical uncertainty distances calculated for the Pedal-Curve Radius, and the Cylinder Surface was $k = 3.058$.

For the numerically calculated individual directional uncertainties, the term σ_D becomes $\sigma_D = \frac{\sqrt{\sigma_1^2(r) + \sigma_2^2(r)}}{k_{num}}$, where $k_{num} = 3.058$ is the scaling factor used to calculate the tridimensional surfaces.

Chapter 5

Case of Study

5.1 Methodology

This chapter describes the test data, the well paths, and the different scenarios and implementations used. The complete workflow for all calculations and the results will also be provided.

5.1.1 Test Data

The selection of the test data is an essential subject for this work. Evaluating the separation distance between wells is a crucial subject to guarantee safety in the drilling environment. Failure to select the well path direction without considering all the errors from the reference and adjacent wellbore can result in catastrophic outcomes. Today, as already mentioned, there is no standard way to calculate the safety distance between wells.

The Industry Steering Committee on Wellbore Survey Accuracy, which primary mission is to produce and maintain standards for the industry relating to wellbore survey accuracy (ISCWSA, n.d.) has been producing many publications about the topic trying to engage the industry to create a standard procedure (equation (4.17)) to define the safety margins. The group recently proposed an equation for calculating the safety factor that encompasses not only the radius of each wellbore but also a surface safety margin, that is used to regulate the minimum distance between wellheads and the σ_{pa} that takes into consideration the uncertainty in the projection ahead of the current survey station (Sawaryn et al., 2019). This equation is used as a baseline for this work, and all other safety factors calculated from the other equations will be subject to comparison with results provided by ISCWSA.

In order to compare the safety factor estimations presented in this work with an equation that is used in real operations, the Equinor's Safety Factor equation (4.15) was selected. The Norwegian Energy Company, Equinor, utilizes a different version of the safety factor equation on its drilling operations. When comparing the Equinor equation with ISCWSA version, it is noticeable the absence of the surface safety margin S_m and the project-ahead uncertainty σ_{pa}. Equinor also uses a different scaling factor, $k = 2.878$, (confidence level 95.95%) than the recommended by ISCWSA where $k = 3.5$, giving a confidence level of 99.34%. All the safety factor calculations were done throughout this work with a scaling

factor of $k = 3.058$, which gives a reasonably high confidence level of 97.50%, although the common scaling factor for both Equinor and ISCWSA recommended equations are also display as a reference.

A simplified version of the safety factor equation (4.14) was also used in the analysis. The equation present by Mansouri et al. (2020) not only does not consider the surface safety margin nor the projected-ahead uncertainty but also does not use the radius of the wellbore and the Offset for its estimation. This equation is considered the least robust of all three equations, and it is displayed to contrast to the other two. In section 5.2, the necessary steps to calculate and evaluate the safety factor shall be presented.

5.1.2 Reference and Offset Wells

The wellbores were selected from the ISCWSA clearance table, which was designed to help others implement and verify their anti-collision algorithms. The clearance table ISCWSA (2017b) has one reference well and 11 offset wells. For this thesis, only the reference well and four offsets wells were selected. Below the list of wellbores.

Table 5.1: The Reference well and a comparison with offset wells.

Wellbore Name	MD Total [m]	Inc. Max. [°]	Azi Range [°]	TVD Total [m]	Local North [m]	East [m]	Ref Well Depth [m]	Closest C-C Distance [m]
Reference Well	2940	90	180-180	1903.00	0	0	-	-
North100	3090	90	180-180	2002.64	100	0	2910	99.64
East10	2820	85	175-190	1915.22	0	10	990	10.00
East20	2850	90	182-200	1863.92	0	20	1770	9.91
Angular	2655	77	145-145	1949.99	-50	-500	2250	29.81

The calculations used the following constants throughout this work:

Table 5.2: The constants used for the calculations.

Setup Information	
Projection	ED50 / UTM Zone 31 North
Facility Reference	Latitude $\mid$ 60º 00' 00.00" N Longitude $\mid$ 3º 00' 00.00 E
Gravity $[m/s^2]$	9.80665
Magnetic Field [nT]	50000
Dip [°]	70
Declination [°]	0
Grid Convergence [°]	0
Azimuthal Reference	Grid North
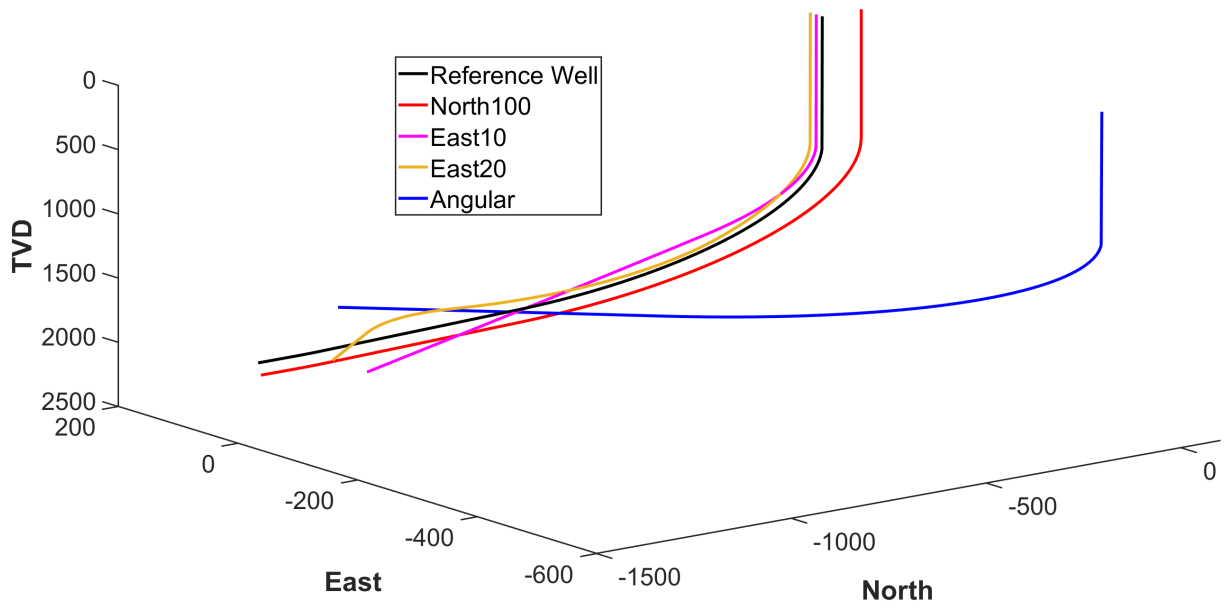
(a) 3D View of All Offset Wells and the Reference Well.
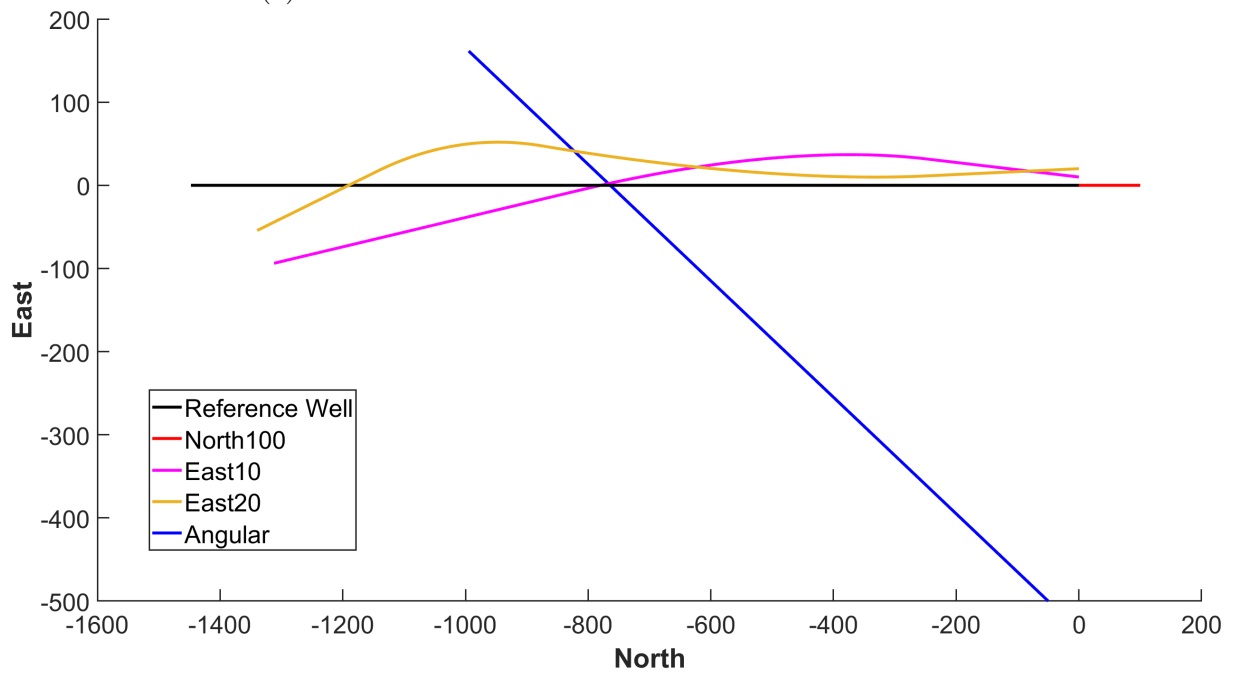
(b) Offset Wells Horizontal View.
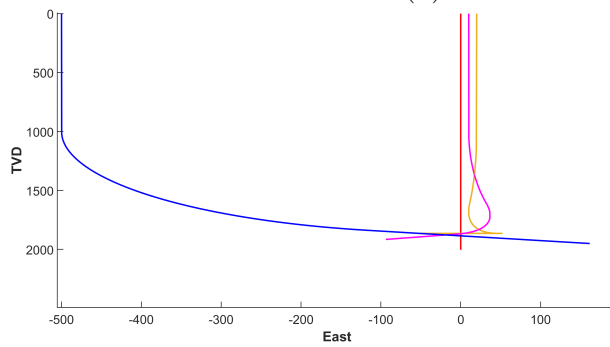
(c) Offset Wells East View.
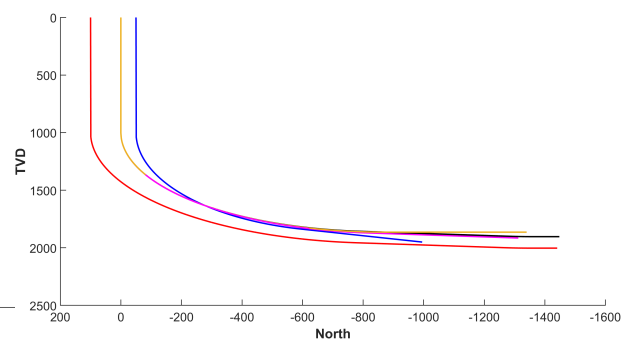
(d) Offset Wells North View

Figure 5.1: The Reference plotted in Horizontal, North and East Views.

Reference Well Path

The reference well has a straightforward J-Type design, with a 180° of Azimuth and achieving 90° of inclination at 2940 m Measured Depth, TVD of 1903 m. The reference well path can be found in the table B.1 in the Appendix B.
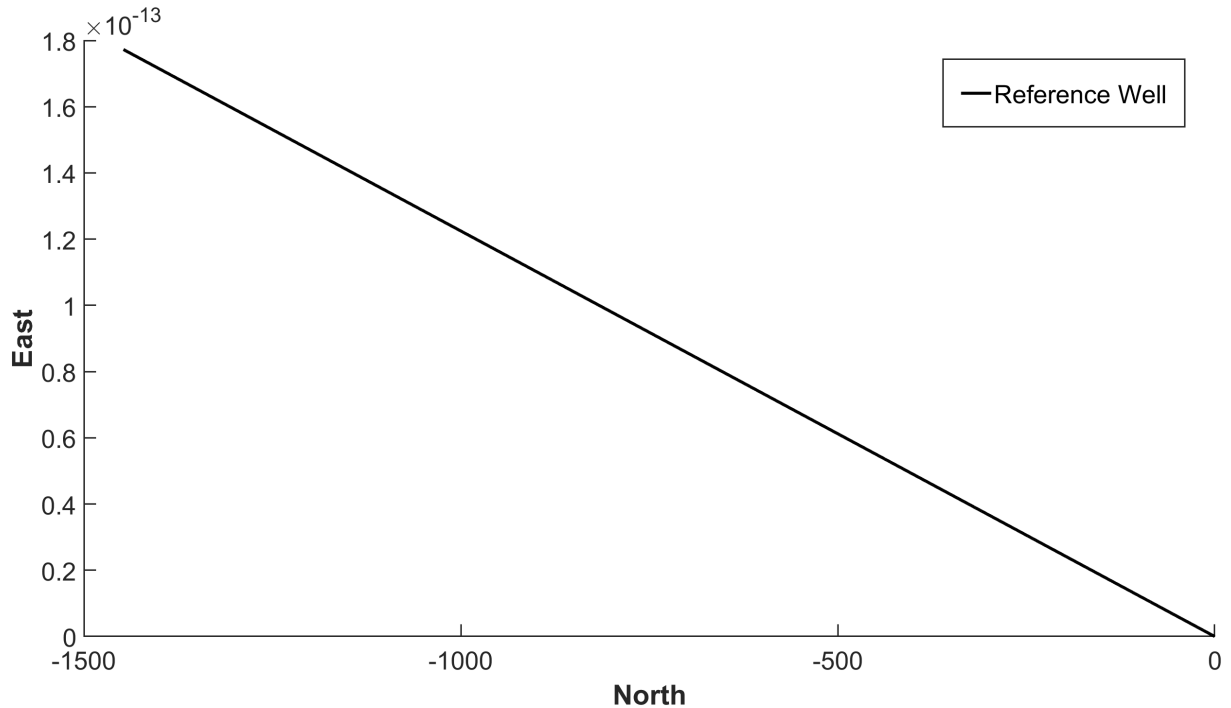

(a) Reference Well Horizontal View.
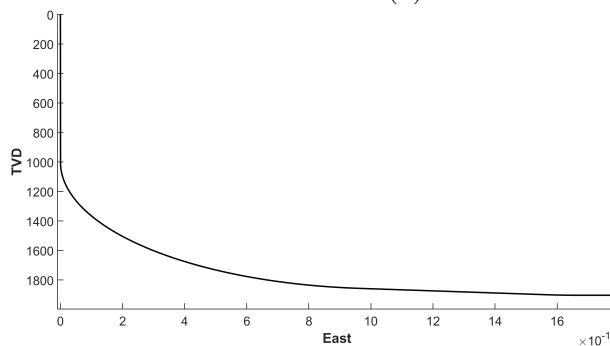
(b) Reference Well East View.
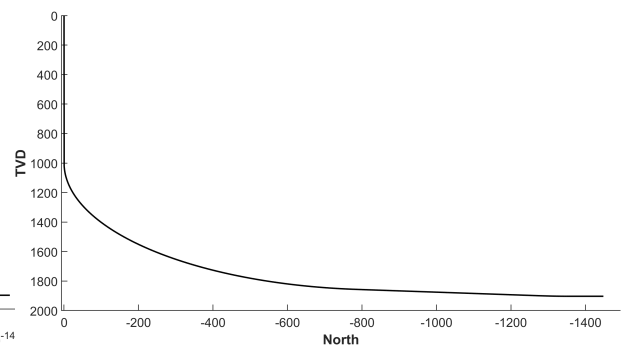
(c) Reference Well North View

Figure 5.2: The Reference plotted in Horizontal, North and East Views.

Offset Well: North100

The North100 Offset well starts 100 m North from the reference well. It is a simple J-Type well going from 0° to horizontal (90°) at 3000 m Measured Depth at a 180° Azimuth. A horizontal tangent section starts from 3000 m to 3090 m it is also present. The well is almost parallel to the reference well, with the closest distance of 99.64 m at 2910 m MD of the Reference well. Check the table B.2 Appendix B for the North100 well path.
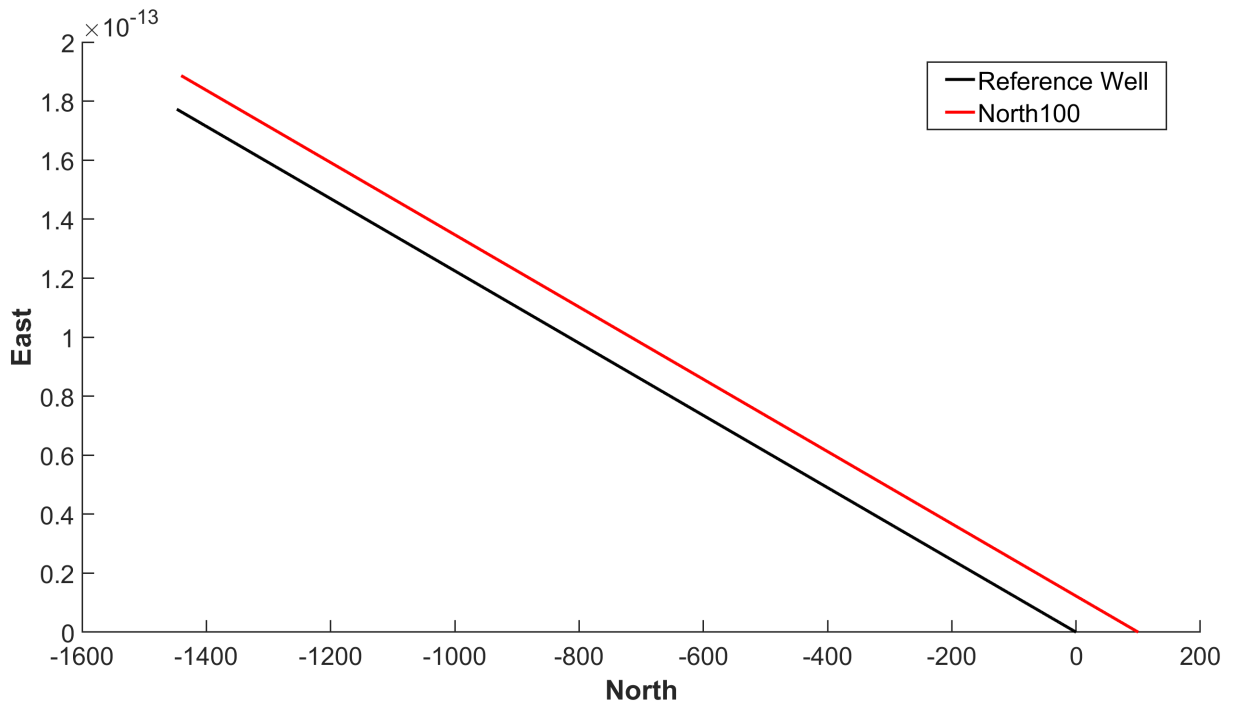
(a) North100 Offset Well Horizontal View.
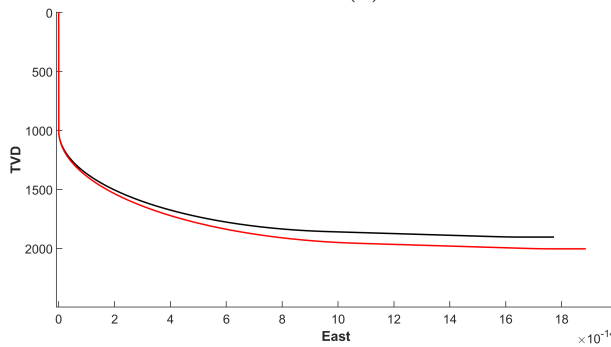
(b) North100 Offset Well East View.
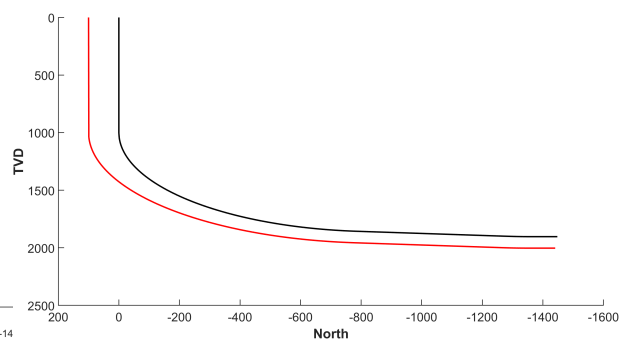
(c) North100 Offset Well North View

Figure 5.3: The North100 Offset Well plotted in Horizontal, North and East Views.

Offset Well: East10

The East10 offset well is a 3D directional well that starts 10 m east of the reference well and kicks off at 990 m. It builds from 0° to 85° inclination and turns right from 175° to 190° of Azimuth. The closest distance to the reference Well is 10 m, around 990 m MD of the Reference well. The East10 well path can be found in the table B.3 of the Appendix B.
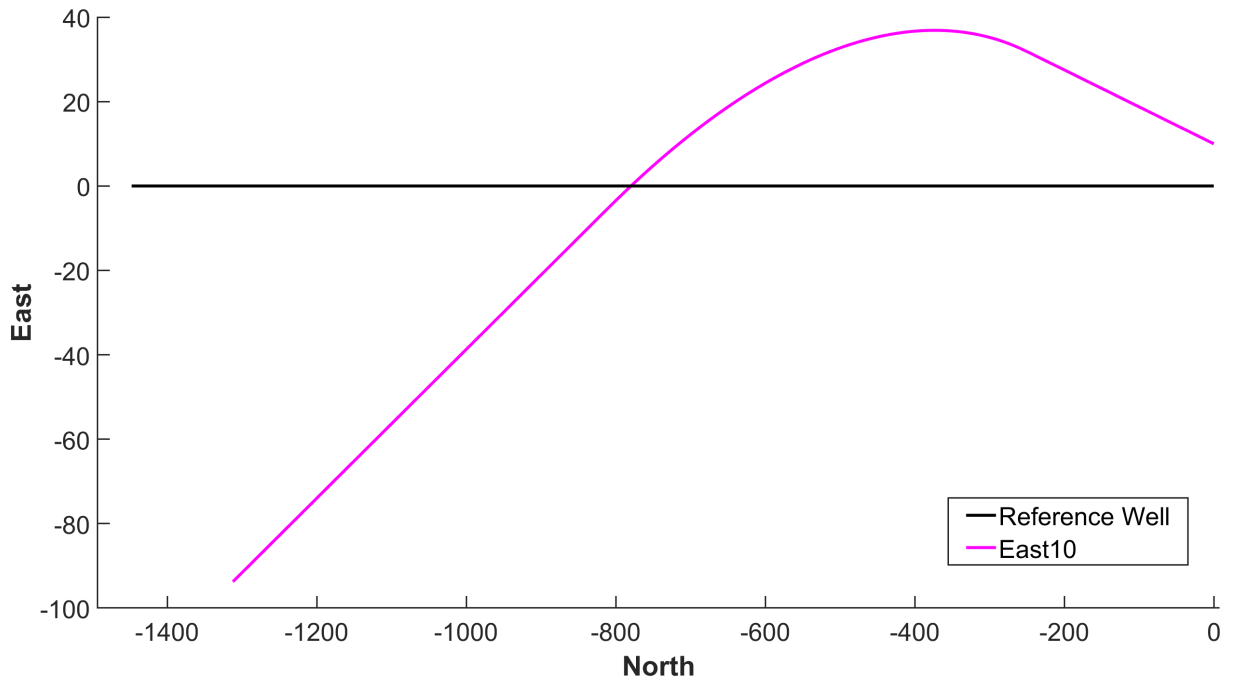
(a) East10 Offset Well Horizontal View.
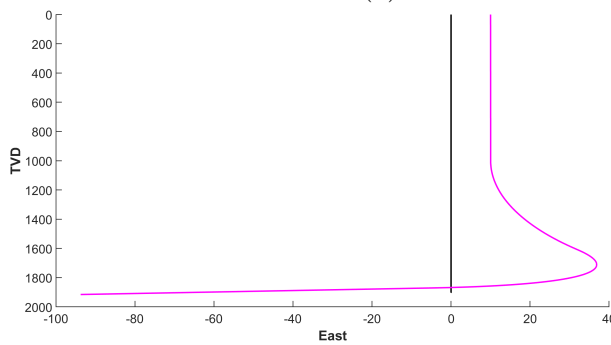
(b) East10 Offset Well East View.
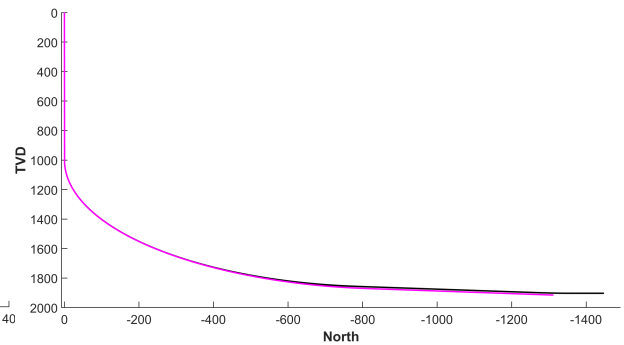
(c) East10 Offset Well North View

Figure 5.4: The East10 Offset Well plotted in Horizontal, North and East Views.

Offset Well: East20

The East20 Offset well is a 3D directional well that starts 20 m east from the reference well. It builds inclination from 0° reaching horizontal (90°) at 2370 m MD. At the same time, it turns left from 182° to 173° Azimuth at 2370 m MD. It starts a flat turn to the right from 2370 m, from 173° to 200°. The closest distance is 9.91 m at 2250 m of the reference well. The well path for the offset well East20 is listed in the table B.4 of the Appendix B.
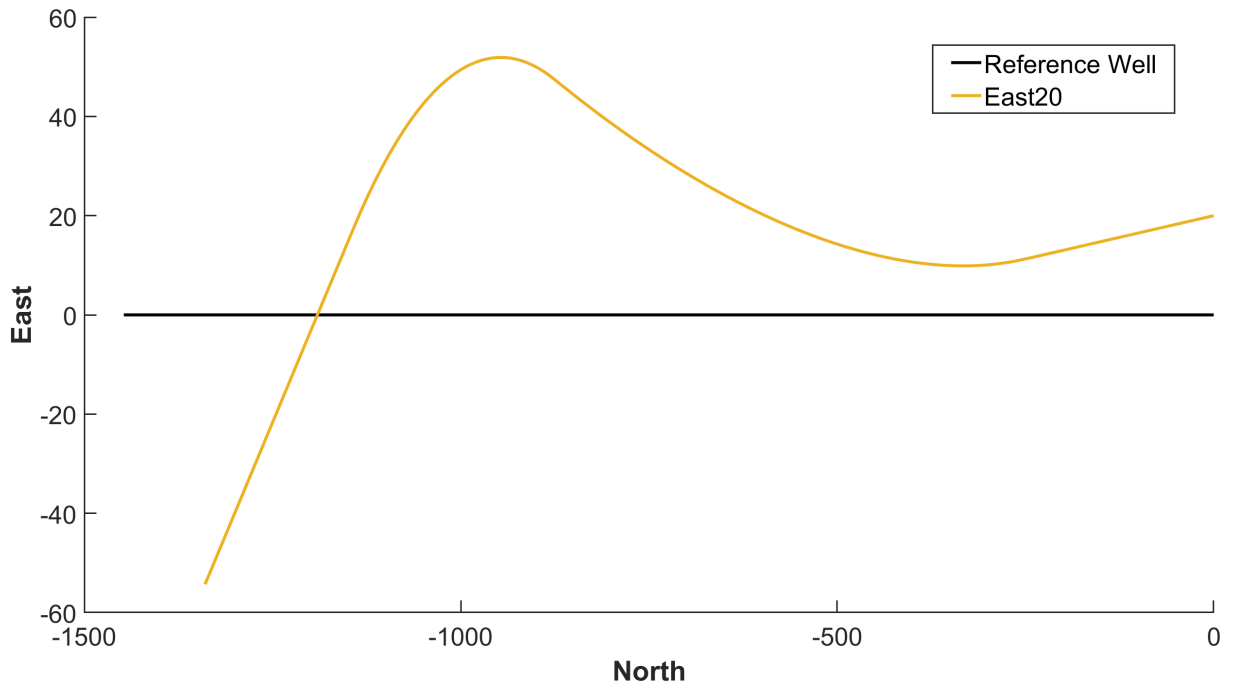
(a) East20 Offset Well Horizontal View.
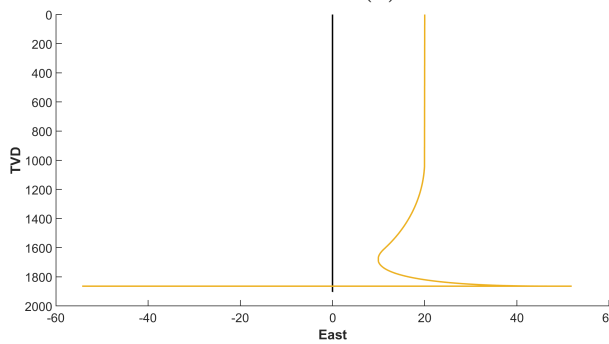
(b) East20 Offset Well East View.
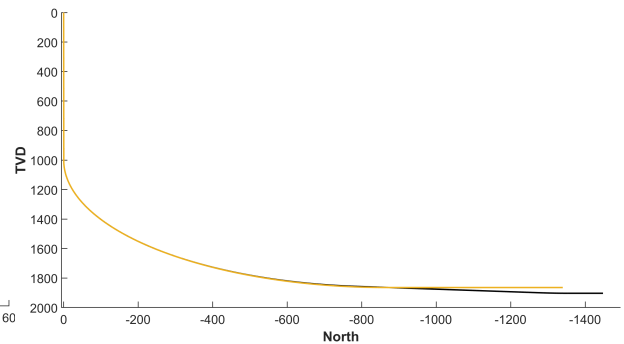
(c) East20 Offset Well North View

Figure 5.5: The East20 Offset Well plotted in Horizontal, North and East Views.

Offset Well: Angular

The Angular Offset well is a J-type wellbore that starts at -50 m north and -500 east from the reference well. It builds inclination from 0° to 77° at 2160 m MD, where keeps a tangent all the way down to the end at 2655 m MD. It keeps the Azimuth 145° throughout the path. The table B.5 in the Appendix B lists the well path for Angular Offset well.
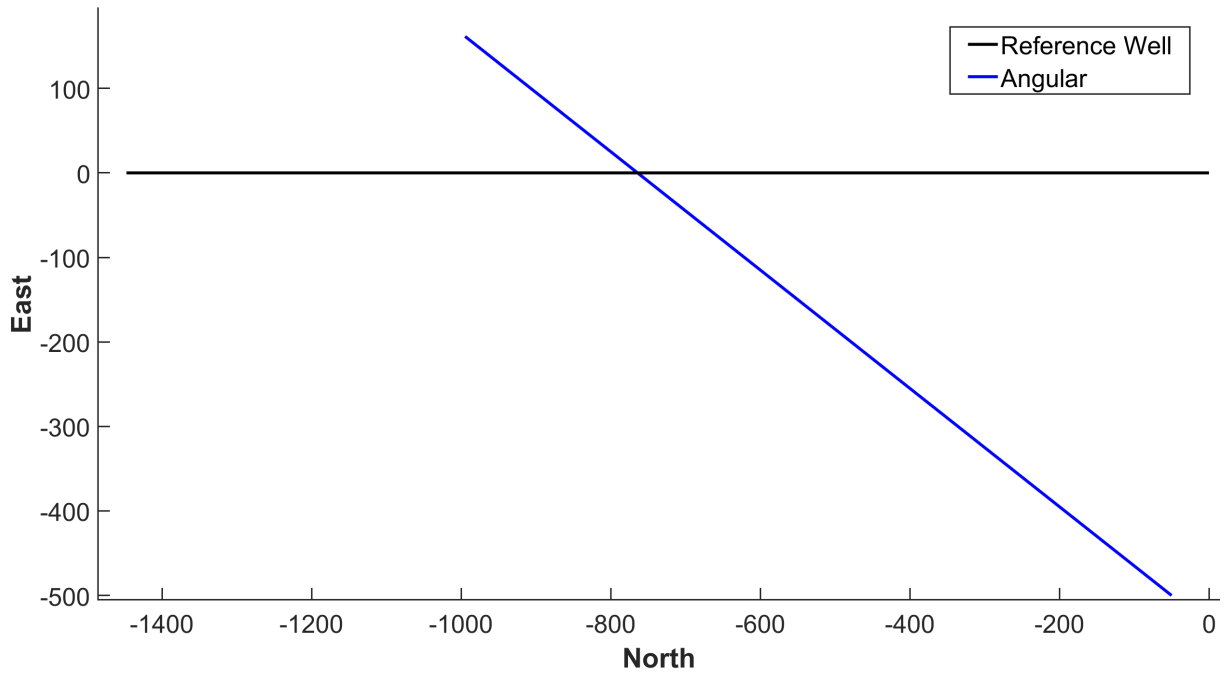
(a) Angular Offset Well Horizontal View.
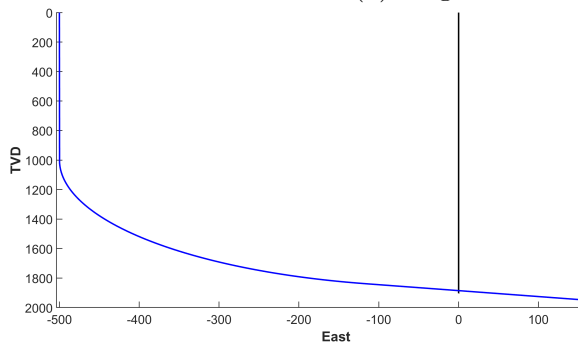
(b) Angular Offset Well East View.
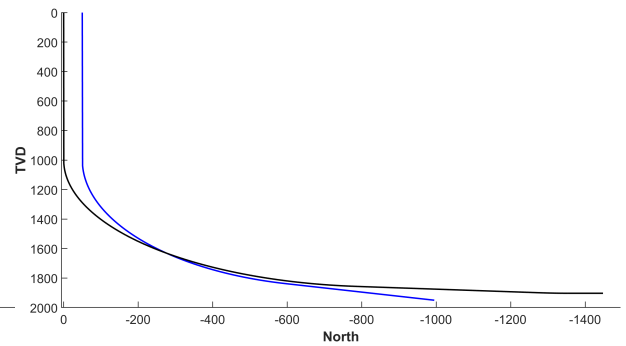


(c) Angular Offset Well North View

Figure 5.6: The Angular Offset Well plotted in Horizontal, North and East Views.

5.2 Implementation Routine

During this thesis, an algorithm to derive the safety factor was developed, from getting the survey measurements to outputting the anti-collision report listing the safety factors per MD. The algorithm was build using Python and Matlab. The steps used to construct the test model were:

1. **Selection of the data**

   Intending to help other companies implement the best anti-collision practices, the ISCWSA group has made freely available a complete data set where the error model was implemented (ISCWSA, 2016). The error model was implemented using the available wellbores in the data set, and the results were compared with the results provided in the same dataset.

2. **Conversion of the Survey Measurements into Global Coordinate System (NEV)**

57

The Global Coordinates were calculated from the Measured Depth, Inclination, and Azimuth survey measurements using the Minimum-Curvature Method. The method implemented uses a vector equation to calculate the North, East, and Vertical positions presented by Sawaryn and Thorogood (2005), and it was thoroughly described in the subsection 2.4.3.

3. **Definition of the Error Sources**

As described by ISCWSA (2017a), the purpose of the error model is to evaluate the effects of the various physical factors which lead to errors in the survey measurements. Those physical factors need to be identified for a given surveying tool (i.e., MWD Tools), and effects on each of the measurements (Measured Depth, Inclination, and Azimuth) must be determined. The combination of all individual errors gives the uncertainty in the position.

ISCWSA also provided a list of 27 error sources to be used in the position uncertainty calculations. Those error sources are only related to the MWD surveying tool. As mentioned before, this work does not consider error sources from other surveying tools than MWD tools, for example, Gyro Surveying Tools.

Each error source has a *Magnitude*, *Weighting Functions* and *Propagation Mode*. The magnitude is defined as the standard deviation of the error (ISCWSA, 2017a). The Weighting Functions describe how the error effects the MD, *Inc.* and *Azi.* by a set of equations. Finally, The Propagation Mode defines how correlated the errors are to each other. The complete set of error sources is available in the table A.1 to A.3 in the Appendix A.

4. **Evaluation of the Position Uncertainty**

After we have defined the error sources with its magnitudes, weighting function, and propagation type, we need to calculate the size of the uncertainty error in NEV coordinate system. the core formula of $e_{i,k}$ was presented in the equation (3.1) and (3.4). The Balanced Tangential Method was used to calculate the effect of the error source in the survey measurements $\frac{d\Delta r_k}{dp_k}$ and $\frac{d\Delta r_{k+1}}{dp_k}$. As mentioned by ISCWSA (2017a), it would not affect the precision of the data using this survey calculation method.

5. **Finding the Covariance Matrix**

With the $e_{i,k}$ and $e_{i,k}^*$ for each survey station, Covariance Matrix for that particular error source can be easy find from the equation (3.15) for Random error sources and equation (3.16) for Systematic and Global error sources. Per error source a covariance (3×3) matrix will be generated in the NEV for each survey station k:

$$COV_{NEV,k} = \begin{bmatrix} \sigma_N^2 & Cov(N,E) & Cov(N,V) \\ Cov(N,E) & \sigma_E^2 & Cov(E,V) \\ Cov(N,V) & Cov(E,V) & \sigma_V^2 \end{bmatrix} \qquad (3.17)$$

The summation of all $COV_{NEV,k}$ generated that way will produce the final Covariance matrix per survey station used to calculate the Ellipsoid, Cylinder, and safety factors.

6. **Calculation of the Minimum Distance or Closest Approach**

The Minimum Distance, also known as Closest Approach, was the scanning method chosen for this thesis. As mentioned by Rocha et al. (2011), the minimum distance method is the most conservative method, and it will always find the closest point in the adjacent offset well. At each survey station of the Reference Wellbore, a scan algorithm was used to find the Offset Wellbore's closest 3D point. Check the section 4.2 for more details.
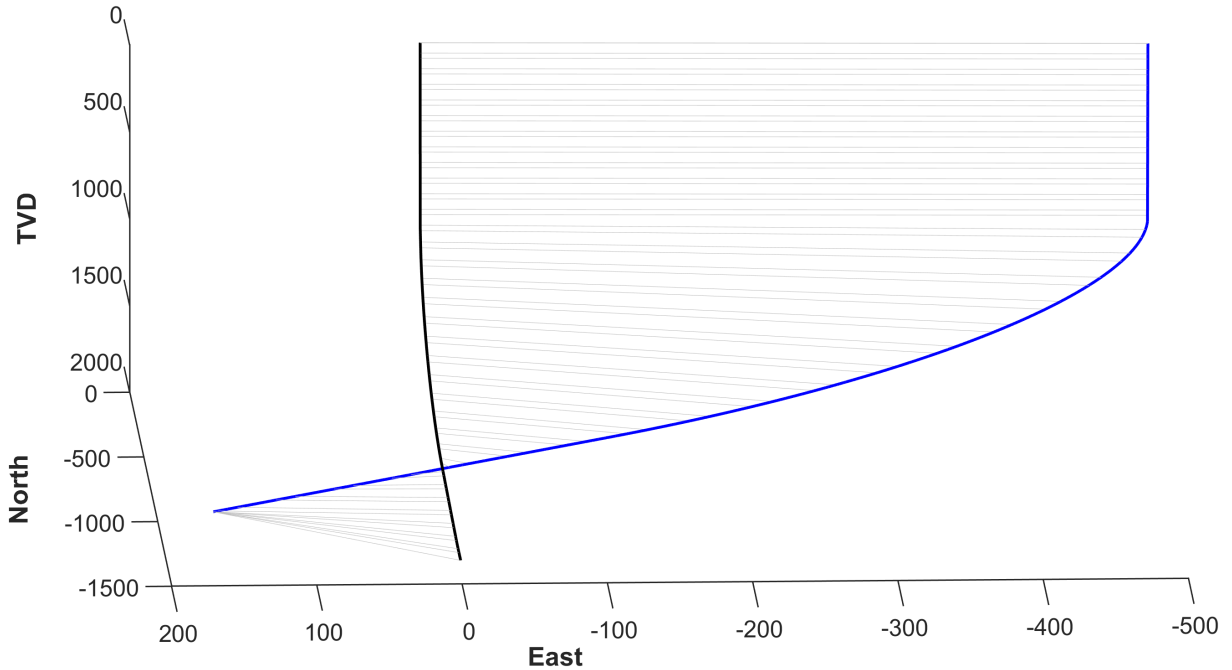

Figure 5.7: An example of the Minimum Distance calculation.

In the example above, the gray lines are the minimum distance of the reference wellbore (in black) survey point to a point in the offset wellbore (in blue).

7. **The Ellipsoid of Uncertainty**

   Since the Covariance Matrix is a positive semi-definite matrix and assuming the positional error has a normal distribution, it can be represented by a Statistical Ellipsoid for 1σ, as mentioned in the section 3.6.

$$E = \{r|(r - c)^T COV_{NEV}^{-1}(r - c) = k^2\} \tag{3.19}$$

   The principal radii of the statistical ellipsoid for COV_{NEV}^{-1}, centered at the point in space c is $R_i = k\sqrt{\lambda_i}$, where k is dimensionless the scaling factor defined by the degrees of freedom and the level of confidence of the uncertainty data. Also, the rotation of the Ellipsoid of Uncertainty can be found by the eigenvectors of COV_{NEV}^{-1}.

8. **Calculating the Individual Directional Uncertainties using the Pedal Curve Radius Method**

   The pedal curve is defined as the orthogonal projection of the ellipsoid over the C-C minimum distance line. The equations for calculating the Pedal Radius for the Ellipsoid were given in section 4.3.1. In this work we calculate the radius from

59

the equation (4.1) presented by Bang et al. (2020) and numerically by using the equations (4.2) to (4.5).

An example of the pedal curve calculated from an ellipsoid is presented below. The dashed black line is the C-C ($\vec{r}$) line, and the dashed magenta line is representing the plane that is orthogonal to $\vec{r}$ and tangential to the ellipsoid.
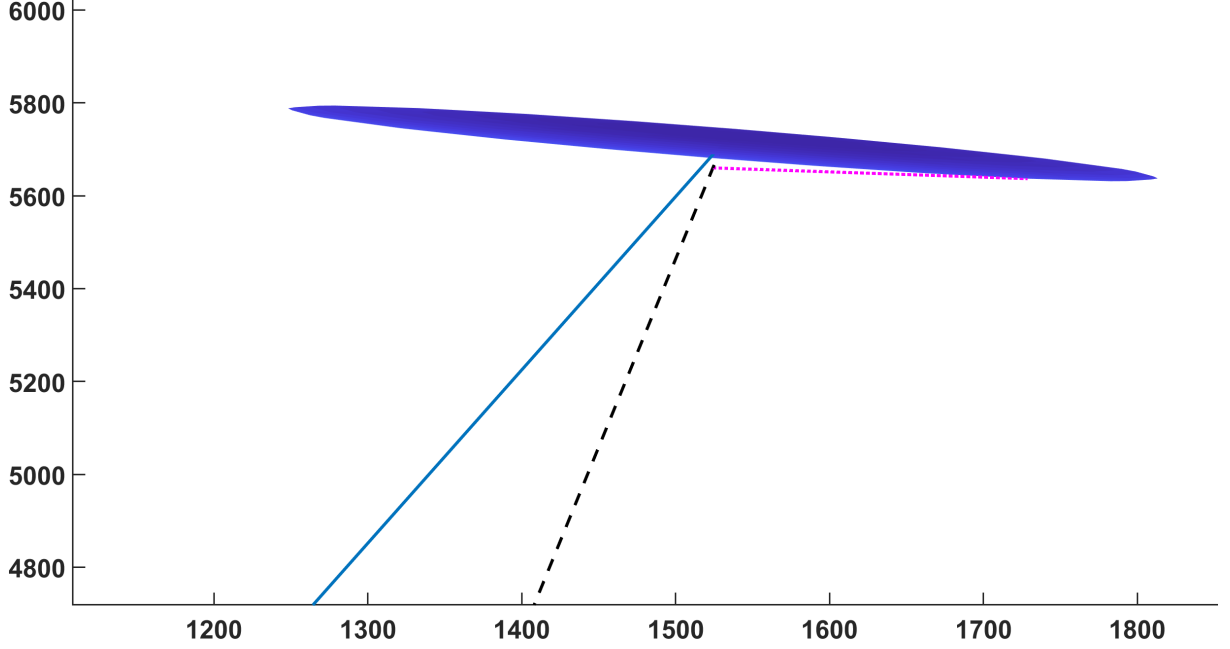

Figure 5.8: An example of the pedal curve calculated for a ellipsoid

9. **Finding the Twisted Elliptic Cylinder of Uncertainty**

As mentioned in the section 3.7, the Twisted Elliptic Cylinder of Uncertainty (TECoU) of was characterized by Liu (2019) and its principal radii and rotation angle can be find using the equations (3.21) to (3.24).

From the basic definition of a Elliptic Cylinder, the parametric equations for the lateral sides of an elliptic cylinder of height h, semi-major axis $R_{cyl,1}$ and $R_{cyl,2}$ are:

$$
\begin{aligned}
x &= R_{cyl,2} \cos\theta \\
y &= R_{cyl,1} \sin\theta, \quad \text{where} \quad \begin{cases} \theta \in [0, 2\pi] \\ v \in [0, h] \end{cases} \\
z &= v
\end{aligned}
\tag{5.1}
$$

For a Measure Depth point along the well path defined as MD_k and the point exactly before as MD_{k-1}, then the difference between those points can be defined as $\Delta\text{MD} = \text{MD}_k - \text{MD}_{k-1}$. For a very small values of ΔMD the height h can be defined as $h = \Delta\text{MD}$.

Using the parametric equations above, the Twisted Elliptic Cylinder is found in the $[x, y, z]$ axes and it needs to be rotated to the NEV axes. Multiplying the transformation matrix T to each of the $[x, y, z]$ components, the coordinate system will be changed to NEV axes. The new parametric equations of the TECoU are:

$$N = Tx$$
$$E = Ty \qquad (5.2)$$
$$V = Tz$$

10. **Calculating the Individual Directional Uncertainties using the Surface-Vector Method**

    The method to calculate the individual directional uncertainties $\sigma_1(r)$ and $\sigma_2(r)$ for the Cylinder Surface Radius were presented in the section 4.3.2. The Ellipsoid Radius was also used in this work in order to differentiate between both methods explicitly.

11. **Calculating the Separation Factor**

    From the chapter 4, section 4.4, it was established the three equations for the separation factor that shall be used throughout this work. The equation (4.17) provide by ISCWSA in the articles Sawaryn et al. (2019) and Bang et al. (2020). The Equinor's Safety Factor equation (4.15), that is currently being used in real life drilling operations. Finally the equation (4.14), which is a simplified version of the other two, recently presented by Mansouri et al. (2020).

    Both ISCWSA and Equinor's equations calculate the pedal distance of the ellipsoid directly from the Covariance matrix at the survey point and unit vector of the C-C line from the survey station point p_0 to closest approach distance in the Offset well, p_{min}. To use the cylinder and ellipsoid pedal curve distances calculated numerically, it was required to replace the σ_1 and σ_2 from those equations with these calculated distances. The results were compared with the already established equations to determine the applicability of the cylinder and the ellipsoid.

5.3   Results

5.3.1   The Covariance Matrix

After calculating and summing the elements $e_{i,k}$ and $e_{i,k}^*$, the Covariance Matrix COV_{NEV} is obtained. The matrix was calculated for each wellbore, including the reference well, and the elements were plotted for comparison.
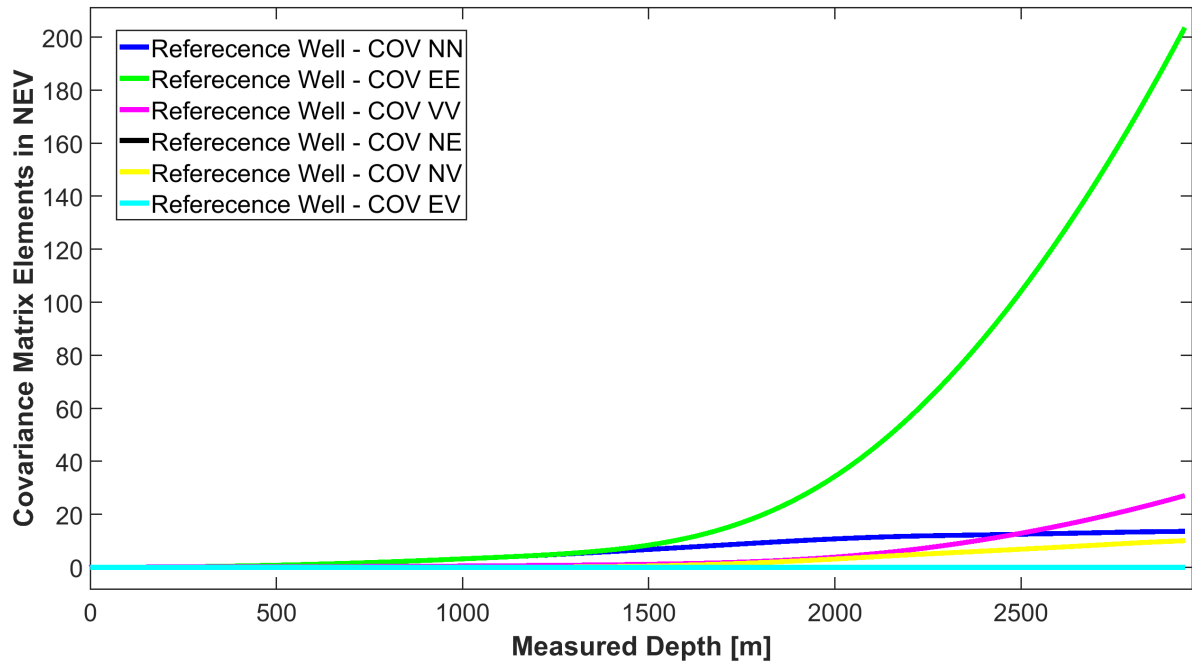
Figure 5.9: The Covariance Matrix Elements of the Reference Well in NEV Coordinate System
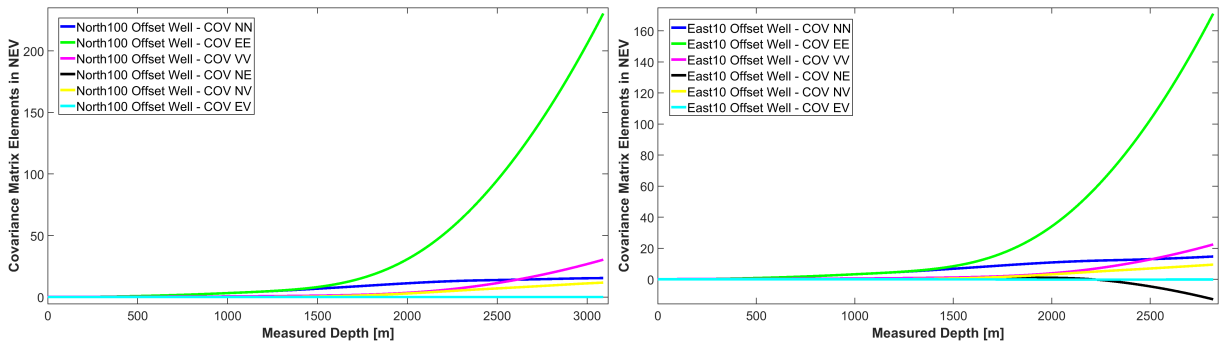

Figure 5.10: The Covariance Matrix Elements of the North100 and East10 Offset Wells in NEV Coordinate System
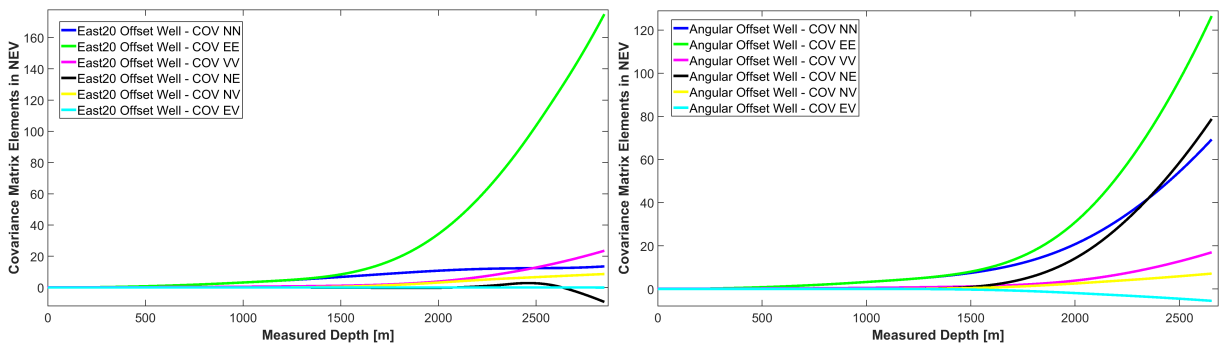

Figure 5.11: The Covariance Matrix Elements of the East20 and Angular Offset Wells in NEV Coordinate System

As shown in the Figures above, the most significant error is always in the East component

of the covariance matrix, representing the variance σ_E^2 in the east direction. The second-largest error is usually in the Vertical component of COV_{NEV}, except in the Angular Offset well, where the North-East covariance and the North variance elements are the second and third largest, respectively. This element represents the variance σ_V^2 in the vertical direction. This element reinforces the concept that the errors are highly dependent on the well path's depth and direction.

5.3.2 The Ellipsoid of Uncertainty

The radii of the statistical Ellipsoid of Uncertainty were defined as the square-root of the Covariance Matrix's eigenvalues, COV_{NEV}^{-1}, as already states throughout this thesis. The level of confidence selected for this thesis was 97.5%, meaning that there is a confidence that at least 97.5% of the positional error is taken into consideration when calculating the Ellipsoid of Uncertainty, giving a scaling factor k of 3.058. The scaling factor k, is then multiplied to the ellipsoid radii, increasing its size.

When comparing the ellipsoid sizes used by ISCWSA and Equinor, with a scaling factor k of 3.5 and 2.878, respectively, the selected confidence level stays in a middle way. The usage of 97.5% of confidence level is not so conservative as ISCWSA, which confidence level is 99.34%, neither optimistic as Equinor that has a confidence level of 95.95%.

The North100 wellbore has the highest ellipsoid major semi-axis magnitude at the end of the well path and is also the deepest wellbore.
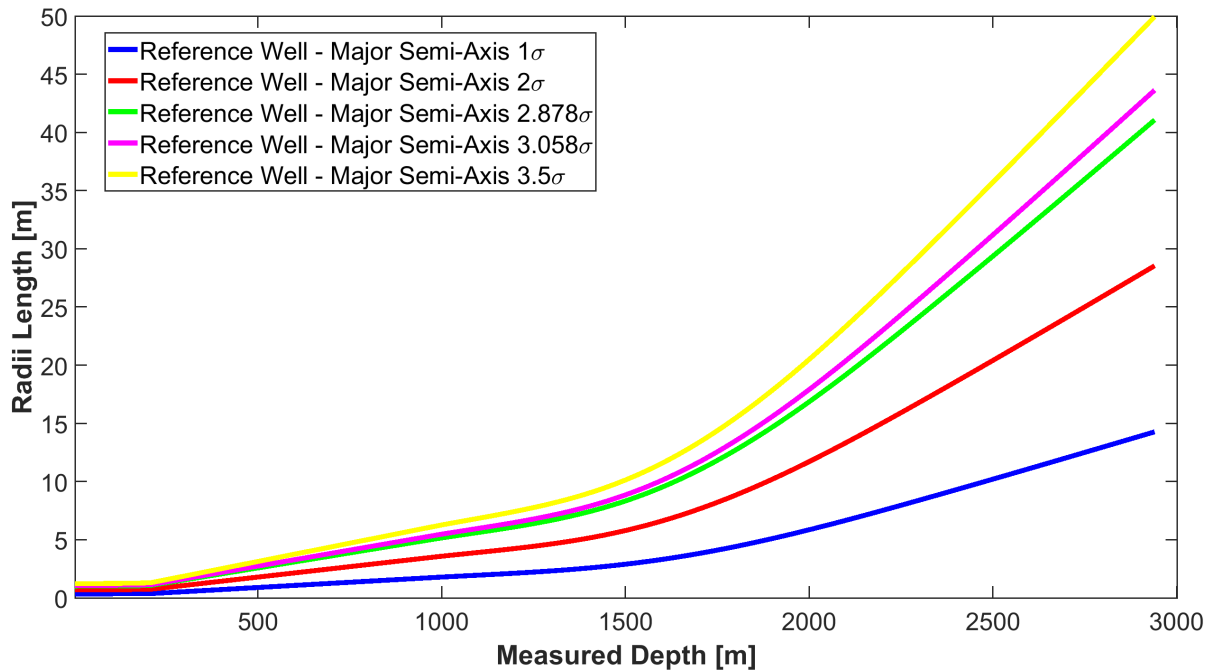

Figure 5.12: The Ellipsoid of Uncertainty Major Semi-Axis Magnitude of the Reference Well for Different Standard Deviations.
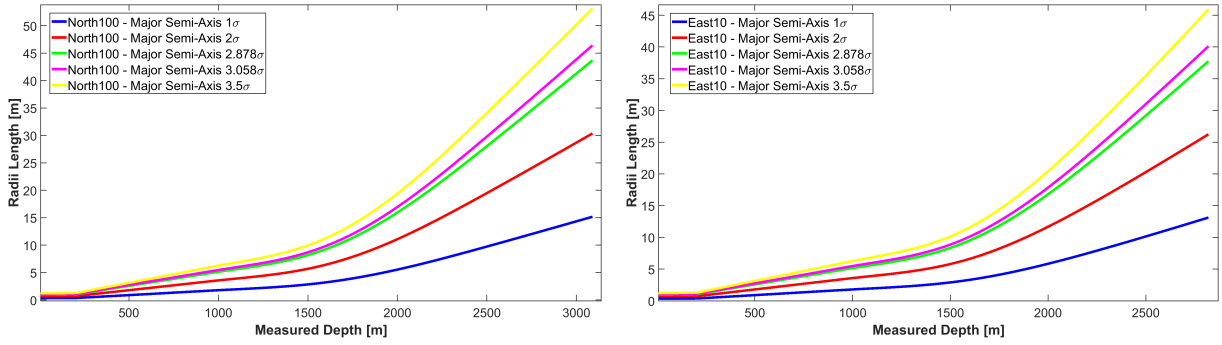
Figure 5.13: The Ellipsoid of Uncertainty Major Semi-Axis of the North100 and East10 Offset Wells for Different Standard Deviations.
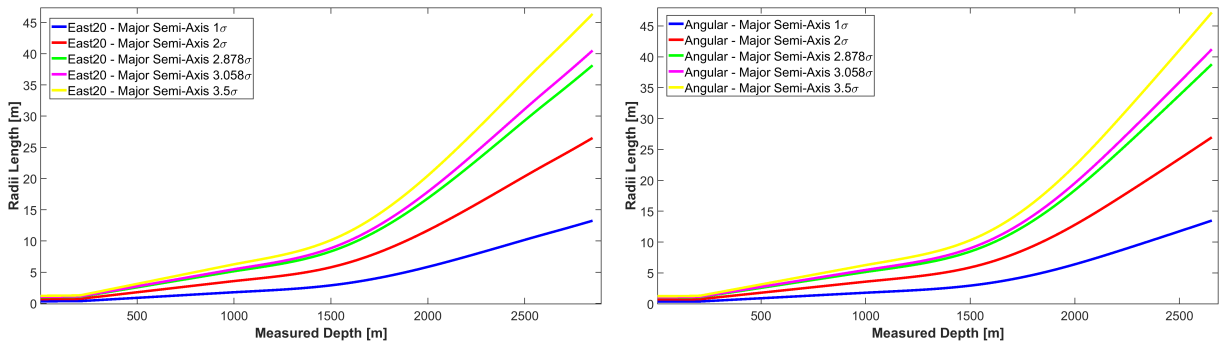

Figure 5.14: The Ellipsoid of Uncertainty Major Semi-Axis of the East20 and Angular Offset Wells for Different Standard Deviations.

5.3.3 The Twisted Elliptic Cylinder of Uncertainty

The Twisted Elliptic Cylinder of Uncertainty is a surface very hard to define mathematically. It is a function of the Measured Depth, Inclination, and Azimuth, which changes the principal radii size and its posture as the path gets deeper. The equations give the cylinder principal radii length (3.24), and they were calculated for a confidence level of 97.5%, a scaling factor k of 3.058. As expected, the major semi-axis lengths are similar to the ellipsoid major semi-axis since the cylinder can also be described as a series of ellipses connected. Below the graphs comparing the cylinder distances for the different standard deviations.
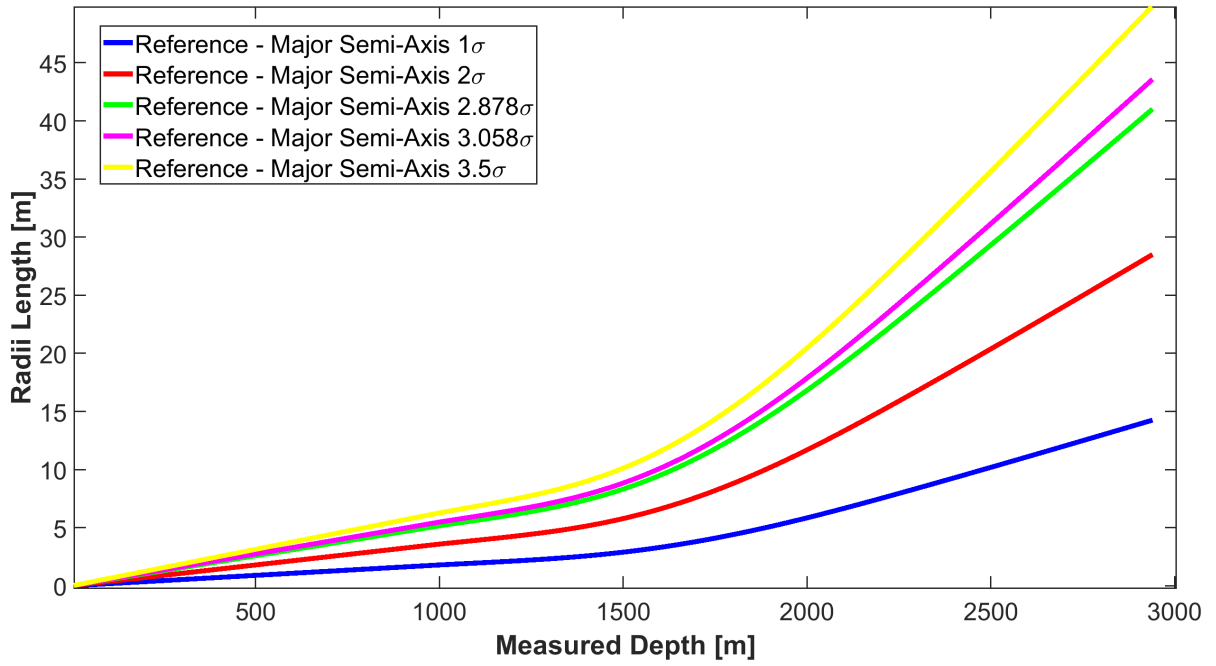
Figure 5.15: The Twisted Elliptic Cylinder Major Semi-Axis Magnitude of the Reference Well for Different Standard Deviations.
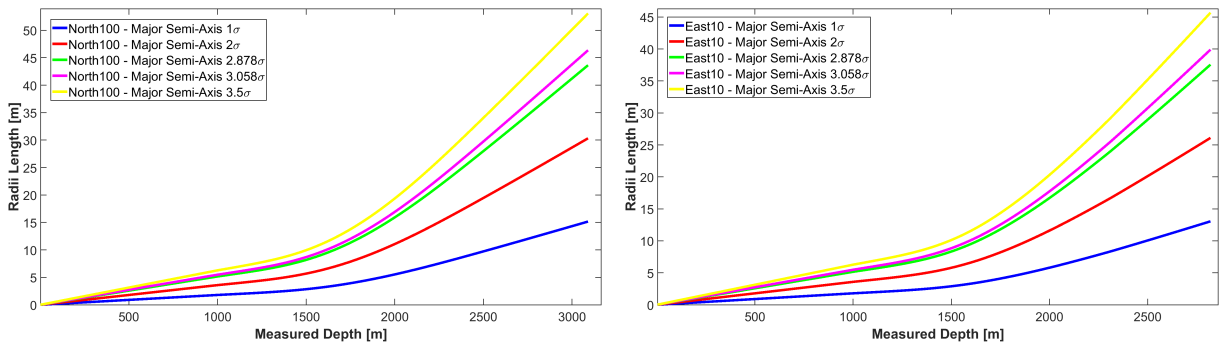

Figure 5.16: The Twisted Elliptic Cylinder Major Semi-Axis of the North100 and East10 Offset Wells for Different Standard Deviations.
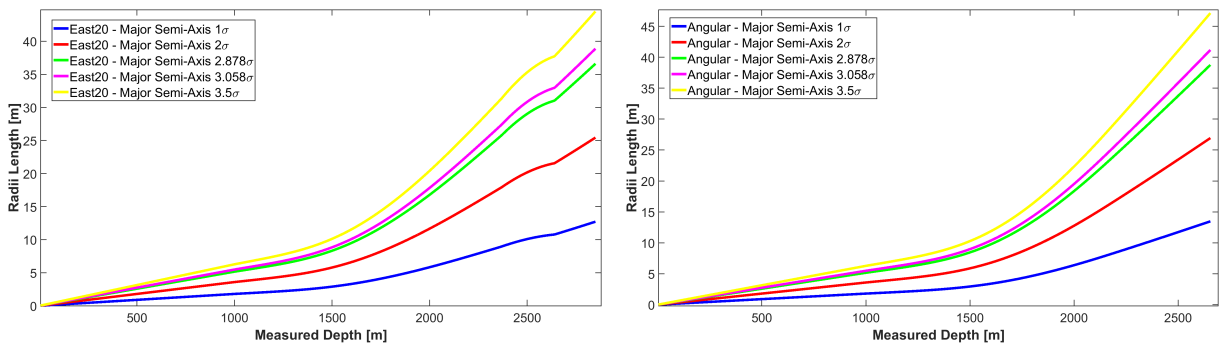

Figure 5.17: The Twisted Elliptic Cylinder Major Semi-Axis of the East20 and Angular Offset Wells for Different Standard Deviations.

5.3.4 C-C, Ellipsoid and Cylinder Distances

The distance C-C was calculated using the Minimum Distance scanning method, as already stated before. All safety factor equations are a ratio between the C-C distance and the sum of the distances between the survey point to pedal distance (Ellipsoid) or the point where the C-C line "touches" the surface of the cylinder. Different methods were used throughout this thesis to calculate those distances.

ISCWSA, for example, uses the equation (4.1) to calculate the pedal curve radius for the ellipsoid and its summation are done by the by the σ_D equation (4.18). Equinor calculates its ellipsoid distance by combining both Ellipsoid of Uncertainty and deriving its σ_D equation as in (4.16), which produces the same distances was the individual distance produced by ISCWSA. In this thesis, the pedal curve distance, as well as the cylinder distance, were calculated numerically as already explained in section 5.2 and its summation is following the summation recommend by ISCWSA and defined by the equation (4.18).
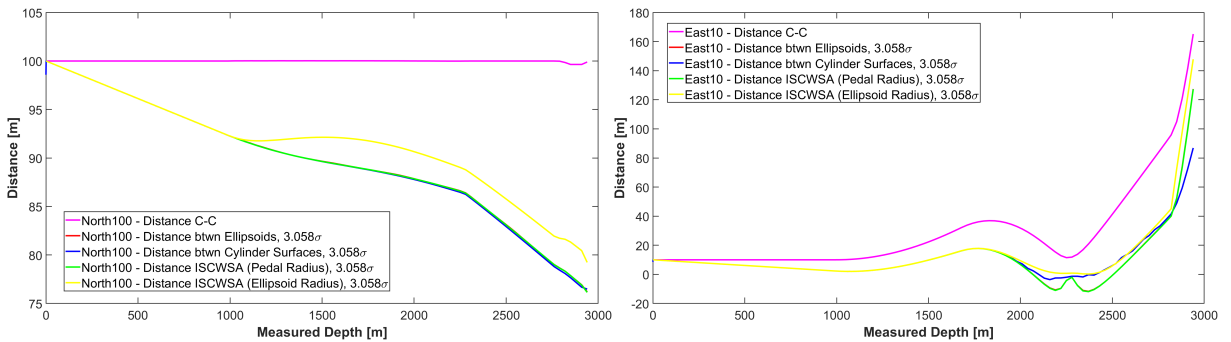

Figure 5.18: The Distances C-C, Between Ellipsoids, Cylinder Surfaces and Calculated by ISCWSA Comparison for the Offset wells North100 and East10.
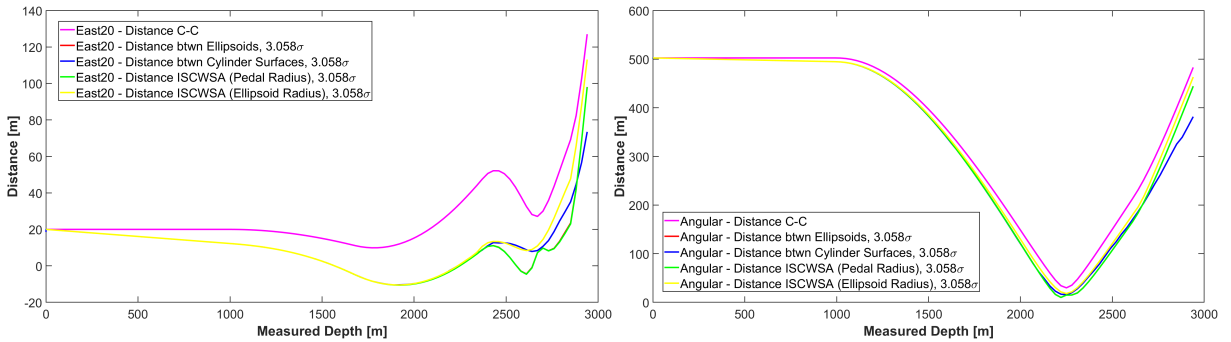

Figure 5.19: The Distances C-C, Between Ellipsoids, Cylinder Surfaces and Calculated by ISCWSA Comparison for the Offset wells East20 and Angular.

The graphs above are comparing the four types of distances calculated. The pink distance is the C-C distance between a point the in the reference well and the offset well. The other distances were calculated by subtracting both $\sigma_1(r)$ and $\sigma_2(r)$ from the C-C distance as in the equation $||\vec{r}|| - \sigma_1(r) - \sigma_2(r)$. The distances in red and blue are the distances between numerically calculated ellipsoids and numerically calculated cylinder surfaces. Finally, the green and the yellow lines are the distance between ellipsoids when calculating $\sigma_1(r)$ and $\sigma_2(r)$ by the Pedal Radius Method and Ellipsoid Radius Method, respectively, from Bang et al. (2020) equations.

First, in red, the distance between the numerically calculated ellipsoids is presented. As it can be seen, the distance is matching almost perfectly with the ISCWSA pedal radius calculation in green, as expected. Using the numerically calculated value or ISCWSA's pedal radius should produce the same safety factors effectively.

The yellow curve is the distance between ellipsoids calculated using the Ellipsoid Radius method, present by Bang et al. (2020). It uses the equation (4.6) to define the point where the C-C line "touches" the ellipsoid boundary. This curve was plotted to contrast with the Cylinder Surface distance, which also uses the concept of C-C line intersecting the surface.

The cylinder surface can be defined as the sum of ellipses of uncertainty throughout the whole well path. As displayed by the graph above, the distance between the survey point and the cylinder surface considers all the ellipsoid of uncertainty. While both Pedal curve radius and the Ellipsoid Radius methods are only considering the ellipsoid associated with the actual survey point. In extreme cases, using only the minimum distance scanning method, using only the pedal curve radius or the ellipsoid radius method, can make the separation factor more optimistic than in reality.

As it can be seen in the Figures 5.18 and 5.19, when the wellbores are almost parallel to each other, as the North100 offset well is to the reference well, the distances are almost the same, except for the Ellipsoid Radius method (yellow curve) that after 1100 m MD starts to present separation from the other distances.

For the Offset wells East10 and East20, it is observed negative distance, and it is possible due to the sum of individual directional uncertainties $\sigma_1(r)$ and $\sigma_2(r)$ of the ellipsoid pedal radius or the cylinder distances are more significant than the C-C distance. This situation can mean that either the Ellipsoids or the Cylinder Surfaces from both reference and offset wells are "touching" each other or, in the case of the pedal curves radius, the summation of the distances are more significant than the C-C distance.
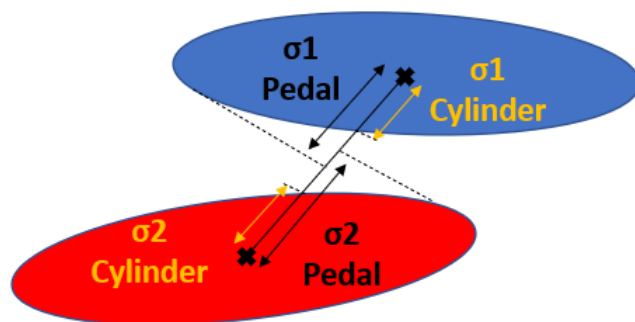

Figure 5.20: Comparison between the Ellipsoid Radius distance, Pedal Radius Distance and the Cylinder Distance.

This Pedal Curve Radius limitation was pointed out in the Jamieson et al. (2007) work, where depending on the ellipsoids' posture and how close they are to each other, the pedal radius method can be very pessimistic (low Separation Factor values) as if the surfaces were touching each other. As shown in Figure 5.20, the ellipsoids are not touching

each other, which could still be considered a safe situation (depending on the confidence level chosen for each ellipsoid). However, the safety factor out of this radius would be potentially less than 1, unnecessarily alerting for a collision situation that did not happen. On the other hand, when using the Cylinder Surface radius, it shows precisely that, although the wellbores are reasonably close to each other, the uncertainty areas are not touching each other, and it is not considered a technical collision. The safety factor using the cylinder surface distance would be a small value, maybe below most of the operator's safety criterion, but not below one that would characterize a collision issue.

The situation presented in Figure 5.20, both safety factors calculated by Cylinder Surface Distances or the Ellipsoid Radius Distance method, would be potentially precisely the same. It does not mean that solutions are similar. In Figure 4.8, the safety factors calculated by the Cylinder Surface Distance and the Ellipsoid Radius Distance would be dramatically different depending on the direction of the C-C curve. The cylinder's safety factor would be much smaller than the one produced by the Ellipsoid Radius Distance or even the Pedal Radius Distance.

5.3.5 The Separation Factors

The main separation factor equations were defined in the section 4.4 and equations (4.14), (4.15) and (4.17). The ISCWSA equation is considered throughout this thesis as the base equation and is effectively being used to compare and verify the results using the cylinder surfaces distances instead of the classic Ellipsoid Pedal Radius Distance. The Equinor's equation was brought to this discussion as an example of a safety factor used daily in the field in real operations. At last, the simplified version of the safety factor ratio, that was recently mentioned by Mansouri et al. (2020) in their paper as an alternative way of calculating the importance factor, was utilized in this work to compare its performance facing the other two, apparently more robust, safety factors.

As mentioned by Bang et al. (2020), the ratio-type safety factor $SF_{generic} = \frac{D}{k\sigma_D}$ is widely used by the industry and was also selected for this work. All three basic equations have different ways of calculating the σ_D variable.

1. **ISCWSA**: the σ_D variable used in the generic equation can also be referred as $\sigma_{(D,global)}$ for the ISCWSA equations, which is the Root-of-Sum-of-Squares (RSS) between the actual σ_D and the σ_{pa}.

$$SF_{ISCWSA} = \frac{D - R_r - R_o - S_m}{k\sigma_{(D,global)}}, \quad \text{where} \quad \left\{ \sigma_{(D,global)} = \sqrt{\sigma_D^2 + \sigma_{pa}^2} \right. \quad (4.17)$$

The term σ_D of the equation above is defined by the equation (4.18). It is important to note that, as mentioned by Bang et al. (2020) there are two ways of summing the individual uncertainties $\sigma_1(r)$ and $\sigma_2(r)$: a simple linear summation or using the Root-of-Sum-of-Squares (RSS). In this thesis, ISCWSA equation's for both Pedal and Ellipsoid Radius equation utilizes only the RSS summation since it was pointed out by Bang et al. (2020) as the most correct option.

Also, $\sigma_1(r)$ and $\sigma_2(r)$ can be calculated using two different approaches as already mentioned in the section 4.4, the Pedal Radius, which is considered the most conservative option and recommended by ISCWSA and the Ellipsoid Radius, which is not currently implemented in any commercial software neither is recommended

by ISCWSA. The Ellipsoid Radius was used to compare with the Cylinder Surface Radius cases, where similarly to the Ellipsoid Radius, the C-C line also intersects its surface.

2. **Equinor**: the σ_D is calculated by equation (4.16), which uses the combined error from the Reference and Offset well to calculated the Pedal Radius, as pointed out in the article from Bang and Nyrnes (2015). Combining the error produces the same results as calculating the σ_D by its individual uncertainties.

3. **Simplified Equation**: the term σ_D is the linear summation of the $\sigma_1(r)$ and $\sigma_2(r)$. Since the values for the numerically calculated $\sigma_1(r)$ and $\sigma_2(r)$ had already incorporated the scaling factor $k = 3.058$, the factor k from the equation (4.14) needs to be set to 1.

All equations mentioned above were initially recommended to be used with a different scaling factor of k. In order to compare the results, a common scaling factor had to be used, and in this case, since both Ellipsoid and Twisted Elliptic Cylinder of Uncertainty was calculated using $k = 3.058$, equivalent to a confidence level of 97.5%, this was the natural and straightforward choice to make.

Comparison: Simplified Equation and other Basic Equations

When comparing the simplified version of the safety factor equation to the other basic equations, ISCWSA and Equinor's, using a scaling factor $k = 3.058$, the results output by this equation were more conservative (smaller value of the safety factor) than the others. Also, the equation does not consider the radius of the reference and the offset wellbores, which makes it less robust and safer than the other two.
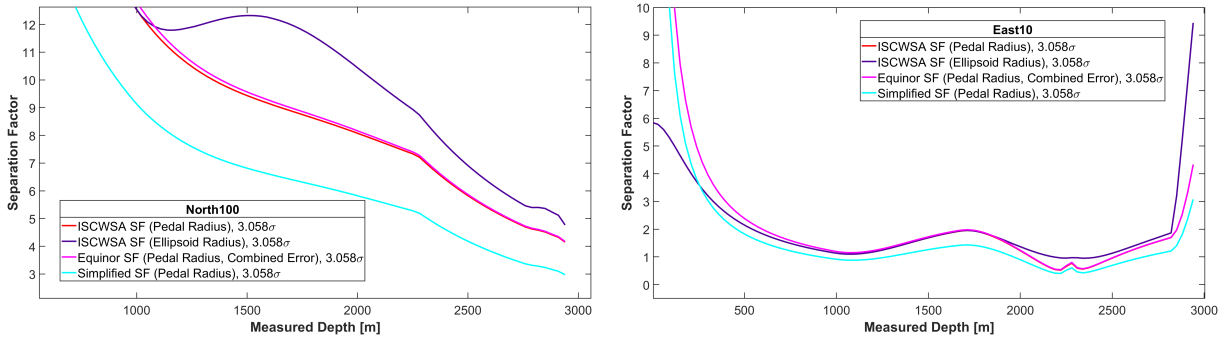
Figure 5.21: A Comparison between the 3 Basic Separation Factor Equations for the Offset wells North100 and East10.

69
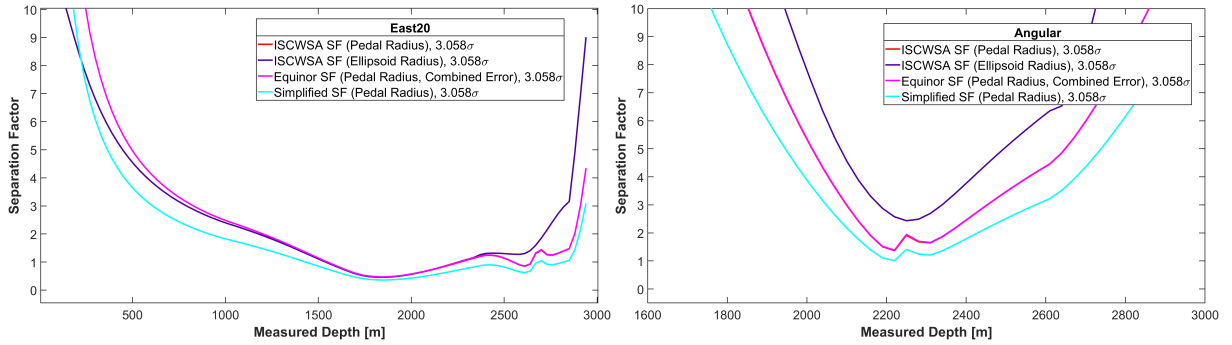
Figure 5.22: A Comparison between the 3 Basic Separation Factor Equations for the Offset wells East20 and Angular.

As can be seen from above Figures 5.21 and 5.22 the differences between the ISCWSA and Equinor equation for the Pedal Radius distance are marginal while the Simplified equation presents in general a smaller safety factor than the other two equations.

Comparison: Ellipsoid Pedal Radius Numerically Calculated and the ISCWSA and Equinor Methods

In order to check if the calculation of the Ellipsoid Pedal Radius was correctly calculated, the safety factors results were compared with ISCWSA and Equinor's equations that use the equations (4.1) and (4.16), respectively, to its pedal distances. For each basic equation, the $\sigma_1(r)$ and $\sigma_2(r)$ were replaced by the Ellipsoid Pedal-Curve Radius calculated in the equations (4.2) and (4.3). In the case of the Equinor's Equation, which uses the combined uncertainties to calculate the uncertainty in the distance, the variable σ_D used was the same as for ISCWSA σ_D, using the RSS for summation.

Since the Ellipsoid Pedal Radius calculated numerically already had the confidence level of 97.5%, the scaling factor k was set to 1 in both ISCWSA and Equinor's equations.
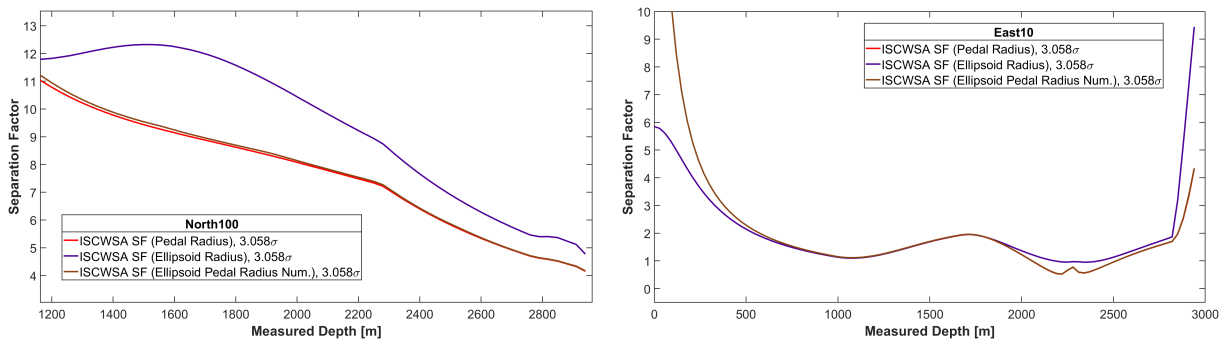
Figure 5.23: A Comparison between Safety Factors Originated by the Ellipsoid Numerically Calculated Pedal Radius and ISCWSA Basic Safety Factor Equation for the Offset wells North100 and East10.
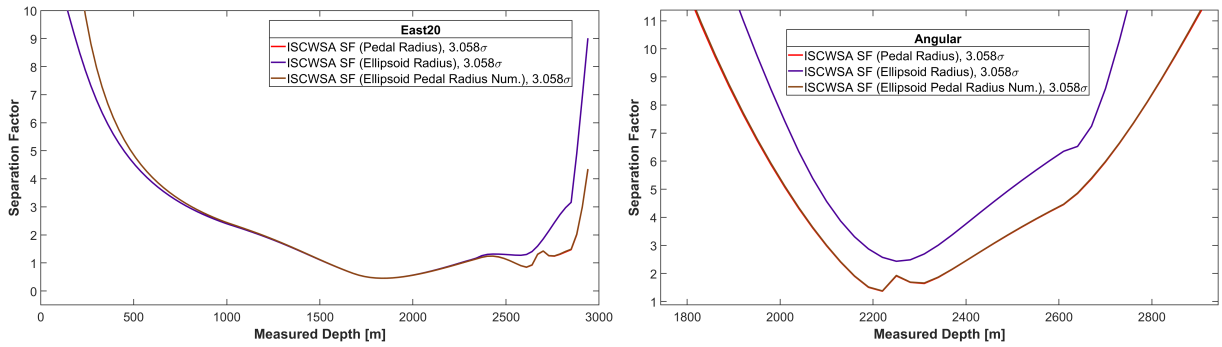
Figure 5.24: A Comparison between Safety Factors Originated by the Ellipsoid Numerically Calculated Pedal Radius and ISCWSA Basic Safety Factor Equation for the Offset wells East20 and Angular.
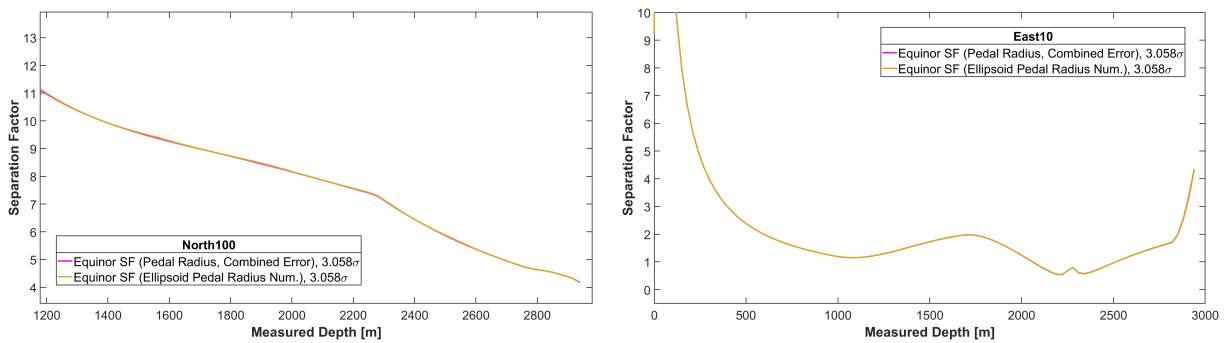
Figure 5.25: A Comparison between Safety Factors Originated by the Ellipsoid Numerically Calculated Pedal Radius and Equinor's Basic Safety Factor Equation for the Offset wells North100 and East10.
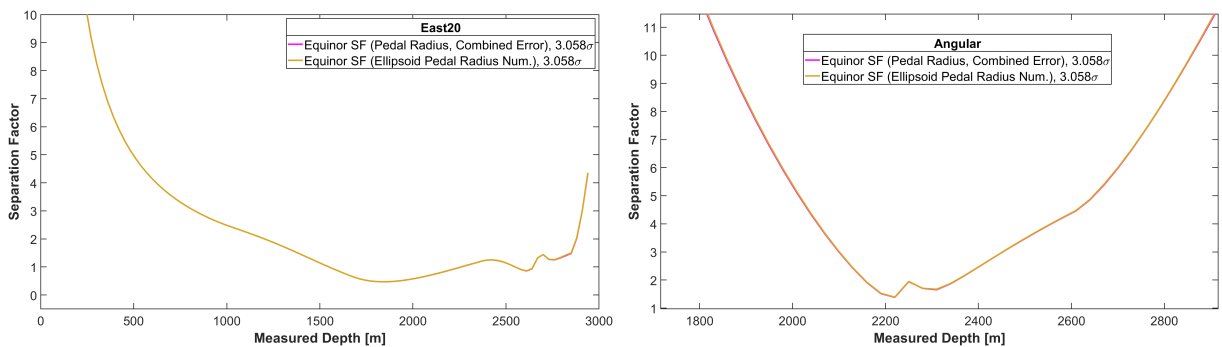

Figure 5.26: A Comparison between Safety Factors Originated by the Ellipsoid Numerically Calculated Pedal Radius and Equinor's Basic Safety Factor Equation for the Offset wells East20 and Angular.

Higher differences in both ISCWSA and Equinor's equations cases were observed, incredibly close to the surface due to some possible rounding errors. As the well path gets more profound, the curve starts matching each other almost perfectly, demonstrating that the numerically calculated pedal radius equations are valid, although it needs some refinements at the surface/shallower depths.

Comparison: TECoU Safety Factor and ISCWSA and Equinor's Methods

The distance between the survey point and the point that the C-C line intersects the cylinder surface is called the *Cylinder Surface Radius*. The distance was found numerically as described in the section 5.2, item 10. Both distances for the reference and offset wells were found and used in ISCWSA safety factor equation (4.17) by replacing the $\sigma_1(r)$ and $\sigma_2(r)$. It is also important to remember that the Cylinder principal axis was calculated for a confidence level of 97.5%, a scaling factor of $k = 3.058$. When using both ISCWSA and Equinor's equations together with the Cylinder Surface Distances, the scaling factor k of those equations had to be set to $k = 1$.
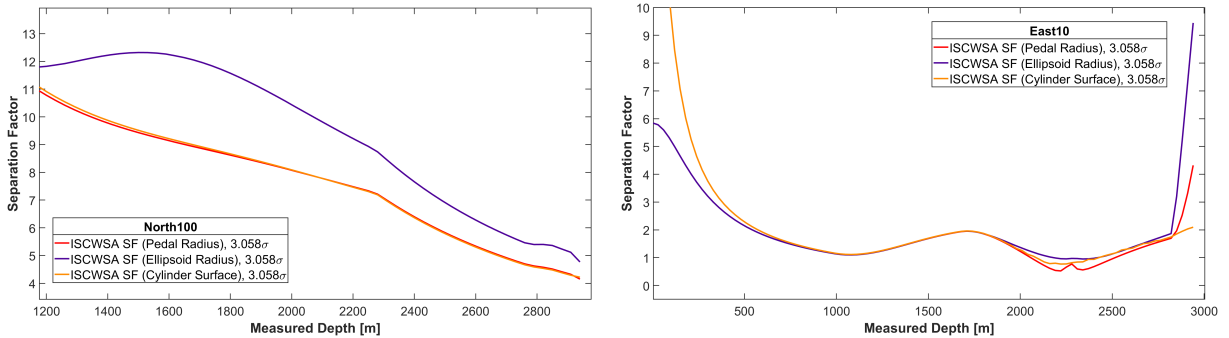
Figure 5.27: A Comparison between Safety Factors Originated by the TECoU Surface Distance and ISCWSA Basic Safety Factor Equation for the Offset wells North100 and East10.
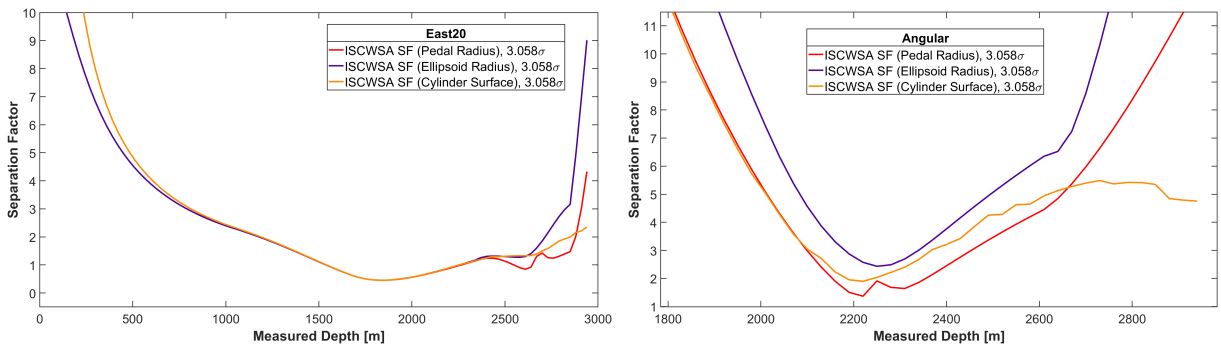
Figure 5.28: A Comparison between Safety Factors Originated by the TECoU Surface Distance and ISCWSA Basic Safety Factor Equation for the Offset wells East20 and Angular.

72
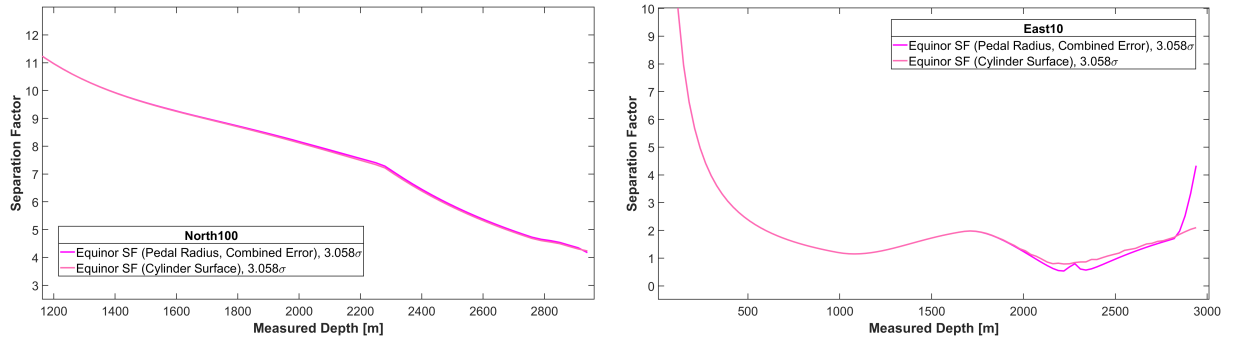
Figure 5.29: A Comparison between Safety Factors Originated by the TECoU Surface Distance and Equinor's Basic Safety Factor Equation for the Offset wells North100 and East10.
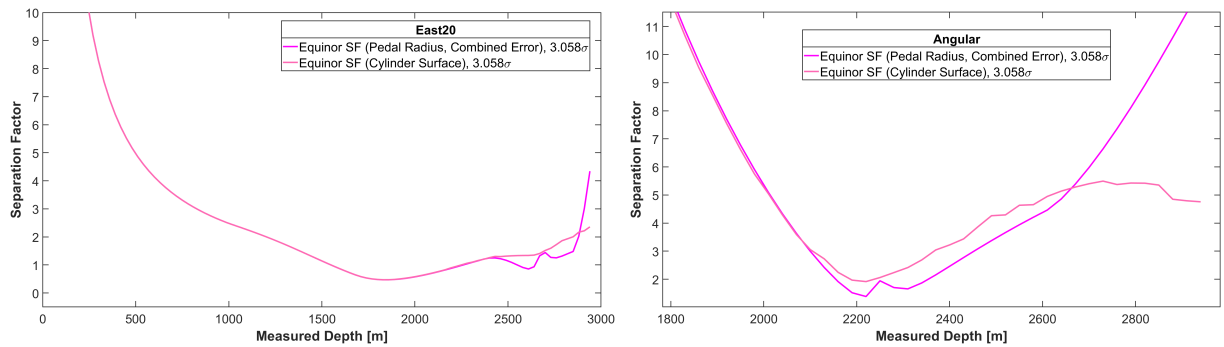
Figure 5.30: A Comparison between Safety Factors Originated by the TECoU Surface Distance and Equinor's Basic Safety Factor Equation for the Offset wells East20 and Angular.

As it can be seen above, for both ISCWSA and Equinor's equations cases, the Cylinder Surface case was matching almost perfectly to its respective equation until the geometry and the attitude of the wellbores (reference and offset) towards each other started to play a significant role in the calculation. Except in the offset well North100, which is parallel to the reference well, the offset wells' safety factors started to present differences after a certain depth.

In the offset well East10, the curves until around 2000 m MD were matching very closely. After that depth, the distances, as observed in Figure 5.18, also started to reduce. The Pedal Radius distance reduces faster than the cylinder surface distance, reaching the 0 distance much earlier. The Ellipsoid Radius method took longer to identify the risk than the other two reflecting in the separation factors at the same depth, with both equations for ISCWSA and Equinor reaching the separation factor 1, which the critical limit, faster than using the cylinder. Although when $SF \leq SF_{critic}$ means that Ellipsoids are touching each other, it is not always the case. It means that $k\sigma_D$ term of the safety factor equation is equal to or greater than D.
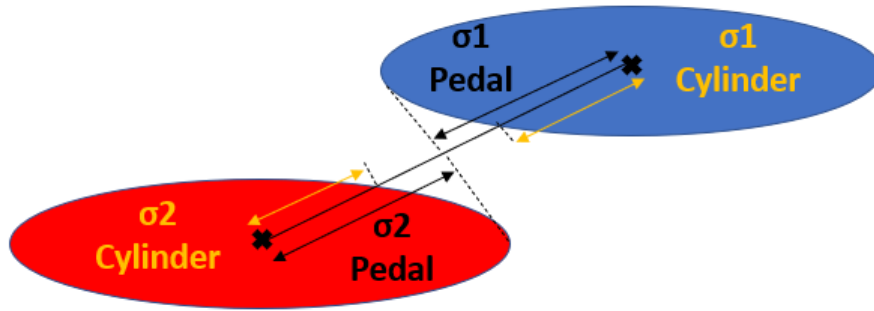
Figure 5.31: A comparison between the cylinder surface distance and pedal radius

As displayed in the Figure 5.20 and 5.31 the Pedal Radius method can be very pessimistic, presenting a situation where the sum of the $\sigma_1(r)$ and $\sigma_2(r)$ are greater than D, while the cylinder would present a smaller value for both terms. For some situations, especially when the C-C is almost orthogonal to both reference and offset well paths, the Cylinder Surface distance and the Ellipsoid Radius will be the same. On the other hand, when the angle between the C-C line for the minimum approach scanning method and the path is less than 90°, the cylinder will present a much more accurate safety factor than the other two. The Figures 4.8 and 5.32 show an example of the advantages of using the Cylinder Distances instead of the Pedal or Ellipsoid radius methods.
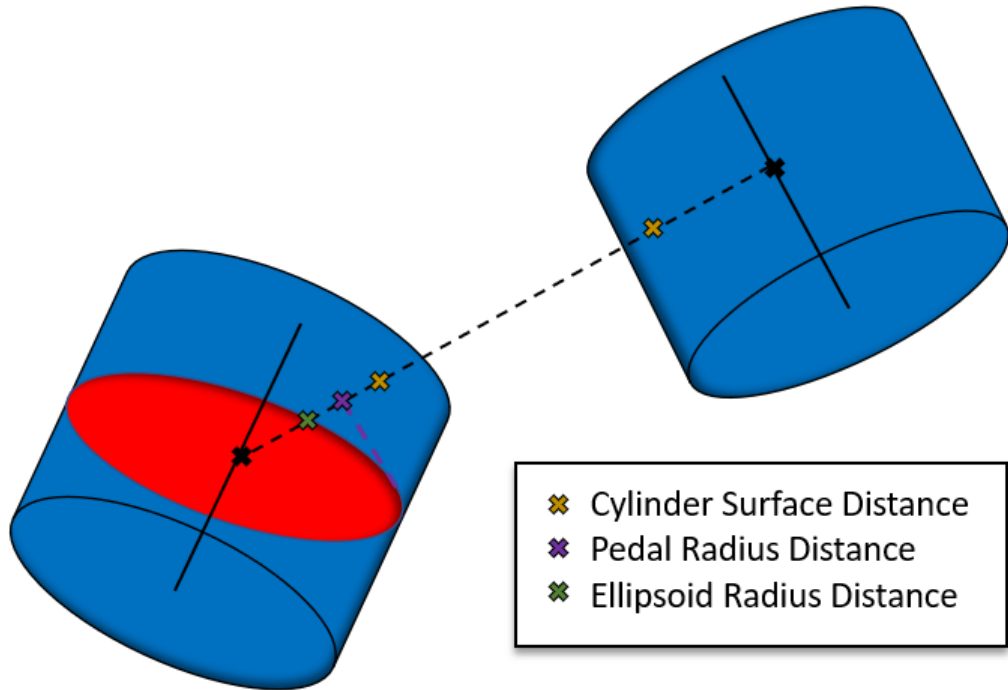
Figure 5.32: Example of the advantage of using the Cylinder Surface Distance instead of the Pedal and Ellipsoid Radius Methods

On the other hand, when it has analyzed the relationship between the reference and the Angular offset well, it was observed that when calculating the distances using the Pedal Radius, the distance between ellipsoids is reduced to less than 0 while the Cylinder Surface distances are still in the positive side. For certain situations, both the Ellipsoid Radius method and the Cylinder Surface distance method share the same weakness: it can be very optimistic, leading to possible collisions (Figure 5.33). However, the Ellipsoid Radius method results are quite different from the Cylinder Surface results in the Angular Offset well case.
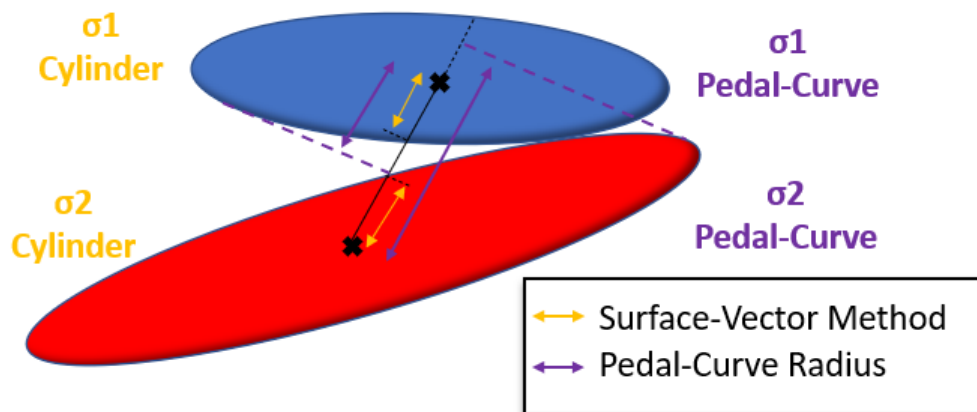
Figure 5.33: Example of the issue share by both Ellipsoid Radius and Cylinder Surface Distance methods.

5.4 Summary

The process of calculating and comparing the different types of separation factors has proven to be challenging. All three basic equations presented very consistent results. The Simplified Version (4.14) was the equation that presented more differences when comparing to the others. The equation has presented itself as the most conservative (smaller separation factor values) of all three. It did not consider the radius of the wellbores, which are quite crucial in the anti-collision analysis.

Equinor's equation, with the combined uncertainty, presented minor differences when comparing with the ISCWSA's for an equal scaling factor. On the other hand, it does not consider a surface safety margin, neither an uncertainty in the projection ahead of the current survey station. Finally, the ISCWSA equation used as a baseline for this study, which is more robust and stable than the other first two, was the most adequate for the challenging drilling environments with multiple wellheads and well path legs being used in the field.

Calculating the separation factors using the Pedal-Curve Radius distance is becoming the standard procedure, and it is available in, possibly, all anti-collision applications. Pedal Radius is the most conservative method than the Ellipsoid Radius and the Cylinder Surface Radius methods presented in this thesis and it can help users navigated safely around other wells nearby. As mentioned, it is also very pessimistic where the safety factor calculated out of the pedal distance can already display a collision alarm much earlier in some situations (Figure 5.20 and 5.31). This excess of conservatism can make navigation in very busy fields, with a high density of wellbores per squared meter like the Troll field, to be particularly challenging. In those situations, the Cylinder Surface Distance is a valid method.

The Cylinder Surface distance method displayed in this thesis is an alternative method to calculate the safety factor. Although it presents a similar issue as in the Ellipsoid Radius

method for certain situations, the method is more robust and reliable since it considers the uncertainty at a specific survey depth and the past uncertainty represented in the cylinder surface.

Chapter 6

Conclusion and Future Work

6.1 Conclusion

The Twisted Elliptic Cylinder of Uncertainty (TECoU) has proven to be a valid representation of the position uncertainty, although the process to generate it is computational more challenging than the Ellipsoid. The analysis of the separation factor using the individual direction uncertainties, $\sigma_1(r)$ and $\sigma_2(r)$, for any of the three Separation Factor Equations, has presented a less pessimistic (greater separation factor) result than using the Ellipsoid Pedal-Curve Radius method.

In more crowded fields, the Pedal Radius method can falsely indicate that two wells are close to collided, triggering an early than necessary stop drilling process while using the Cylinder Surface Method, the operation could safely proceed. The method presented in this thesis still needs refinements to prevent wells with long lateral position uncertain and specific postures to collide, as in Figure 5.33. Despite the difficulties of mathematically describing the Twisted Elliptic Cylinder of Uncertainty, the method should be considered an alternative to the Pedal Radius distance.

When reviewing the process to calculate the position uncertainties for each wellbore, it is important to notice the efforts from ISCWSA to standardize the anti-collision analysis of all the necessary data to achieve the task. It is also important to note that the error sources provided by them are just generic and do not represent the reality in the field, where the MWD and Gyro tools present a higher number of error sources. Those errors can vary from tool to tool, from manufacture to manufacture, and engineers considering implementing the method would need to replace the error sources with the ones provided by tool manufacture.

The process of finding the Ellipsoid and Cylinder of uncertainties has proven to be challenging. The numerical approaches taken in this work have proven to be successfully implemented, especially when comparing the numerically calculated Ellipsoid Pedal Radius method and the method provided by Bang et al. (2020). The Twisted Elliptic Cylinder of uncertainty is extremely hard to describe mathematically, and all calculation of the individual direction uncertainties, $\sigma_1(r)$ and $\sigma_2(r)$, was also computational challenging, where each of the surface individual points in the area nearby the C-C line had to be tested against the equation (4.9). As a recommendation, the cylinder's surface should be formally described to improve the efficiency of the calculations.

From the three separation factors used, the Simplified, Equinor and ISCWSA, it is clear that the equation provided by the WPTS is the most robust and less prone to numerical errors than the other two. It was demonstrated in this work that the Simplified version way more pessimistic, displaying much smaller safety factors than the others when using the Pedal-Curve method. It also does not use both wellbores' radius in the calculation, making it dangerous to be used. Because of that, it is not recommended to be used. The biggest difference between the Equinor and ISCWSA's equation are the additions of the safety margin and the projected-ahead uncertainties introduced by ISCWSA. Those terms consider a minimum separation between the wellheads and the projection uncertainties, making the equation from ISCWSA more robust and adequate to be used in real operations.

By comparing the three methods to calculate the individual directional uncertainties, $\sigma_1(r)$ and $\sigma_2(r)$, it is clear that the Pedal-Curve radius is the most conservative, displaying the smallest safety factors as the two wellbores, the reference, and the offset, are getting close to each other. As already explained, the reason is due to the very nature of how the Peda-Curve is derived, and it can cause an earlier stop drilling. The Cylinder Surface Method is presented as a valid alternative to the Pedal-Curvel, although it faces some issues similar to the Ellipsoid Radius method. To overcome this issue, the well planning engineer would have to determine the smallest distance between the two ellipsoids to ensure the position uncertainties do not overlap each other, which would characterize as a well collision.

With more wellbores being drilled in the same area in the past few years, it is now more than important to define an industry-standard way to defined how safe is to drill in the area, avoiding costly well collisions, without forgetting its precision. The Twisted Elliptic Cylinder of Uncertainty should be considered as a viable alternative to the Pedal-Curve, although it still needs refinements on its methods. Hopefully, in the future, more research can be done in the same area.

6.2   Future Work

In this section, the writer's recommendations to help future students continue the work developed in this thesis.

- **Describe the Twisted Elliptic Cylinder of Uncertainty Surface**: As mentioned throughout the thesis, the surface of the twisted elliptic cylinder is very hard to describe mathematically. In order to derive the position uncertainties for the Cylinder Surface Method, a numerical approach was taken. This numerical approach was proven to be very computationally expensive. An accurate description of the surface would reduce the computational effort, increase the speed of the method.

- **Improve Cylinder Surface Method**: Although the Cylinder Surface method has proven to be a viable replacement to the Pedal-Curve method, it is not perfect and requires an additional calculation of the minimum distance between Ellipsoids to ensure the position uncertainties are not overlapping each other. An improvement in the method would be beneficial in determining the safety of the operation when using the Cylinder Surface Method.

- **Use the anti-collision technique in the automated drilling systems**: The methods presented so far are mostly used offline, while in the planning phase or after the survey was taken during drilling. The Automated Drilling System would require a computationally fast method, where the safety factor is constantly being calculated as new data is received for every single offset well in the same area. Today, there are no automated drilling applications with that capability.

References

Adams, N. J., & Charrier, T. (1985). *Drilling Engineering - A Complete Well Planning Approach.* PennWell Publishing Company.

Ajetunmobi, M. O. (2012). *Depth Issues in the Oil Patch - A Study of Wellbore Position Uncertainty in the Ekofisk Field* (Doctoral dissertation). University of Stavanger.

Baker Hughes. (1998). *Wellbore Positioning - Training Manual* (tech. rep. July). Baker Hughes. Houston, Texas.

Bang, J., Inc, G., Nyrnes, E., Asa, E., Wilson, H., & Hughes, B. (2020). Evaluation of Separation Factors Used in Wellbore Collision Avoidance. https://doi.org/10.2118/200475-PA

Bang, J., & Nyrnes, E. (2015). Collision Risk Analysis - Pedal Curve vs. Ellipse.

Brooks, A., & Wilson, H. (2005). *Quantification of Depth Accuracy*, SPE.

Butler, B. (2018). Unlocking Production With Multilateral Wells. https://www.hartenergy.com/exclusives/unlocking-production-multilateral-wells-31250

Cattell, R. B. (1988). Variance-Covariance Matrix. https://www.encyclopedia.com/social-sciences/applied-and-social-sciences-magazines/variance-covariance-matrix

Choudhary, D. (2011). Directional Drilling Technology. http://directionaldrilling.blogspot.com/2011/07/toolface-magnetic-tool-face-mtf-gravity.html

Cumming, M. (2017). WHICH WAY TO GO: What is Slant, Directional & Horizontal drilling? https://www.machines4u.com.au/mag/slant-directional-horizontal-drilling/

Friendly, M., Monette, G., & Fox, J. (2011). *Understanding Statistical Methods Statistical Methods through Elliptical Geometry* (tech. rep.). York University.

ISCWSA. (n.d.). About ISCWSA - The Industry Steering Committee on Wellbore Survey Accuracy - International Organization - Affiliated with the Society of Petroleum Engineers - SPE. https://www.iscwsa.net/about/

ISCWSA. (2013). *Collision Avoidance Calculations - Current Common Practice* (tech. rep.). Industry Steering Committee on Wellbore Survey Accuracy. https://www.iscwsa.net/media/files/files/b6fb074d/current-common-practice-in-collision-avoidance-calculations-oct-2017.pdf

ISCWSA. (2016). Error Model Example File 1 - MWDRev4 ISCWSA - 11-14-2016 : Wellbore Standards in Houston, Texas USA. https://www.iscwsa.net/articles/error-model-example-file-1-mwdrev4-iscwsa/

ISCWSA. (2017a). *Definition of the ISCWSA Error Model* (tech. rep. September). ISCWSA.

ISCWSA. (2017b). Standard Set of Wellpaths for Evaluating Clearance Scenarios - Excel WorkBook. https://www.iscwsa.net/articles/standard-wellpath-revision-4-excel/

Jamieson, A., McGregor, A., Stigant, J., Weston, J., Grindrod, S. J., McRobbie, D., & IS-CWSA. (2007). *Introduction to Wellbore Positioning.* University of the Highlands; Islands.

Johnson, R. A. (2017). *Probability and Statistics for Engineers* (Miller & Freund's, Ed.; 9th). Pearson Education Limited.

Jones, J. (n.d.). Statistics: Chi-Square Distribution. https://people.richland.edu/james/lecture/m170/ch12-int.html

Krishnan, A., & Kulkarni, A. (2016). Well Trajectory Survey of a Directional well. *International Research Journal of Engineering and Technology, 3*(7). www.irjet.net

Liu, X. (2019). Borehole trajectory uncertainty and its characterization. *Petroleum Exploration and Development, 46*(2), 407–412. https://doi.org/10.1016/S1876-3804(19)60021-2

Mansouri, V., Khosravanian, R., Wood, D. A., & Aadnøy, B. S. (2020). Optimizing the separation factor along a directional well trajectory to minimize collision risk. *Journal of Petroleum Exploration and Production Technology, 10*(5), 2113–2125. https://doi.org/10.1007/s13202-020-00876-7

Mitchell, R. F., & Miska, S. Z. (2016). *Fundamentals of Drilling Engineering* (R. F. Mitchell & S. Z. Miska, Eds.; Vol. 12). Society of Petroleum Engineers. https://doi.org/10.1002/9781119083931

Muhammadali, S. (2017). *Error and Ellipses of Uncertainty Analysis in Far North* (Doctoral dissertation). Norwegian University of Science and Technology.

PetroWiki. (n.d.). Directional survey. https://petrowiki.org/Directional_survey

Poedjono, B., Lombardo, G. J., & Phillips, W. (2009). *Anti-Collision Risk Management Standard for Well Placement* (tech. rep.).

Rocha, L. A. S., Azuaga, D., Andrade, R., Vieira, J. L. B., & Santos, O. L. A. (2011). *Directional Drilling* (3rd). Interciência. https://books.google.no/books?id=d0ZMSAAACAAJ

Sawaryn, S. J., & Thorogood, J. L. (2005). *A Compendium of Directional Calculations Based on the Minimum Curvature Method* (tech. rep.).

Sawaryn, S. J., Wilson, H., Allen, W. T., Clark, P. J., Mitchell, I., Codling, J., Sentance, A., Poedjono, B., Lowdon, R., Bang, J., & Nyrnes, E. (2018). Well Collision Avoidance Management and Principles. *SPE Drilling and Completion, 33*(4), 335–350. https://doi.org/10.2118/184730-PA

Sawaryn, S. J., Wilson, H., Bang, J., Nyrnes, E., Sentance, A., Poedjono, B., Lowdon, R., Mitchell, I., Codling, J., Clark, P. J., & Allen, W. T. (2019). Well Collision Avoidance Separation Rule. *SPE Drilling and Completion, 34*(1), 1–15. https://doi.org/10.2118/187073-PA

Thorogood, J. L., Sawaryn, S. J., & BP Exploration. (1990). *The Travelling Cylinder: A Practical Tool for Collision Avoidance* (tech. rep.). SPE. Houston, Texas.

Torkildsen, T., Håvardstein, S. T., Weston, J., & Ekseth, R. (2008). *Prediction of Wellbore Position Accuracy When Surveyed With Gyroscopic Tools* (tech. rep.).

Walstrom, J. E., Brown, A. A., & Harvey, R. P. (1969). *An Analysis of Uncertainty in Directional Surveying Introduction and Model Description* (tech. rep.). SPE. Houston, Texas.

What-when-how. (n.d.). Datums, Coordinate Systems, and Map Projections (GPS) Part 2. http://what-when-how.com/gps/datums-coordinate-systems-and-map-projections-gps-part-2/

Wikipedia. (n.d.). Ellipsoid. https://en.wikipedia.org/wiki/Ellipsoid

Williamson, H. S. (2000). *Accuracy Prediction for Directional Measurement While Drilling* (tech. rep.).

Wolff, C. J. M., Laboratorium, P., & De Wardt, J. P. (1981). *Borehole Position Uncertainty – Analysis of Measuring Methods and Derivation of Systematic Error Model* (tech. rep.).

Appendix A

List of Error Sources and Weighting Functions

Table A.1: The MWD Tool Error Sources, their magnitudes and propagation mode provided by ISCWSA

No	Code	Type	Magnitude	Units	Prop.
1	DRFR	Depth	0.35	m	R
2	DSFS	Depth	0.00056	-	S
3	DSTG	Depth	0.00000025	1/m	G
4	ABXY-TI1S	Sensor	0.004	m/s2	S
5	ABXY-TI2S	Sensor	0.004	m/s2	S
6	ABZ	Sensor	0.004	m/s2	S
7	ASXY-TI1S	Sensor	0.0005	-	S
8	ASXY-TI2S	Sensor	0.0005	-	S
9	ASXY-TI3S	Sensor	0.0005	-	S
10	ASZ	Sensor	0.0005	-	S
11	MBXY-TI1S	Sensor	70	nT	S
12	MBXY-TI2S	Sensor	70	nT	S
13	MBZ	Sensor	70	nT	S
14	MSXY-TI1S	Sensor	0.0016	-	S
15	MSXY-TI2S	Sensor	0.0016	-	S
16	MSXY-TI3S	Sensor	0.0016	-	S
17	MSZ	Sensor	0.0016	-	S
18	DECG	AziRef	0.36	deg	G
19	DECR	AziRef	0.1	deg	R
20	DBHG	AziRef	5000	deg.nT	G
21	DBHR	AziRef	3000	deg.nT	R
22	AMIL	Mgntcs	220	nT	S
23	SAG	Align	0.2	deg	S
24	XYM1	Align	0.1	deg	S
25	XYM2	Align	0.1	deg	S
26	XYM3	Align	0.1	deg	S
27	XYM4	Align	0.1	deg	S

Table A.2: The Weighting Functions for each MWD Surveying Tool Error Sources provided by ISCWSA (ISCWSA, 2016)

No	Code	Type	Weighting Functions		
			Depth	Inclination	Azimuth
1	DRFR	Depth	1	0	0
2	DSFS	Depth	MD	0	0
3	DSTG	Depth	MD TVD	0	0
4	ABXY-TI1S	Sensor	0	$\frac{\cos(Inc)}{G_{ield}}$	$\frac{\tan(Dip)\cos(Inc)\sin(Azi_M)}{G_{field}}$
5	ABXY-TI2S	Sensor	0	0	$\frac{\tan(\frac{pi}{2}-Inc)-\tan(Dip)\cos(Azi_M)}{G_{field}}$
6	ABZ	Sensor	0	$\frac{--\sin(Inc)}{G_{field}}$	$\frac{\tan(Dip)\sin(Inc)\sin(Azi_M)}{G_{field}}$
7	ASXY-TI1S	Sensor	0	$\frac{\sin(Inc)\cos(Inc)}{\sqrt{2}}$	$\frac{-\tan(Dip)\sin(Inc)\cos(Inc)\sin(Azi_M)}{\sqrt{2}}$
8	ASXY-TI2S	Sensor	0	$\frac{\sin(Inc)\cos(Inc)}{2}$	$\frac{-\tan(Dip)\sin(Inc)\cos(Inc)\sin(Azi_M)}{2}$
9	ASXY-TI3S	Sensor	0	0	$\frac{\tan(Dip)\sin(Inc)\cos(Azi_M)}{2}$
10	ASZ	Sensor	0	$-\sin(Inc)\cos(Inc)$	$\tan(Dip)\sin(Inc)\cos(Inc)\sin(Azi_M)$
11	MBXY-TI1S	Sensor	0	0	$\frac{-\cos(Inc)\sin(Azi_M)}{B_{field}\cos(Dip)}$
12	MBXY-TI2S	Sensor	0	0	$\frac{\cos(Azi_M)}{B_{field}\cos(Dip)}$
13	MBZ	Sensor	0	0	$\frac{-\sin(Inc)\sin(Azi_M)}{B_{field}\cos(Dip)}$
14	MSXY-TI1S	Sensor	0	0	$\frac{\sin(Inc)\sin(Azi_M)\tan(Dip)\cos(Inc)+\sin(Inc)\cos(Azi_M)}{\sqrt{2}}$
15	MSXY-TI2S	Sensor	0	0	$\frac{\sin(Azi_M)\tan(Dip)\sin(Inc)\cos(Inc)-\cos(Inc)^2\cos(Azi_M)-\cos(Azi_M)}{2}$
16	MSXY-TI3S	Sensor	0	0	$\frac{\cos(Inc)\cos(Azi_M)^2-\cos(Inc)\sin(Azi_M)^2-\tan(Dip)\sin(Inc)\cos(Azi_M)}{2}$
17	MSZ	Sensor	0	0	$-(\sin(Inc)\cos(Azi_M)+\tan(Dip)\cos(Inc))\sin(Inc)\sin(Azi_M))$
18	DECG	AziRef	0	0	1
19	DECR	AziRef	0	0	1
20	DBHG	AziRef	0	0	$\frac{1}{B_{field}\cos(Dip)}$
21	DBHR	AziRef	0	0	$\frac{1}{B_{field}\cos(Dip)}$
22	AMIL	Mgntcs	0	0	$\frac{\sin(Inc)\sin(Azi_M)}{B_{field}\cos(Dip)}$
23	SAG	Align	0	$\sin(Inc)$	0
24	XYM1	Align	0	$|\sin(Inc)|$	0
25	XYM2	Align	0	0	-1
26	XYM3	Align	0	$|\cos(Inc)|\cos(Azi_T)$	$\frac{-|\cos(Inc)|\sin(Azi_T)}{\sin(Inc)}$
27	XYM4	Align	0	$|\cos(Inc)|\sin(Azi_T)$	$\frac{|\cos(Inc)|\cos(Azi_T)}{\sin(Inc)}$

Table A.3: Error Sources that present Sigularity when Vertical

No	Code	Type	Singularity When Vertical		
			North	East	Vertical
5	ABXY-TI2S	Sensor	$\frac{-\sin(Azi)}{G_{field}}$	$\frac{\cos(Azi)}{G_{field}}$	0
26	XYM3	Align	1	0	0
27	XYM4	Align	0	1	0

Appendix B

The Reference and Offset Well Paths

Table B.1: The Wellpath of the Reference Well.

Type	MD [m]	Inclination [°]	Azimuth [°]	TVD [m]	North [m]	East [m]	DLS [°]/30 m
	0	0.00	180.00	0.00	0.00	0.00	0.00
Vertical	990	0.00	180.00	990.00	0.00	0.00	0.00
2D Arc	1020	1.33	180.00	1020.00	-0.35	0.00	1.33
2D Arc	2250	83.33	180.00	1853.67	-759.73	0.00	2.00
2D Arc	2280	85.00	180.00	1856.72	-789.70	0.00	1.67
Tangent	2760	85.00	180.00	1898.55	-1267.75	0.00	0.00
2D Arc	2790	86.00	180.00	1900.91	-1297.65	0.00	1.00
2D Arc	2850	90.00	180.00	1903.00	-1357.60	0.00	2.00
Tangent	2940	90.00	180.00	1903.00	-1447.60	0.00	0.00

Table B.2: The Wellpath of the North100 Offset Well

Type	MD [m]	Inclination [°]	Azimuth [°]	TVD [m]	North [m]	East [m]	DLS [°]/30 m
	0	0.00	180.00	0.00	100.00	0.00	0.00
Vertical	990	0.00	180.00	990.00	100.00	0.00	0.00
2D Arc	1020	1.19	180.00	1020.00	99.69	0.00	1.19
2D Arc	1110	6.56	180.00	1109.76	93.61	0.00	1.79
2D Arc	1140	8.36	180.00	1139.50	89.71	0.00	1.80
2D Arc	1290	17.31	180.00	1285.61	56.43	0.00	1.79
2D Arc	1320	19.11	180.00	1314.10	47.05	0.00	1.80
2D Arc	1470	28.06	180.00	1451.43	-12.90	0.00	1.79
2D Arc	1500	29.86	180.00	1477.68	-27.43	0.00	1.80
2D Arc	1680	40.60	180.00	1624.50	-131.11	0.00	1.79
2D Arc	1710	42.40	180.00	1646.97	-150.99	0.00	1.80
2D Arc	1830	49.56	180.00	1730.30	-237.23	0.00	1.79
2D Arc	1860	51.36	180.00	1749.40	-260.36	0.00	1.80
2D Arc	2010	60.31	180.00	1833.55	-384.35	0.00	1.79
2D Arc	2040	62.11	180.00	1848.00	-410.64	0.00	1.80
2D Arc	2190	71.06	180.00	1907.54	-548.15	0.00	1.79
2D Arc	2220	72.80	180.00	1916.84	-576.67	0.00	1.80
2D Arc	2400	83.60	180.00	1953.50	-752.63	0.00	1.79
2D Arc	2430	85.00	180.00	1956.48	-782.48	0.00	1.40
Tangent	2910	85.00	180.00	1998.31	-1360.65	0.00	0.00
2D Arc	2940	86.11	180.00	2000.64	-1390.56	0.00	1.11
2D Arc	2970	88.11	180.00	2002.15	-1420.52	0.00	2.00
2D Arc	3000	90.00	180.00	2002.64	-1450.52	0.00	1.89
Tangent	3090	90.00	180.00	2002.64	-1540.52	0.00	0.00

Table B.3: The Wellpath of East10 the Offset Well

Type	MD [m]	Inclination [°]	Azimuth [°]	TVD [m]	North [m]	East [m]	DLS [°]/30 m
	0	0.00	175.00	0.00	0.00	10.00	0.00
Vertical	990	0.00	175.00	990.00	0.00	10.00	0.00
2D Arc	1020	1.33	175.00	1020.00	-0.35	10.03	1.33
2D Arc	1650	43.33	175.00	1589.79	-233.50	30.43	2.00
3D Arc	1680	45.31	175.18	1611.26	-254.38	32.22	1.98
3D Arc	1770	50.89	178.13	1671.35	-321.21	36.05	2.00
3D Arc	1800	52.77	179.02	1689.89	-344.79	36.63	2.01
3D Arc	1980	64.14	183.54	1783.94	-497.83	32.85	2.00
3D Arc	2010	66.04	184.20	1796.58	-524.97	31.07	1.99
3D Arc	2250	81.38	188.96	1863.72	-753.02	4.31	2.00
3D Arc	2280	83.31	189.52	1867.72	-782.37	-0.46	2.01
3D Arc	2310	85.00	190.00	1870.78	-811.78	-5.52	1.76
Tangent	2820	85.00	190.00	1915.22	-1312.12	-93.74	0.00

Table B.4: The Wellpath of the East20 Offset Well

Type	MD [m]	Inclination [°]	Azimuth [°]	TVD [m]	North [m]	East [m]	DLS [°]/30 m
	0	0.00	182.00	0.00	0.00	20.00	0.00
Vertical	990	0.00	182.00	990.00	0.00	20.00	0.00
2D Arc	1020	1.33	182.00	1020.00	-0.35	19.99	1.33
3D Arc	2070	70.87	176.11	1815.76	-583.25	19.16	2.00
3D Arc	2100	72.85	175.77	1825.10	-611.69	21.18	2.01
3D Arc	2130	74.82	175.43	1833.45	-640.41	23.39	2.00
3D Arc	2160	76.80	175.10	1840.81	-669.40	25.79	2.01
3D Arc	2190	78.77	174.78	1847.15	-698.60	28.37	1.99
3D Arc	2220	80.75	174.46	1852.49	-727.99	31.14	2.00
3D Arc	2250	82.72	174.15	1856.80	-757.53	34.09	1.99
3D Arc	2280	84.70	173.83	1860.08	-787.19	37.21	2.01
3D Arc	2310	86.67	173.52	1862.34	-816.92	40.51	1.99
3D Arc	2340	88.65	173.21	1863.57	-846.69	43.97	2.00
3D Arc	2370	90.00	173.00	1863.92	-876.47	47.57	1.37
3D Arc	2400	90.00	175.95	1863.92	-906.33	50.46	2.95
3D Arc	2640	90.00	199.95	1863.92	-1142.29	17.51	3.00
3D Arc	2670	90.00	200.00	1863.92	-1170.48	7.26	0.05
2D Arc	2850	90.00	200.00	1863.92	-1339.63	-54.31	0.00

Table B.5: The Wellpath of the Angular Offset Well

Type	MD [m]	Inclination [°]	Azimuth [°]	TVD [m]	North [m]	East [m]	DLS [°]/30 m
	0	0.00	145.00	0.00	-50.00	-500.00	0.00
Vertical	990	0.00	145.00	990.00	-50.00	-500.00	0.00
2D Arc	1020	1.33	145.00	1020.00	-50.29	-499.80	1.33
2D Arc	2130	75.33	145.00	1831.47	-575.81	-131.82	2.00
2D Arc	2160	77.00	145.00	1838.64	-599.67	-115.11	1.67
Tangent	2655	77.00	145.00	1949.99	-994.76	161.53	0.00